12-2021

Injection Studies on a Small-Scale Rotating Detonation Engine with Improved Flow Control

Jonathan J. Wyatt

Injection Studies on a Small-Scale Rotating Detonation Engine with Improved Flow Control

THESIS

Jonathan J. Wyatt, 2d Lt, USAF

AFIT-ENY-MS-21-D-080

DEPARTMENT OF THE AIR FORCE
AIR UNIVERSITY

AIR FORCE INSTITUTE OF TECHNOLOGY

Wright-Patterson Air Force Base, Ohio

AFIT-ENY-MS-21-D-080

INJECTION STUDIES ON A SMALL-SCALE ROTATING DETONATION ENGINE WITH IMPROVED FLOW CONTROL

THESIS

Presented to the Faculty

Department of ENY

Graduate School of Engineering and Management

Air Force Institute of Technology

Air University

Air Education and Training Command

in Partial Fulfillment of the Requirements for the

Degree of Master of Astronautical Engineering

Jonathan J. Wyatt, BS

2d Lt, USAF

December 2021

AFIT-ENY-MS-21-D-080

INJECTION STUDIES ON A SMALL-SCALE ROTATING DETONATION ENGINE WITH IMPROVED FLOW CONTROL

THESIS

Jonathan J. Wyatt, BS
2d Lt, USAF

Committee Membership:

Dr. Fred R. Schauer
Chair

Dr. Marc D. Polanka
Member

Dr. S. Alex Schumaker
Member

Abstract

The Rotating Detonation Engine (RDE) has gained increasing attention in recent years for its potential advantages over typical deflagration combustion. Current interest resides in stretching the operating limits of RDEs with low mass flow rates and small channel diameters. Small scale RDEs could offer a research tool that can be quickly and cheaply modified while also not requiring the numerous facility safety accommodations that usually accompany RDE testing. Thus, a Micro-RDE design was developed with an outer diameter of 28 mm and a channel gap of 2 mm operating on Ethylene and Nitrous Oxide as the fuel and oxidizer, respectively. This small scale engine was designed to operate on mass flows between 25 - 75 g/s. Detonations have been successfully achieved in this rig, however further optimization to produce stable detonations at the design frequency of 20 kHz is an ongoing process.

Initial testing on this rig exhibited unstable wave modes with a frequency range of 11.7 - 14 kHz while using a Jets in Crossflow (JIC) injection geometry and a spark plug as an ignition mechanism [1]. It was hypothesized that non-ideal mixing and flow field reactions with the spark plug were the causes of the unstable wave behavior and low frequencies. Thus, changes to the injection scheme and ignition mechanism were made to improve the mixing quality of the reactants while also reducing the destabilizing interactions experienced with the spark plug. A Partially-Premixed JIC which moved the point of crossflow from inside the detonation chamber to 2 mm before the entrance was implemented to replace the traditional JIC scheme [2]. A pre-detonator device replaced the spark plug as the ignition mechanism, and iterations on the placement of the pre-detonator along with the experimentation of different materials, such as Inconel, were performed to reduce erosion in the Micro-RDE. This

new configuration had an increase of observed frequencies ranging from 13 - 19.1 kHz, and though not all waves were stable, the first single wave propagating mode was seen in an RDE of this scale [2]. Additional research was needed to further optimize the Micro-RDE and allow for an increased understanding of how an RDE at this scale and the detonations it produces are influenced by certain parameters.

Key parameters that influence the detonation wave mode are cell size, fill height, and wave speed, which are heavily influenced by injection schemes. Previous testing utilized a partially premixed jets in crossflow (JIC) injection scheme, while tests before that used a traditional JIC scheme. A Simplex and Counter-jet injection scheme were added to the configuration to explore other options of injecting the fuel and oxidizer. The goal of this research was to characterize the operating limits of the injection schemes and understand their effects on the detonation wave stability in a small-scale RDE. The traditional JIC scheme produced the largest operating map detonating at oxidizer mass flow rates from 55 g/s to as low as 12 g/s. However, it's average wave frequency observed was 12.6 kHz, 38 % from the design frequency of 20 kHz. The partially-premixed JIC produced higher wave frequencies averaging 16.9 kHz which equated to 16 % from the design frequency, while a specific configuration of the Counter-jet produced an average wave speed of 17.3 kHz equating to 14 % from the design frequency. The Simplex produced frequencies averaging 13.3 kHz which was 34 % from the design, and also possessed the most limited operating map. An optical outerbody was incorporated to provide visualization of the detonation within the channel. Testing using the optical outerbody was intended to further explore the detonation dynamics in the chamber and assess the cell size, fill height, and wave speed, but limitations of the high-speed cameras utilized prevented an in-depth assessment of the parameters in question.

This work is dedicated to my family and friends back in Southeast San Diego, California and all across the country. Your support during this challenging time as a Master's student has been unwavering and has helped me get through this process. You all are the reason that I push myself so hard. I hope I can continue to make you all proud and represent for the city I come from. I also hope that by showing this is possible, other's will follow in my footsteps. Can't wait to celebrate with you all back home, but until then, The Marathon Continues.

- Jonathan J. Wyatt

Acknowledgements

I would like to thank all the people who helped this research possible. Thanks to my advisor, Dr. Schauer, and predecessors Joe Dechert and Nathan Fiorino for giving me the opportunity to continue this project. It has been both a privilege and a challenge to follow on such a difficult project developed by such intelligent people. To Nathan Snow, thanks for all the constant help and guidance throughout my time in the Dbay. A lot of this project would not have been possible without you, and I'll always remember the countless hours we spent trying to make this research both successful and educational.

To Riley Huff, Kavi Muraleetharan, Peter Keller, and the many others who were in and out of the lab, thanks for coming in to test with me in the early mornings and well after it was time to go home. I hope to pay it forward one day. Special thanks to the Dbay cadre, Brian, Kevin, Curtis, Matt F., Rob, RJ, Matt P. and John for always being willing to share their expertise and for allowing me time to test when you all had your own research to do. I enjoyed being able to witness projects that are changing the propulsion world today. Lastly, to my committee members, Dr. Marc Polanka and Dr. Alex Schumaker, thank you for the consistent editing and revisions that helped improve the quality of this research. While it made this thesis project all the more challenging, I believe I am better equipped to conduct research as an engineer because of it.

Jonathan J. Wyatt

Table of Contents

Page

List of Figures

List of Tables

Nomenclature

Symbol		Page
λ	Cell Size	17
h	Fill Height	17
l_c	Channel Length	18
Δ	Channel Gap	18
h_D	Wave Height	19
J	Momentum Flux Ratio	24
C_D	Discharge Coefficient	24
α	Spray Angle	24
Q	Total Flow Rate	24
R_o	Radius of the Orifice	25
ρ	Liquid Density	25
ΔP	Pressure Drop	25
v	Average Tangential Velocity	25
ϵ	Throat to Chamber Area Ratio	30
ϕ	Equivalence Ratio	30
α	Oblique Shock Angle	40
β	Shear Layer Angle	40
ε	Detonation Wave Angle	40
θ	Contact Surface Angle	40
δ	Characteristic Reaction Zone Width	43
E_a	Activation Energy	43
R	Universal Gas Constant	43

Symbol Page

List of Abbreviations

Abbreviation		Page
RDE	Rotating Detonation Engine	1
JIC	Jets-in-Crossflow	1
DERF	Detonation Engine Research Facility	3
AFRL	Air Force Research Laboratory	3
CJ	Chapman-Jouget	10
FJ	Fickett-Jacobs	14
PDE	Pulsed Detonation Engine	15
DDT	Deflagration to Detonation Transition	15
SIJ	Semi-Impinging Jet	22
DAQ	Data Acquistion Controller	46
CTAP	Capillary Tube Average Pressure	86
FFT	Fast Fourier Transform	112

INJECTION STUDIES ON A SMALL-SCALE ROTATING DETONATION ENGINE WITH IMPROVED FLOW CONTROL

I. Introduction

This document presents the continued research efforts on the previously developed small-scale Rotating Detonation Engine (RDE), also called the "Micro-RDE". These efforts included the characterization of the influence of various injection schemes on the stability and operability in the Micro-RDE. Stability of the detonation wave in the RDE was based on its proximity to the design frequency 20 kHz while the operability was based on the ranges of detonable mass flows and equivalence ratios. Optical access was gained into the detonation chamber to further assess the detonation waves produced by each injection scheme, with properties such as the fill height, cell size, and wave speed being used for comparison. The Micro-RDE was designed with a channel diameter of 28 mm and operated on nitrous oxide (N_20) and ethylene (C_2H_4) as the oxidizer and fuel, respectively. Changes to the mass flow control system were made to improve the stability and reliability of metered flow in the RDE system. Four injection schemes were tested in this research: a traditional (Plain) Jets in Crossflow (JIC) injection scheme, a Partially-Premixed JIC scheme, a modified Simplex swirl nozzle, and a Counter-jet injection mechanism. Additionally, optical access was gained into the small scale detonation engine to provide visual data of the propagating wave in the detonation chamber and help further characterize the performance of the various injection schemes in the Micro-RDE.

1.1 Motivation and Background

Detonations are a mode of combustion in which the combustion reaction is preceded by a leading shock/compression wave. This shock wave forms due to the flame front traveling at super sonic speeds, its speed being what separates detonative combustion and deflagrative combustion where flame fronts travel at subsonic speeds [3]. The strong shock compressions cause a steep rise in pressure before the reaction zone creating more favorable conditions for combustion (as opposed to deflagration where pressure is nominally constant throughout the reaction). As a result from the high pressure rise the amount of extractable work from a detonation or pressure-gain combustion process is greater than that of a deflagrative or constant pressure process [4]. This theoretical increase in more extractable work can be seen in the P-v diagram in Figure 1 which compares a detonation cycle to the Brayton cycle, a typical deflagration process.

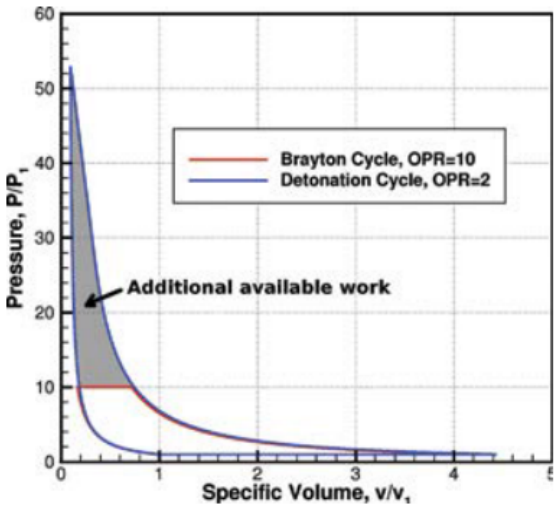

[5]

Figure 1. Comparison of Brayton Cycle to Detonation Cycle for Typical Operating Pressure Ratios (OPR)

Detonation engines were designed to harness this theoretical increase in work pictured in Figure 1. A specific type of detonation engine, the Rotating Detonation

Engine (RDE), is designed to continuously propagate a detonation wave around an annulus. Fundamentally, the detonation wave can be sustained in an RDE as long as fresh reactants are supplied to it with each passing wave. If there aren't sufficient reactants entering the combustion chamber before the detonation wave completes a full rotation then the wave will no longer be able to sustain itself. To reach this self sustaining wave, not only must fresh reactants be replenished into the chamber, but combusted reactants must simultaneously be exhausted the remaining length of the chamber to allow for the new reactants to continuously enter the chamber [6]. No moving parts are required in an RDE to achieve this self-sustaining detonation.

Common RDEs generally have channel diameters around 150 mm and operate on mass flows on the order of kilograms per second [1]. Testing RDEs usually involve numerous hazards which can include explosive gases and high levels of noise. Therefore, most RDE research is conducted in test facilities similar to the Detonation Engine Research Facility (DERF) of the Air Force Research Laboratory (AFRL) which possesses certain safety precautions to account for the storage of highly reactive fuel and oxidizers, high operating noises, and potential explosions. Due to the numerous accommodations necessary to safely house and run an RDE, there are a limited number of locations in which RDE research can be conducted. Consequently, research into small scale rotating detonation engines has been conducted to create an operable device that does not require the typical facility restrictions of most RDEs.

The Micro-RDE designed by Dechert was intended to reduce the hazards associated with typical RDE experiments while also developing an understanding of RDE operation on a smaller scale [1]. He designed a small scale RDE with a channel diameter of 28 mm, a channel gap of 2 mm, and a channel length of 30 mm. This RDE design was made to run on mass flow rates between 25 - 75 g/s (orders of magnitude less than typical flow rates in RDEs) and produce detonation frequencies at

20 kHz. These lower mass flow rates would lessen the amount of hazardous materials needed to conduct testing and consequently ease the requirements necessary of a facility. The higher frequencies that could be achieved in the engine because of its smaller size would also reduce the hearing safety requirements typically required of facilities to prevent hearing damage. Additional benefits from an RDE at this size could translate to portability, as its smaller setup would enable it to be moved to lab environments previously inaccessible to RDEs. With these potential benefits in mind, along with the desire to push the limits of RDE operation, research on the Micro-RDE was conducted.

Initial research in the Micro-RDE conducted by Dechert showed that detonations were achievable at some of the intended mass flow rates, however the detonation waves produced in the configuration were universally unstable as detonation frequencies fell below 30 % of the design frequency. It was hypothesized that this unstable behavior was due to a lack of mixing quality and issues with the ignition mechanism (a spark plug) which caused protrusions in the detonation chamber that the wave would attach to [1].

Following Dechert's research, Fiorino made modifications to the original Micro-RDE configuration to improve the stability of the detonation waves observed. To do so, Fiorino altered the injection scheme and ignition mechanism, both believed to be contributing factors to the instability seen in the small-scale engine. The traditional Jets in Crossflow (JIC) injection scheme was replaced with a Partially-Premixed JIC where the point of crossflow was moved from inside the detonation chamber to inside the oxidizer plenum to allow the reactants more time to mix before being consumed by the passing detonation wave [2]. Additionally, the previous spark plug configuration was replaced with a pre-detonator which used a deflagration-to-detonation transition (DDT) to ignite the reactants without causing a protrusion in the chamber that the

detonation wave could attach itself to. These major design changes accompanied by a few minor changes (see [2]) resulted in the increased stability of detonations in the Micro-RDE, realized by multiple detonation frequencies only falling 16 % below the design frequency. The detonations accompanied by these higher detonation frequencies also exhibited stable single wave mode behavior showing further improved signs of stability. However, the objective of reaching a stable detonation at the design frequency was still not achieved.

Further analysis in Fiorino's research revealed issues with the mass flow control system which could not adequately compensate for the backpressure produced by detonation events. Because the flow system used, Alicat SLPM controllers, were unable to compensate for the downstream pressure disturbances, the measured mass flow dropped during detonation conditions causing for a significant difference between the requested and observed mass flow rates for both the fuel and oxidizer. Thus, a new mass flow control system was needed to produce stable flow that could be reliably tested at desired mass flow rates and equivalence ratios.

1.2 Research Objectives

The goal of research in the Micro-RDE remains to reliably produce detonations at low mass flow rates and high frequencies in a small-scale detonation engine. Because it was seen in Fiorino's research that changes to an injection scheme can help increase the frequency and stabilize the wave mode of the detonation, new injection mechanisms were added to the Micro-RDE configuration to examine their effects on detonation stability. To ensure that during this research mass flows were steady and could be reliably tested, a new mass flow control system was implemented. Optical outerbodies were implemented to gather optical data that help characterize the stability of the detonations produced by the different injection schemes. With these changes, the

operability and stability of the RDE could be reliably tested.

Thus, the first objective of the current research was to implement sonic nozzles as a new mass flow control system to reliably meter flow both before and during detonations regardless of downstream pressure disturbances in the chamber. Before testing in the RDE, it had to be verified that the observed mass flows closely matched the requested mass flows to ensure accuracy of the testing map.

The second objective was to compare the performance of various injection schemes and their influence on detonation stability in the Micro-RDE. Operability was desired to be as wide as possible among the tested mass flows and equivalence ratios, and detonations were desired to be as close as possible to the design frequency 20 kHz to characterize stability. Examining these injection schemes was also hoped to provide further insight as to what conditions help produce more stable detonations, and how to manipulate the injection schemes to achieve those conditions.

The final objective was to gain optical access into the detonation chamber to further characterize the performance of the various injection schemes and their influence on cell size, fill height and other detonation parameters. Understanding these parameters could allow for further optimization of the Micro-RDE as they heavily influence the design of rotating detonation engines.

1.3 Research Approach

Chapter II will cover the literature necessary in understanding and implementing the research in this project. These include detonation thermodynamics, detonation wave structure, RDE injector designs, optical access in RDEs, and the previous research on the Micro-RDE. These topics were used during the design and implementation of the various injection schemes and the optically accessible detonation chamber.

Next, Chapter III will cover the methodology of the research. It will begin with an overview of the facility used for testing, the Detonation Engine Research Facility (DERF), and the portions of it used to accomplish this research. Then, the previous work on the Micro-RDE will be covered to establish the state of the RDE when research began and lay the foundation of the purpose of the objectives. Following the previous work, the changes made to the mass flow control methods will be presented to show an improved testability in the current configuration. The RDE design changes will be covered next. The focus of these changes were improving injection, reducing erosion, and gaining optical access into the Micro-RDE. These changes include a new centerbody design, additional injection scheme designs along with those previously tested, and the incorporation of an optical outerbody. The instrumentation of pressure and temperature readings as well as the high-speed camera equipment and setup used to monitor desired testing parameters will be outlined last.

In Chapter IV, the results obtained from the research conducted are presented. The RDE's operating space was tested by sweeping through mass flows from 10 g/s to 50 g/s and equivalence ratios from 0.5 to 1.5. These mass flow rates were swept for each injection scheme beginning at the highest mass flow rate and decreasing until detonations were no longer experienced and the lower limits of the operating maps were characterized. Successful detonations were experienced at flow rates as low as 12 g/s, the lowest seen in this Micro-RDE configuration. Detonation frequencies produced by the various injection schemes ranged from 11 kHz to 18 kHz.

Additionally, plenum pressures of the reactants were found to stabilize with increasing run times and settle to within 5 % of their final value within 1.2 seconds for the fuel and 0.5 seconds for the oxidizer. This was found from a single test that was intentionally ran for 6 seconds, producing the longest recorded detonation wave produced in the Micro-RDE. Optical access was gained into the chamber, however

limitations of the high-speed cameras utilized prevented visualization of specific parameters of the detonation wave's structure along with its cell size and fill height.

Finally, Chapter V reviews the methodology and results, as well as introduces potential avenues for future work. Ideas for future work include changing the oxidizer from nitrous oxide to oxygen to be able to detonate at lower mass flow rates. This move to oxygen would warrant a change in the metal composition of the RDE, potentially from Inconel to a metal like Monel that would be less susceptible to oxidation. Concerning the injection schemes, further optimization can be accomplished to expand their operating map and stability. This could include switching the fuel and oxidizer injectors to observe how the operability would change if the flows were reversed. Additionally, larger injection hole areas for the Simplex are needed to ensure a choking state is achieved across the nozzles and the mass flows tested are reliable. Lastly, changes to the optical configuration must be made to gain sufficient visualization into the chamber to be able to characterize the detonation wave. This can be achieved by replacing the side view Phantom camera with a different high speed camera that allows for a higher frame rate and lower exposure time to properly visualize the detonation wave. Concerning the optical outerbody, further changes must be made to the optical configuration to allow for the consistent survivability of the outerbody while still maintaining its clarity to allow for optical access.

II. Literature Review

Previous research in the operation of a small-scale Rotating Detonation Engine has made great strides towards obtaining a stable detonation [1][2]. Current research aims to pursue increased stability in a detonation while gaining optical access into the detonation chamber. Visualization into the chamber provides a closer view at the detonation wave allowing for further understanding of detonation propagation and future optimization of an RDE. Research will also consist of the comparison of the performance of various injection schemes and the characterization of their operating regimes. Improving the reactant mixing is vital to producing and sustaining a stable detonation, especially dealing with an RDE of this scale. Improved wave stability may detonate closer to 20 kHz, the design frequency of the RDE.

Before research can be conducted, certain background knowledge must be understood. This includes detonation concepts, discussed in Section 2.1, rotating detonation engine concepts, discussed in Section 2.2, and detonation wave propagation, discussed in Section 2.3. These topics allow for a deeper understanding of topics such as injection schemes discussed in Section 2.4, and the review of the Micro RDE discussed in Section 2.5. Optical access, discussed in Section 2.6, is the culmination of the topics as it is the purpose of this research. The following is an overview of the topics. Each section highlights the concepts that inspired the design decisions reviewed in Chapter III.

2.1 Detonation Concepts

Deflagration and detonation are two modes of combustion. Deflagration is characterized as a flame front that travels at subsonic speeds [3]. This form of combustion is seen in most conventional jet and rocket engines today. Deflagration theoretically

retains near constant pressure throughout the reaction and is therefore applied in many familiar thermodynamic cycles such as the Brayton cycle [7]. The alternate stable mode of combustion, detonation, is characterized by a flame front travelling at super sonic speeds. Because of the high velocity of the propagating flame, this reaction is preceded by a strong shock wave which causes a vast increase in pressure [3]. This increase in pressure creates more ideal conditions for combustion reactions and results in a greater potential for high thermodynamic efficiency and rapid energy conversion compared to traditional deflagrative processes [8]. This potential for more extractable work has created an increasing attraction for realizing the theoretical promises of detonation reactions.

There have been many attempts to correctly model a detonation since the phenomenon was first discovered in the late 1800s[4]. Donald Chapman and Ehrile Jouget built upon the work of Raleigh, Rankine, and Hugoniot and developed a quantitative theory that could predict the characteristics of a detonation. Aptly named the Chapman-Jouget theory, it describes relationships between Rayleigh lines and Rankine-Hugoniot curves. Rayleigh lines are formed by possible solutions to the mass and momentum equations between two states while Rankine-Hugoniot curves represent possible solutions to the energy equations between the same states. The Chapman-Jouget theory also accounts for the energy release due to the detonation combustion reaction [4]. In their studies, Chapman and Jouget found a minimum entropy and velocity solution to the previously mentioned equations which directly relate to a point of tangency between the Rayleigh line and the Rankine Hugoniot curve [3]. Figure 2 shows these points of tangency, also known as Chapman-Jouget (CJ) Points, denoted by the black dots along the curve.

Regions above and below the upper CJ point correspond to strong detonations and weak detonations, respectively. The strength of the detonation was dependent

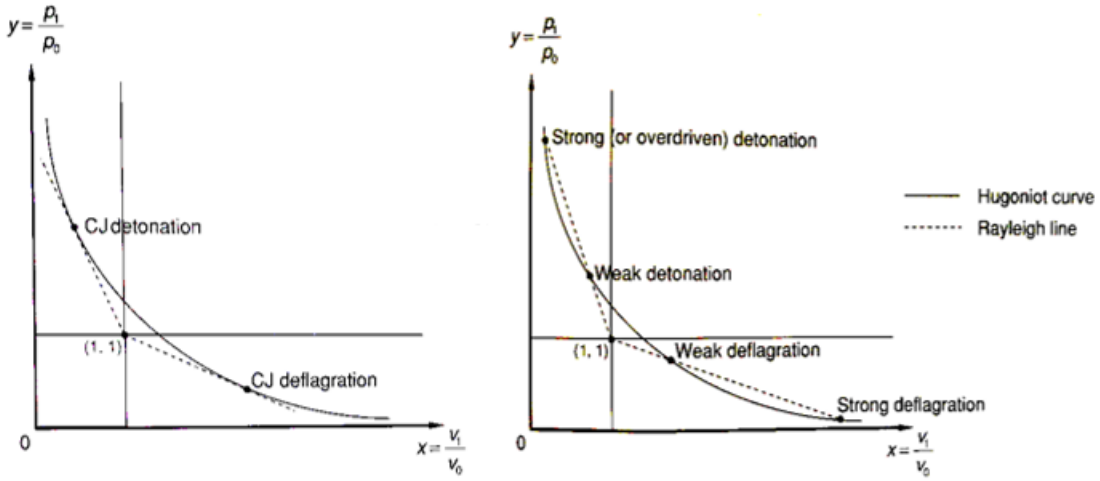

[4]

Figure 2. P-v Diagram of the Rayleigh Line and the Rankine-Hugoniot Curve, a) CJ Points, b) Detonation vs. Deflagration Strength

upon the flow downstream of the leading shock [4]. The velocity of the flow behind the detonation front was subsonic for a strong detonation and supersonic for a weak detonation [4]. At the CJ point previously discussed, the flow reached a sonic condition behind the wave front. The speed of the detonation that corresponds to this sonic condition following the wave front is known as the Chapman-Jouget (CJ) wave velocity. This solution also relates to the minimum entropy state as well and is dynamically stable when compared to other detonation waves [4]. It is important to note the model created from Chapman and Jouget's analysis is a limited 1-D model, however it is a reasonable approximation for actual detonations.

Following the CJ theory, three researchers: Zeldovich, von Neumann, and Doring independently attempted to build off Chapman and Jouget's research by proposing a structure of a detonation at this sonic speed solution. Their solution, the ZND model, provided a one-dimensional model of the detonation structure involving three subcomponents: a compression wave, a reaction zone, and an expansion wave [3]. Figure 3 shows the properties of said model and its components. The compression

wave, annotated in Figure 3 as State 1, is a leading shock wave that creates a sharp rise in pressure, temperature, and density. Following the leading shock is the reaction zone, from States 1 to 2' in Figure 3, where the chemical energy from the combustion reaction is released. The expansion wave trails the reaction zone and results in an increase in temperature from the combustion heat release but a decrease in pressure and density. This region where combusted gases expand occurs between State 2' and State 2 in Figure 3 [3]. The expansion wave drives the compression wave forward and the compression wave provides the energy to continue the reaction, thus allowing for a freely propagating detonation [4].

The ZND model also revealed some limitations with the assumptions of the CJ theory. It concluded that the wave speed solution was not necessarily at the CJ point, but instead was defined by iterative analysis that accounted for the reaction zone. This showed that a solution below the CJ point on the Hugoniot curve, a weak detonation, could not exist. However, although the solutions between the two models typically differ, the difference in their wave speed solutions is on the order of only a few percent [3]. Therefore, the CJ theory provides a fast and accurate estimation while avoiding the more extensive analysis involved with determining the wave speed from the ZND model.

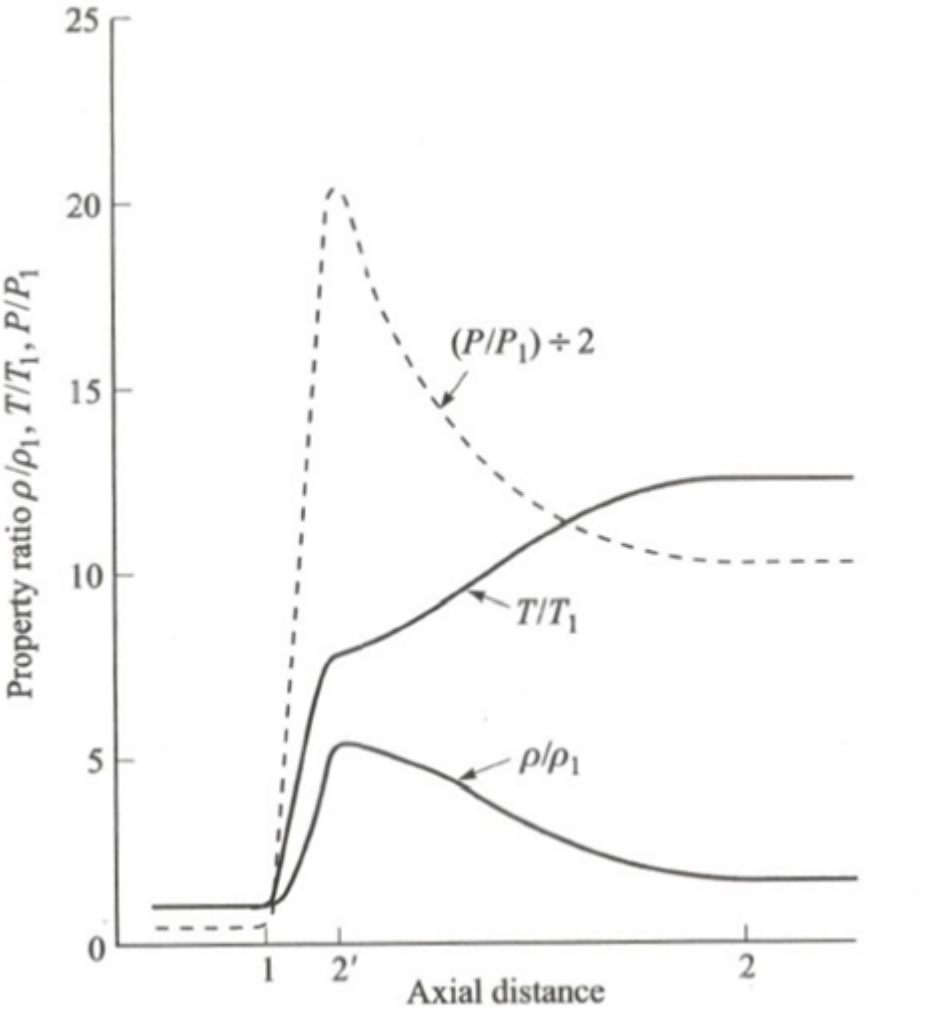

[3]

Figure 3. Representation of ZND Detonation Structure

2.2 Rotating Detonation Engine Concepts

Rotating detonation engines have received increasing attention due to the extreme pressure increases that accompany detonations [9]. These dramatic pressure increases promise a higher potential to extract more work than typical deflagration processes [9]. This can be seen in Figure 4, where combustive cycles Brayton, Humphrey, and Fickett-Jacobs are compared. The Brayton cycle represents typical deflagrative combustion and is a constant pressure reaction while the Humphrey cycle represents

detonative combustion as a constant volume process. The Fickett-Jacobs (FJ) model proposed by Wintenberger and Shepherd is the practical application of CJ detonation theory and is used to compute an upper bound to the amount of work that can be extracted from a detonation [9].

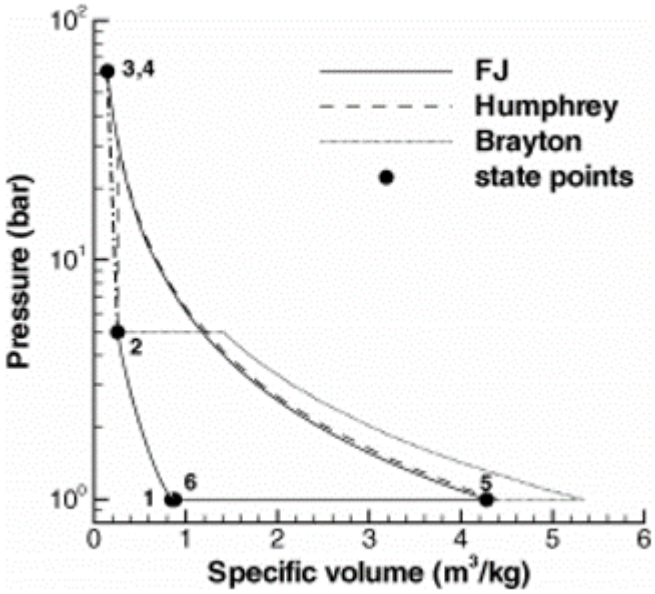

[9]

Figure 4. P-v Diagram for Cycle Comparison

In the Brayton cycle, usually used in turbine and ramjet, gas is compressed and pressure is increased as seen from Points 1 to 2 in Figure 4. The combustion reaction then occurs at a constant pressure resulting in an increase in volume, denoted by the horizontal line from Point 2. The work to be extracted from the expansion of the Brayton cycle can be seen in the right-hand portion of the curve. In the Humphrey and FJ cycles, used to model a detonation, gas is compressed by a shockwave and begins a detonation that continues to increase the pressure as denoted from Points 2 through 4. From Points 4 through 5, work is extracted from the system. The FJ cycle, which also accounts for Rayleigh heat addition, models a propagating detonation closer than the Humphrey cycle [10]. The amount of work that can be extracted from each cycle

is represented by the area under the curve for each respective cycle, which as seen in Figure 4 increases from the Brayton Cycle to the Humphrey and FJ cycle. [9].

The efforts to achieve these theoretical benefits were first realized in Pulsed Detonation Engines (PDE). These engines relied on repeated deflagration to detonation transitions (DDT), which require multiple initiations per second [11]. An alternative, the Rotating Detonation Engine, (RDE) was designed out of the desire to address the unsteadiness of a detonation wave and to propagate a continuous detonation wave, one that only requires a single initiation [12].

RDEs have moved to the forefront of detonative propulsion because of their simplistic design. An RDE has three main parts as pictured in Figure 5: a center body, an outer body, and the feed and injection system for the reactants. The detonation channel is formed by the gap between the center body and the outer body and is where the detonation wave travels around the annulus. Reactants are injected at the base of the detonation channel to feed the detonation. There exist many ways to inject the fuel/oxidizer via different injection schemes as discussed in Section 2.4. To propagate a continuous detonation wave around an annulus, RDEs require that new reactants be replenished after each passing wave and that the used products be exhausted from the channel [6]. Providing new reactants to the detonation wave while expelling the combustion products allows the detonation wave to become self-sustaining for as long as the new reactants are supplied. It is also imperative to understand that the timing window of an RDE is crucial, and too long of a time between the injection of reactants and their ignition can result in an unstable detonation wave. For example, experiments conducted by Braun et al. revealed a timing window for a successful initial ignition in their RDE was less than 20 ms [13]. This fell in the time frame before the detonation was produced. Once a detonation does begin, it reaches supersonic speeds and the time for sufficient reactants to be injected before each passing wave

decreases by orders of magnitude.

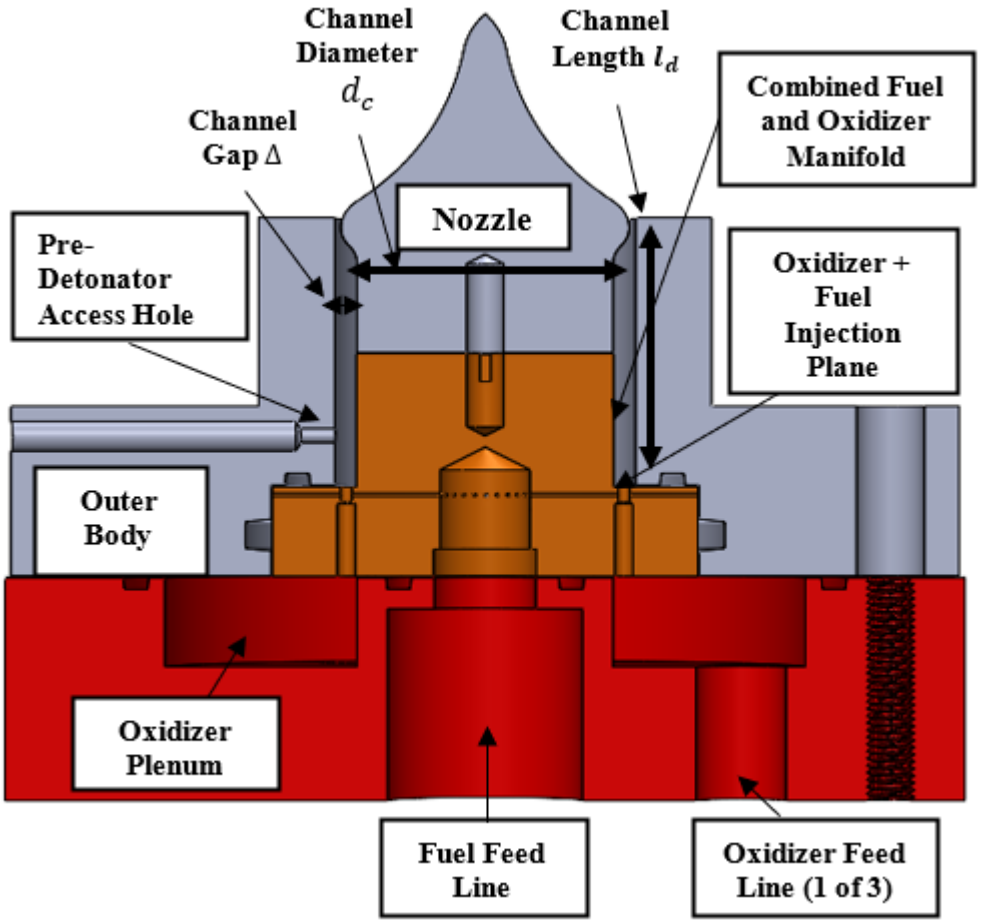

[14]

Figure 5. Dimensions and Components of an RDE

Although often modeled as such, detonations are fundamentally not one-dimensional. A detonation wave consists of three parts as seen in the window of Figure 6: an incident wave, a transverse wave, and a Mach stem. The incident wave travels with the detonation wave and is formed by the original shock wave. The transverse wave travels perpendicular to the incident wave, and the Mach stem is formed by the collision of transverse waves [3]. The point at which they meet is called the triple point, and the unsteady nature of a detonation causes the triple point to propagate downstream and form the triple point trajectory. The propagation of a triple point trajectory can

be seen in Figure 6. By tracing the triple point trajectory, it results in a "fish scale" pattern that create individual cells. The number of cells and cell size, λ , can influence the strength and stability of a detonation, and can also influence the optimal design parameters for a given RDE. These are specifically important as the size of the detonation channel is decreased.

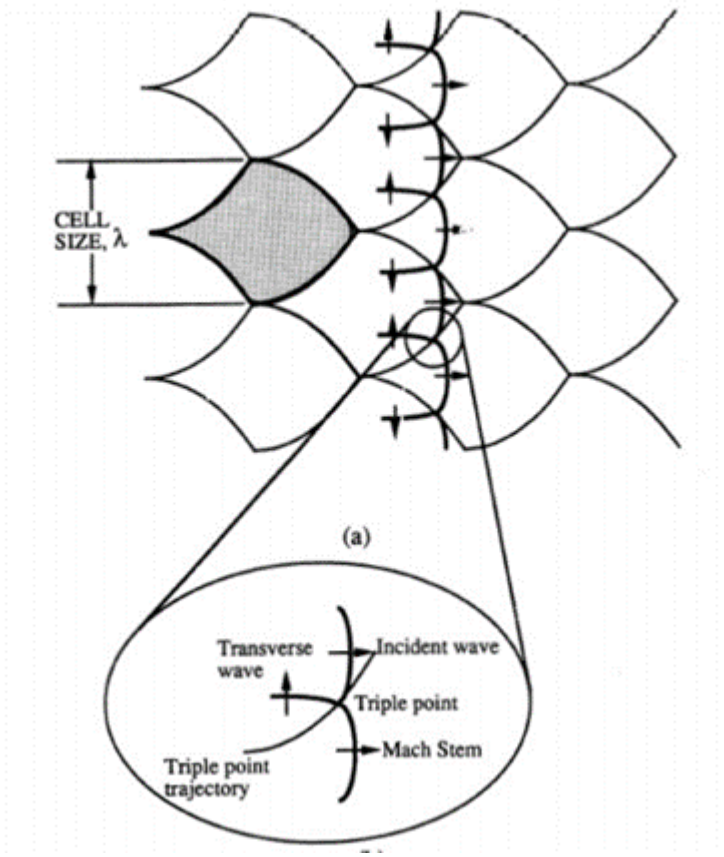

[15]

Figure 6. Detonation Structure and "Fish Scale Pattern"

Bykovskii et al.'s research of the limits of RDE geometries found that the key components of an RDE (detonation channel length, reactant fill height, and detonation channel gap) were heavily dependent on the cell size for a given detonation [16]. The reactant fill height, h, is the distance the reactants travel before being consumed by each passing detonation wave. Bykovskii et al. postulated that the fill height required to sustain detonation is a direct function of cell size as seen in Equation 1.

Detonation channel length, l_c, is the length of the annulus formed by the inner and outer walls of the RDE. As seen in Equation 2, l_c should be at least twice the length of the fill height to be sufficiently long to contain the detonation [16]. The other critical geometry parameter examined by Bykovskii et al. was detonation channel gap, Δ. The detonation channel gap is the distance between the inner and outer walls of the RDE. As seen in Equation 3, it should be at least one-fifth of the fill height. As with detonation channel length, it is dependent on cell size. These equations from Bykovskii et al. were used to design the original micro RDE, which will be discussed in Section 2.5.

$$h = (12 \pm 5)\lambda \tag{1}$$

$$l_c = 2h \tag{2}$$

$$\Delta = 0.2h \tag{3}$$

2.3 Detonation Wave Propagation

To be able to properly analyze the visualization seen on the inside of an RDE, it is important to understand how the detonation wave propagates in the channel. Detonation wave mode transitions and wave interactions significantly affect the performance and stability of RDEs [17]. Figure 7 shows an unwrapped sketch of a detonation wave in an RDE. When examining the figure note that the flow is moving from bottom to top, and the detonation wave is propagating right to left. Also keep in mind that although only a single wave is depicted, multiple detonation waves are possible [18].

As it travels around the circumference of the RDE, the detonation wave propagates at a respective wave speed and forms an associated refill time for the reactants. This reactant fill region forms where reactants are available for consumption upstream of

every passing wave [17]. The minimum distance that reactants travel before they are consumed is known as the fill height [18]. Fill height is an important feature in RDE design because if the fill height is not reached before the detonation wave makes a full rotation (either the wave propagates too fast, or the reactants fill too slowly) then there will not be enough reactants to sustain the detonation and the wave will weaken. The detonation wave also has a height, h_D, which is measured from the injector orifices and can only be as tall as the height of the reactant fill region in front of it.

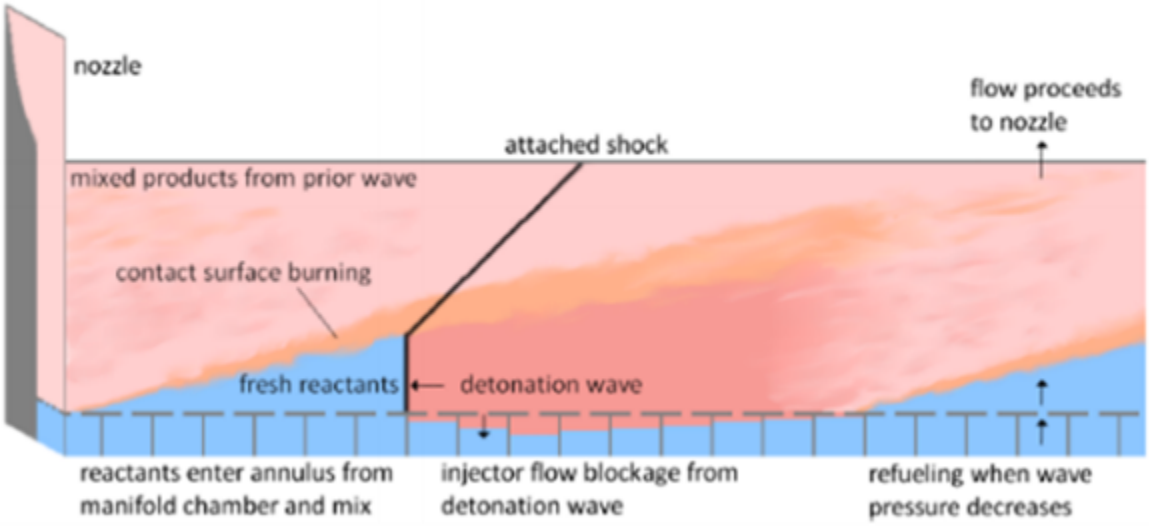

[18]

Figure 7. Sketch of Rotating Detonation Wave Structure

Downstream of the detonation wave is an attached oblique shock as seen in Figure 7. This attached shock is formed between the products behind the detonation, which expand due to side relief, and the products combusted by the previous rotation of the detonation wave [18]. The angle of the slip line formed between the products corresponds to the angle of the attached shock. The shock grows increasingly stronger the closer it gets to the detonation wave and is at its weakest at the furthest point from the wave [18]. The point where the detonation wave and the oblique shock

are attached is the triple point [18]. The cellular triple points can be seen as the internal structure of the detonation, while the recently discussed oblique wave and its characteristics can be viewed as the external structure.

Shepard et al. presented experimental and numerical evidence for the behavior of detonations and concluded that all propagating detonations are fundamentally unstable, but they can exhibit a wide variety of behavior [19]. The weak unstable detonations are nearly laminar with unsteady periodic flow while the strong detonations are turbulent with chaotically unstable flow [19]. According to Shepard, there are three primary factors that contribute to detonation instability: 1) there exists an amplification of acoustic waves trapped in the acoustic resonator which constitutes the region between the lead shock and the end of the reaction zone 2) the chemical reaction rates are sensitive to the thermodynamic state (changes in temperature and pressure) and 3) the hydrodynamic instability of the propagating reaction fronts [19]. This instability causes multiple wave fronts to be formed, broken down, or destroyed and it is these wave fronts that compose the full propagation of the detonation known as the detonation cell. The instability of the wave fronts translates to the non-uniformity and unsteadiness of the cells which result in an unstable detonation wave structure [19].

This instability can be directly seen in the soot foil patterns in Figure 8. A soot foil is simply a surface covered with soot and placed on the side of the channel, and it is commonly used to examine detonation instability [19]. Soot tracks the motion of triple points along the detonation front and the patterns found on the soot foils mark periodic cells and their transverse sizescale, λ, also known as the detonation cell size. Determining cell size is extremely important in the development of an RDE as it is strongly correlated to the ideal length of the reaction zone and thus the critical dimensions for propagation in the RDE [19]. This was seen in the previous section,

Section 2.2, when examining Bykovksii's guidelines for RDE dimensions based on cell size. As seen in Figure 8, cell size is not a well-defined quantity and accurate measurements are limited due to the stochastic nature of detonations [19]. The top portion of Figure 8 coincides with a $2H_2 + O_2 + 12Ar$ reaction and pictures a less periodic but still regular cell pattern with λ = 35 - 45 mm. The bottom portion of 8 coincides with a $H_2 + N_2O + 1.33N_2$ reaction and pictures an irregular cell pattern with λ = 5 - 32 mm [19]. Both reactions are pictured at the same scale at 150 mm high with a 20 kPa initial pressure. In general, ranges of precision between 50 to 100 % are not uncommon when measuring cell size [19]. Although challenging to measure, detonation cell size is critical to sizing an RDE as channel dimensions and λ are key factors that contribute to the "stability" of a detonation.

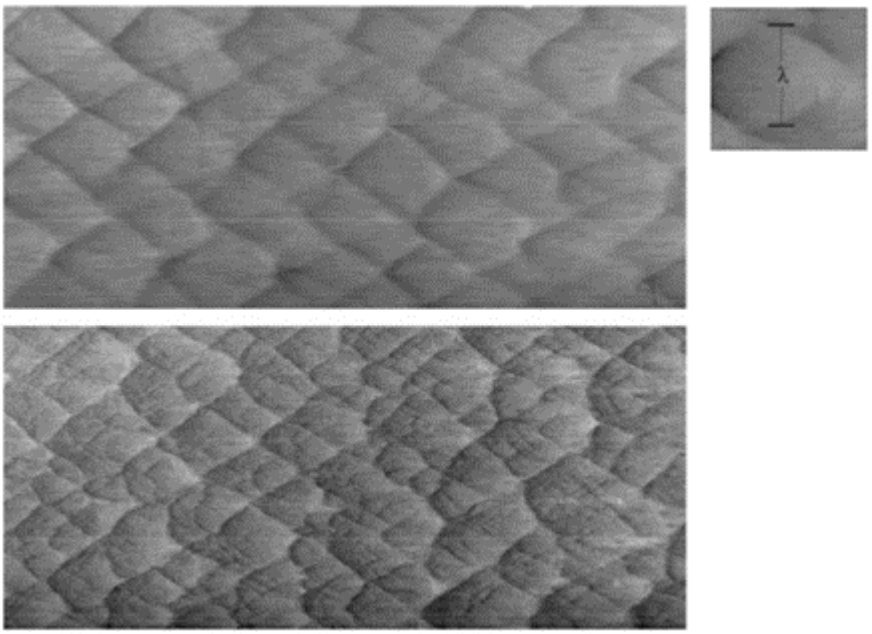

[19]

Figure 8. Soot Foil Records for $2H_2 + O_2 + 12Ar$ (top) and $H_2 + N_2O + 1.33N_2$ (bottom) Reactions at Same Scale (150 mm high and 20 kPa initial pressure)

While all detonations are fundamentally unstable, their differences in stability has still been classified as different detonations produce different wave behaviors and wave

speeds. Kudo et al. classified a stable detonation as one having a wave speed at or above 80 % of its CJ speed [20]. Wave speeds between 60% and 80% of the CJ speed were considered critically stable and wave speeds below 60% of the CJ speed were considered unstable. For the purposes of this paper, when discussing the stability of a detonation Kudo et al.'s classifications will be utilized.

2.4 Injection Schemes

When operating an RDE, the quality of the mixing of the reactants is critical in creating and maintaining a detonation wave [13]. Cell size and thus detonability are optimized at local stoichiometric conditions, and insufficient mixing can result in an unstable or loss of detonation wave. Mixing is heavily influenced by the injection geometry utilized in the RDE, which also plays a role in the pressure recovery in the combustion chamber. In an RDE, there exists potential for flow to become unchoked at the injectors and allow feedback into the supply lines. This backflow can negatively affect the performance of the RDE by reducing fill height and mixing time, so it is important to utilize injection schemes that recover pressure before the detonation wave is lost [21]. Ensuring there is sufficient fuel/oxidizer injection into the chamber and that said fuel/oxidizer is sufficiently mixed is an important design hurdle in the development of RDEs, and this is heavily influenced by its' injection scheme [13].

Experiments by Duvall et al. examined the impacts of three different injection schemes on RDE operation [21]. The injection schemes tested were the Axial Injector (referred to as the Pintle), Jets in Crossflow (JIC), and Semi-Impinging Jet (SIJ). The cross sections of these injection geometries can be seen in Figure 9, where the red and black arrows denote the fuel and oxidizer flow, respectively. The goals of this experiment were to characterize and contrast the operating regimes of each injector and to observe their effects on the detonation wave mode produced [21]. To do this,

Duvall et al. defined five modes of combustion that detailed the behavior seen from each injector and examined the detonation mode produced by each injection scheme at various conditions. These five modes are outlined in Table 1 [21].

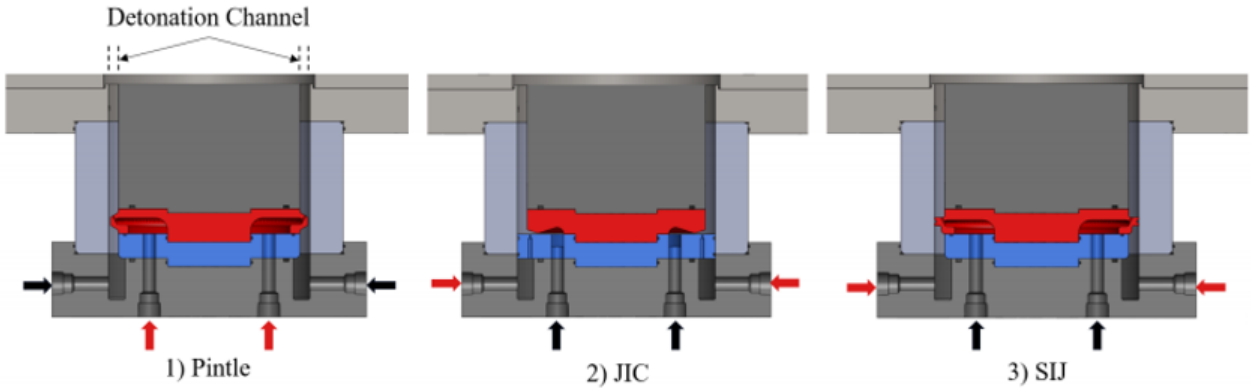

[21]

Figure 9. RDE Cross-Sections of Three Different Injection Schemes

Table 1. Five Modes of Combustion from Duvall et al.

[21]

Mode	Description
1	Stable detonation, single rotating wave
2	Stable detonation, two co-rotating waves
3	Steady deflagration, counter rotating wave structure
4	Unsteady deflagration, no coherent structure
5	Rapid transition between unsteady deflagration and detonation

The Pintle injection scheme consists of the oxidizer flowing axially over a contoured surface and into the detonation chamber. This contoured surface creates an annular slot with the outer wall of the detonation channel. Fuel is injected into the detonation channel from the upper face of the contoured surface from jets situated around its circumference. "The jets are angled and oriented toward the outer wall" [21]. In the JIC injection scheme, oxidizer flows from an inner plenum around a corner from where it expands radially. This flow passes over fuel injectors that are oriented axially, and the fuel flow crashes into the oxidizer flow [21]. Lastly, the SIJ injection scheme utilizes staggered jets for fuel and oxidizer situated around the circumference of the detonation channel. For this particular example, all jets are angled toward the center

of the channel with the fuel and oxidizer being injected from the outer and inner radius, respectively. Additionally, the fuel and oxidizer jets are offset such that only a fraction of their exit areas overlap [21].

Results from Duvall et al.'s experiment revealed the Pintle scheme operated in Modes 1, 4, or 5, the JIC scheme operated in Modes 1, 2, or 4, and the SIJ scheme operated in Modes 1, 3, or 4 [21]. The mode in which the geometry operated was heavily dependent on the mass flow and the momentum ratio, defined in Equation 4 as J, the momentum flux of the fuel divided by the momentum flux of the oxidizer. Both the Pintle and JIC injection schemes detonated frequently at momentum ratios near 0.5-0.6 [21]. The SIJ injection scheme never approached this range of J, usually operating in a range of 0.12-0.28 [21]. It was also found that for SIJ, to reach a stable detonation it was imperative that the choking conditions of the injectors be matched. JIC and the Pintle were not as heavily dependent on the similarities between their choking condition [21]. Finally, it was discovered that the Pintle injector retains its plenum pressure much better than its' counterparts and thus has the best performance for pressure recovery [21]. This phenomenon can be seen in Figure 10.

$$J = \frac{q_{fuel}}{q_{oxidizer}} \tag{4}$$

As expected, injection schemes are not limited to the previously discussed geometries. Amini studied the theoretical effects of pressure swirl nozzles which mix their reactants and propagate them forward using a swirling motion [22]. The goals of his research were to develop a theoretical model for pressure-swirl nozzle flow and examine the effects of the nozzle geometry on parameters that directly correlate to mixing: liquid film thickness, discharge coefficient, and spray angle. Discharge coefficient, C_D, and spray angle, α, can be calculated using Equations 5 and 7, respectively [22]. Discharge coefficient is a function of the total flow rate Q, the radius of the orifice

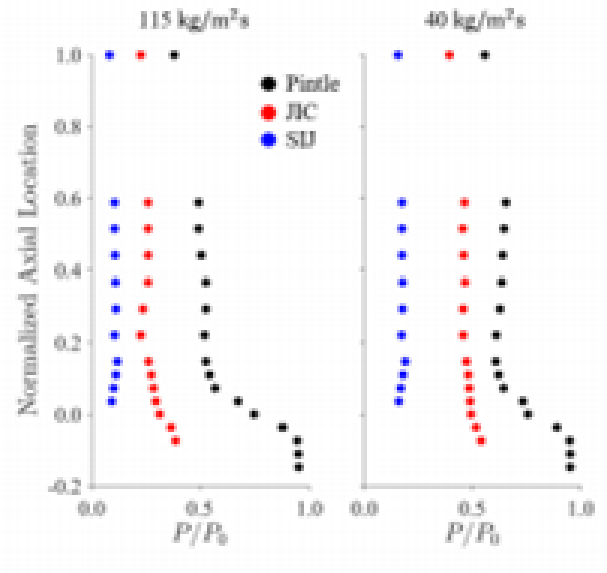

[21]

Figure 10. Non-Dimensional CTAP Plots Showing Pintle's Pressure Recovery

R_o, the density of the liquid ρ, and the pressure drop across the nozzle ΔP. Spray angle is dependent on the total velocity found from the discharge parameter, W, and the average tangential velocity v [22].

$$C_D = \frac{Q}{\pi R_o^2}\sqrt{\frac{\rho}{2\Delta P}} \tag{5}$$

$$W = \frac{Q}{C_d(\pi R_o^2)} \tag{6}$$

$$J = 2\arcsin\frac{v}{W} \tag{7}$$

The pressure swirl nozzle injection scheme investigated, a simplex, consists of four parts: tangential inlet ports, a swirl chamber, a spin chamber, and a discharge orifice [22]. In a simplex nozzle, reactants enter the nozzle through the tangential inlet ports creating a swirling motion in the swirl chamber. From there, centrifugal forces are magnified in the converging spin chamber and the reactants are then expelled through the discharge orifice resulting in a spray cone as shown in Figure 11. When examining

the dimensions of the pressure-swirl nozzles, experiments conducted by Griffin and Mauraszew concluded that parameters such as orifice length, inlet port length, and swirl chamber length have no direct effect on the performance of the injector[23]. They also concluded that swirl plays an important role in ensuring the stability of a rotating detonation wave[23].

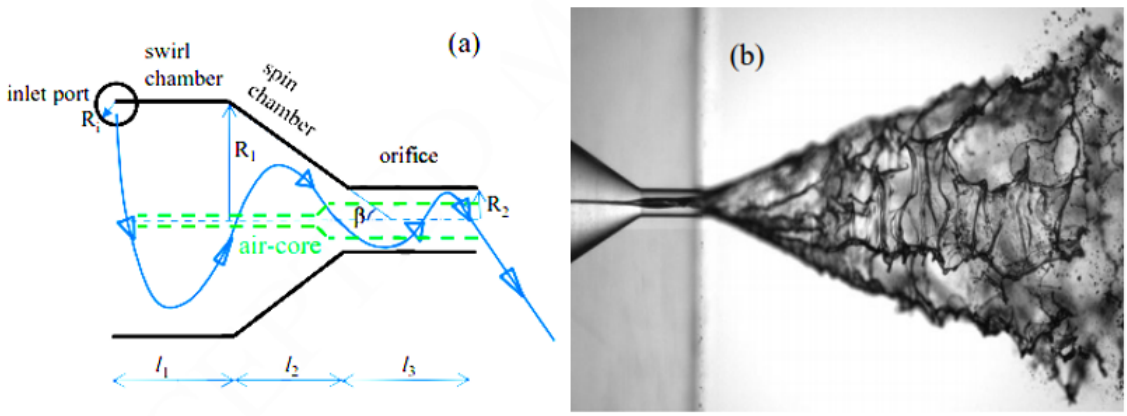

[22]

Figure 11. Key Features of a) Simplex Injection Scheme and b) Spray Cone

Figure 12 defines the operating range of the theoretical, experimental, and numerical approaches in terms of Reynolds number. The theoretical approaches for modeling the nozzle flow are outlined in Table 2. The experimental and numerical approaches were utilized to validate the theoretical for lower and higher mass flow rates, respectively, and provide more detailed results. The results from the different approaches revealed that overall the V2 model most accurately predicts the flow and the V1 model usually overpredicts air core size and angle while underpredicting the discharge coefficient. However, the V1 model tends to be the more accurate on the lower limit of Reynolds numbers while the upper limit asymptotically approaches the solution of the V0 model. Since Reynolds number is the ratio of inertial to viscous forces, it makes sense that the higher the Reynolds number the more aligned with the inviscid case the solutions will become. Results show that if all other dimensions

are constant, changes in length to diameter ratio of swirl chamber, spin chamber, and orifice do not affect the nozzle properties considerably. This can be seen in Figure 13.

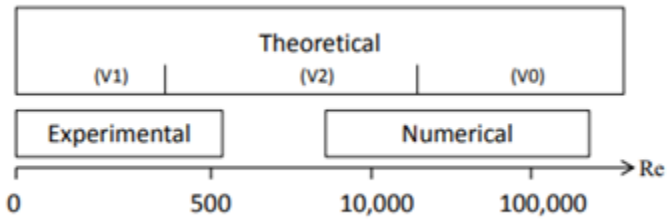

[22]

Figure 12. The Operating Range for the Various Approaches in Predicting Nozzle Flow

Table 2. Theoretical Approaches for Modeling Nozzle Flow

[22]

Approach	Description
V0	Inviscid Flow
V1	Viscous flow neglecting the axial velocity component in the potential core
V2	Viscous flow considering the axial flow in the potential core of the nozzle

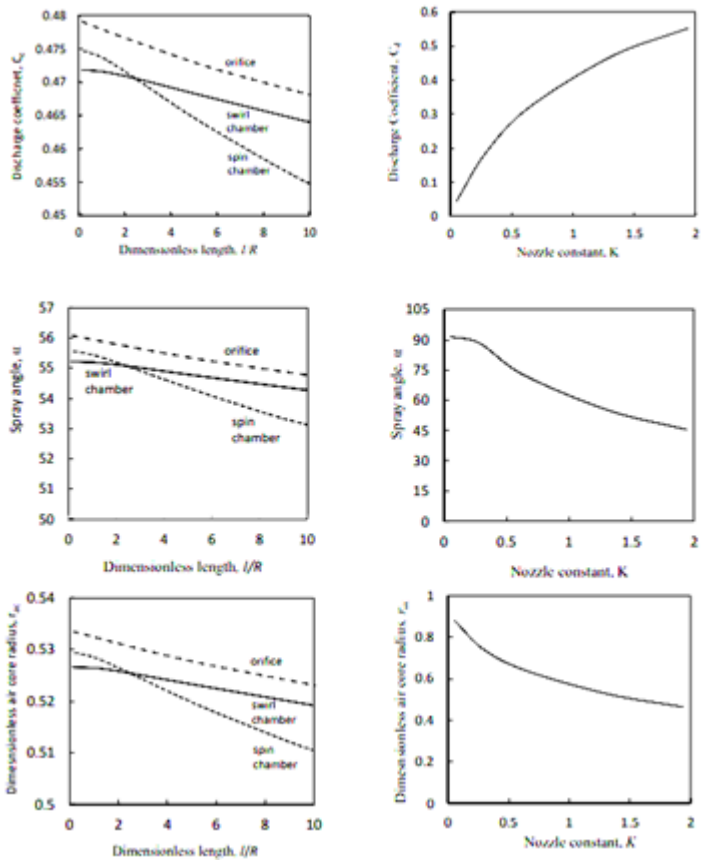

[22]

Figure 13. The Effect of Nozzle Geometry on Discharge Coefficient, Spray Angle, and Air Core Radius

2.5 Review of the Micro RDE

The Micro-RDE has undergone multiple changes since its initial construction by Dechert et al [1]. To grasp the newer iterations of the Micro-RDE discussed in Chapter III, it is important to understand the changes to the initial RDE that have already been made. Section 2.5.1 outlines the first iterations of the small-scale engine designed by Dechert et al. and the results that came from the their testing. Section 2.5.2 outlines the next iterations of the engine designed by Fiorino et al. and his results. The current design discussed in Chapter III is a continuation of their previous designs.

2.5.1 Initial Design (Dechert)

Dechert et al. designed the first iteration of the Micro-RDE to stretch the boundaries of small-scale rotating detonation engines using Bykovskii et al.'s principles for RDE sizing [1]. This RDE was designed with the goal of reaching a stable single propagating detonation wave with a 20 kHz frequency. To reach this goal in a small RDE, and thus a small cell size, nitrous oxide and ethylene were chosen as the reactants for their high reactivity [1]. The cell size for the chosen reactants is not within Kaneshige and Shepard's Detonation Database [24]. Thus, Dechert obtained the cell size from a soot foil of a nitrous and ethane detonation and directly correlated it to estimate the cell size of nitrous and ethylene, yielding a value between 0.5 and 1.75 mm [1]. Using this range of cell sizes, Dechert was able to calculate the sizing dimensions of the Micro-RDE using the guidelines derived by Bykovskii et al. outlined in Section 2.2 [16]. These dimensions can be seen in Table 3.

Table 3. Micro-RDE Sizing Parameters

	Approach	Description
[1]	Cell Size	0.5 - 1.75mm
	Fill Height	Estimated: 3.5 - 12 mm Experimentally Calculated: 3.2 - 8.1 mm
	Channel Gap	2 mm
	Channel Length	30 mm
	Channel Diameter	28 mm

Dechert ran tests on the Micro-RDE across mass flows between 0.025 – 0.075 kg/s and equivalence ratios between 0.5 – 1.5. Initially, reactant flow in the detonation channel reached a velocity nearly six times the turbulent flame speed for the reactants, making flameholding virtually impossible. An aerospike nozzle was situated at the end of the detonation channel to slow the reactant flow and increase the chamber pressure to create more detonable conditions. In addition, the ignition via spark plug was moved from its original location outside of the channel to inside in order to

decrease the distance between the spark and the freshly mixed reactants [1]. This led to successful detonations. The resultant operating maps can be seen in Figures 14 and 15. Tests in Figure 14 represent tests ran using an aerospike nozzle with a throat to chamber ratio $\epsilon = 0.14$ and Figure 15 correspond to those ran with a throat to chamber ratio $\epsilon = 0.4$ [1]. All test points were tested twice. A red point denotes no detonation, a solid green point denotes successful detonations for each point, and an empty green circle denotes only one successful detonation. These single detonations predominately occurred after the RDE was heated from a previous successful test but were unable to detonate after the RDE had cooled down.

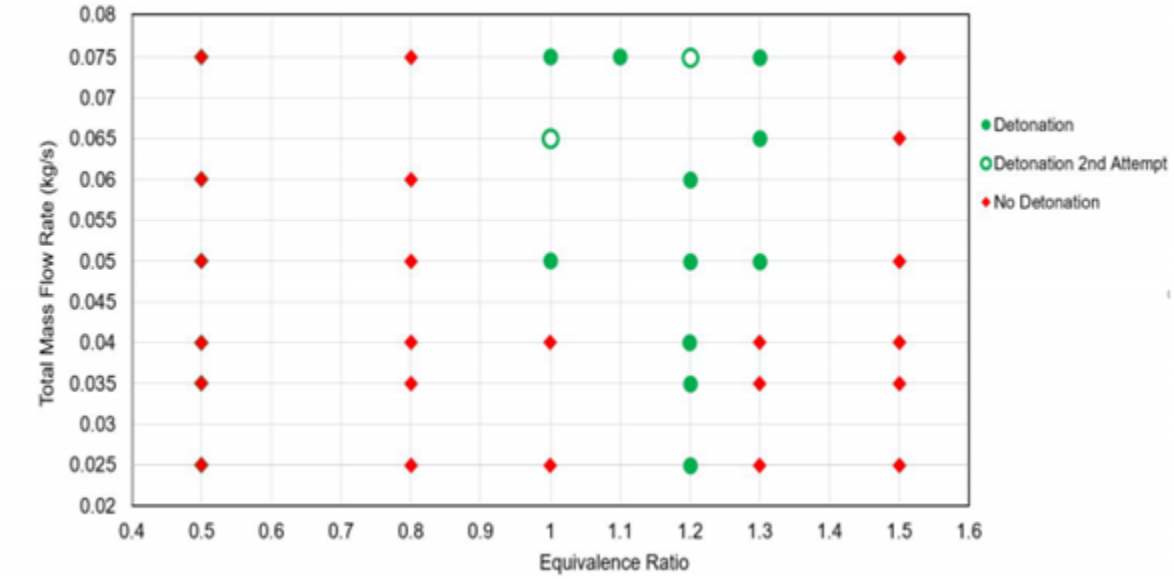

[1]

Figure 14. Operating Map for $\epsilon = 0.14$ from Dechert et al.

Both operating maps show better RDE performance for higher equivalence ratios instead of the expected optimum performance at stoichiometric values ($\phi = 1.0$) . Dechert hypothesized this occurred due to inconsistencies between the global and local equivalence ratios, the global being measured around 1.2 and the local (not measured) was likely around 1.0 . This indicated a lack of mixing of the fuel injected into the flow. Dechert utilized a JIC injection scheme, described in Section 2.4 [1].

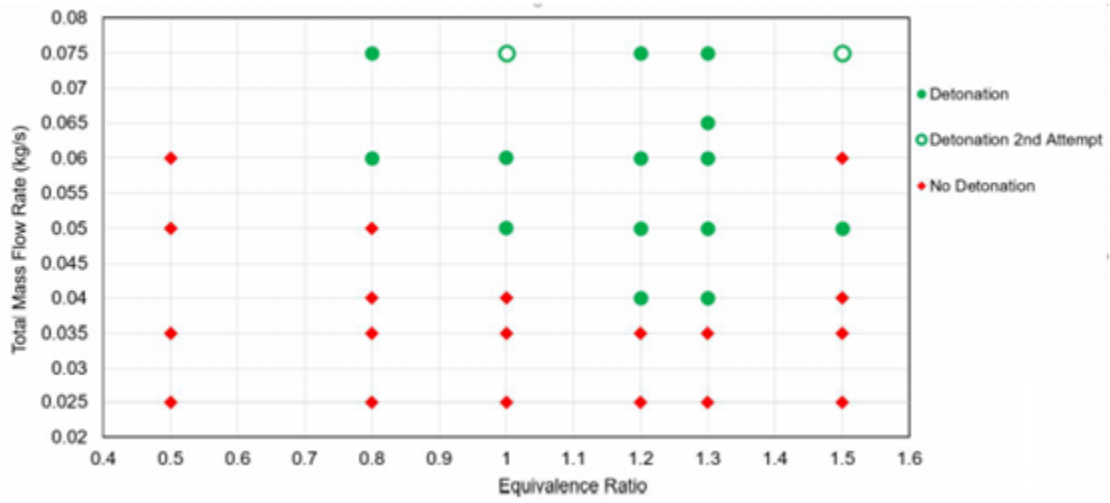

[1]

Figure 15. Operating Map for $\epsilon = 0.40$ from Dechert et al.

To allow for better local mixing, Fiorino modified the JIC injection geometry on the small-scale RDE [2]. These modifications are further discussed in Chapter III.

To ignite the reactants injected from his JIC geometry, Dechert et al. utilized a spark plug [1]. The spark plug was used as an ignition mechanism and provided energy for the injected reactants to start the detonation. While igniting the mixture without issues, this spark plug proved to be a hotspot for the detonation wave to interact with and was suspected of causing clapping, counter-rotation and other unstable behaviors of the wave. Clapping and counter-rotating are detonation wave propagation modes characterized by two waves rotating in the opposite direction or near the same frequency. When the frequencies are the same, the waves collide at the same two stationary collision points giving the appearance of clapping. When the frequencies are different, the two waves appear to be counter rotating where their point of collision can rotate as well. Images inside the chamber taken by a Phantom v711 high-speed camera show this phenomenon in Figure 16. Erosion experienced by the spark plug was believed to be caused by these hot spots in the detonation wave. Many spark plugs were destroyed after only one detonation, causing for constant re-

moval and replacement of the eroded spark plugs. Furthermore, the hole through which the spark plug was inserted became eroded after constant exposure to these hot spots [1].

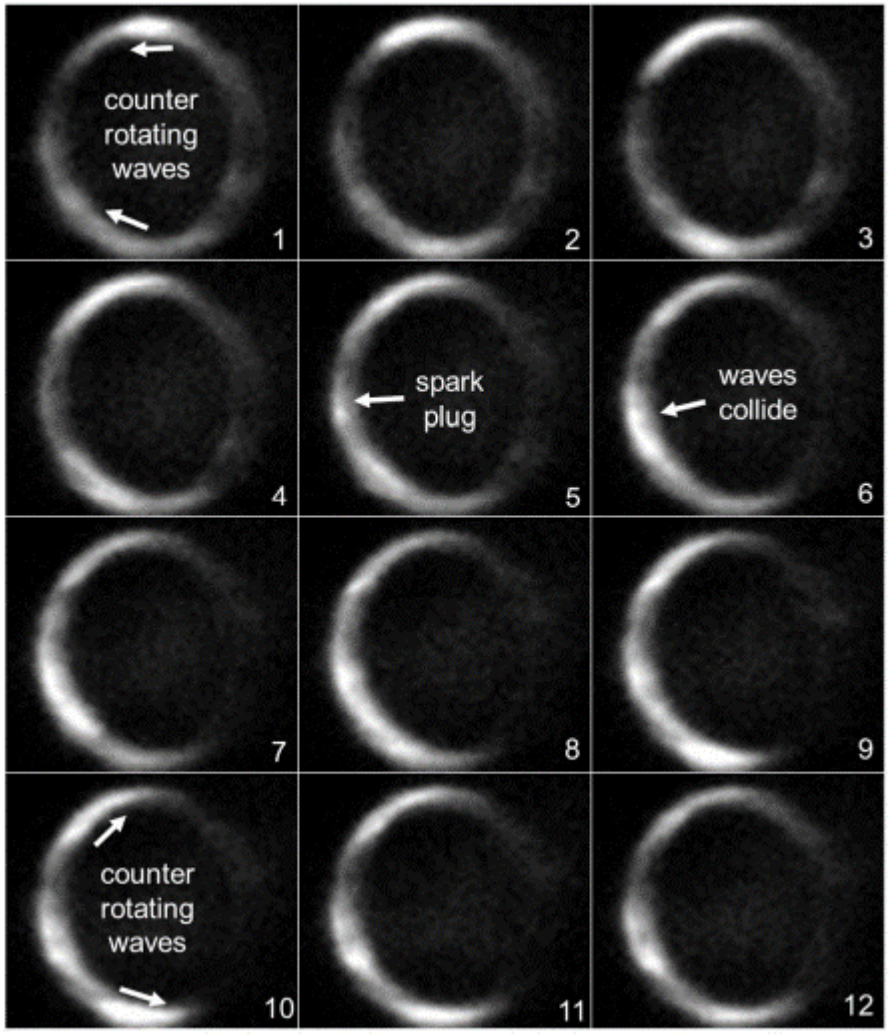

[1]

Figure 16. Detonation Wave Behavior Using Dechert's Rig

Through the video captured by the high-speed camera detonation wave speed and frequency were also examined. Wave speeds of the detonations captured ranged from 1020 to 1230 m/s, lower than the expected value (2080-2291 m/s) by 30-40% [1]. Because the detonations had wave speeds $\sim$ 60 % of their expected CJ speed, the detonations were determined to be unstable. The relatively low wave speeds resulted

in detonation frequencies produced between 11.4 and 14 kHz, well below the desired 20 kHz [1].

2.5.2 Follow-On Design (Fiorino)

To achieve the desired detonation wave speed and frequency, and to also reduce the erosion and improve the testability of the small-scale RDE, Fiorino made certain modifications. Fiorino et al. improved on Dechert's design with the same goal: producing a small scale RDE than can reliably detonate at lower mass flows and reach frequencies at or above 20 kHz [2]. To accomplish this, they implemented a new injection scheme and ignition method. Dechert's previous more traditional injection scheme proved to be ineffective when mixing the fuel and oxidizer before reaching the detonation channel [1]. To improve the mixing of the reactants, a vital part of creating and sustaining a stable detonation wave, Fiorino modified the JIC scheme from Dechert. The intersection of fuel and oxidizer that was originally inside the chamber was moved inside each individual oxidizer injector, giving further time and distance for the reactants to partially mix before reaching the detonation chamber and being consumed by the next passing wave [2]. The specifics of this design change are discussed in Section 3.2.2.

Additionally, the previous ignition mechanism utilized by Dechert, the spark plug, was also modified by Fiorino. The spark plug that proved to be the source of hotspots developing in the passing detonation waves which led to massive erosion and constant need for replacement was replaced by a pre-detonator device [2]. The pre-det offered heat as an ignition source for the detonation wave but required a smaller access hole into the chamber allowing for consistent survivability and less erosion. Iterations on the location of the pre-det were made to further improve the ignition mechanism's susceptibility to damage. To further reduce erosion, new outerbodies made of Inconel

625 were utilized in lieu of the previous 304 Stainless Steel outerbodies which had a lower tensile strength when exposed to higher temperatures [2]. These changes in the Micro-RDE are also further dicussed in Section 3.2.2.

To meter the flow of the reactants MCRQ High Pressure Mass/Gas Flow Controllers from Alicat Scientific were used. Fiorino noticed that for this specific RDE, these controllers were unable to adequately compensate for the back pressure brought by the detonation events. This meant that there were inconsistencies between the requested and the observed mass flow rates outputted by the controllers, making it difficult to reliably execute the intended test matrix. These issues are further discussed in Chapter 3.3.1. Still, using flow rate data gathered from the controllers, Fiorino was able to measure and estimate the true mass flow rates and equivalence ratios for each test on the Micro-RDE, even if they were not the point that was specifically requested [2]. Using the true data for the configuration with the predet (tests were also run on the spark plug), a measured propagating detonation was found from equivalence ratios 0.6 to 1.2 at mass flows between 45 – 60 g/s, as seen in Figure 17 [2].

To characterize the stability of the detonation, Fiorino developed a scoring system from 0-10 to define the stability of a detonation wave, 0 representing pure deflagration and 10 representing a single wave stable detonation. The scores and their corresponding wave modes can be seen in Table 4, with scores increasing as the wave mode becomes less unstable. Multiple detonations exhibited single wave detonation stability with frequencies up to 16.8 kHz. Higher frequencies up to 19.1 kHz were also observed, but these waves exhibited unstable behavior such as clapping or galloping. Figure 18 shows the corresponding wave speed for each wave mode observed in the 48 test cases ran. Despite the progress made in stability and frequency, when outlier cases were removed and the detonation frequencies were averaged their mean was

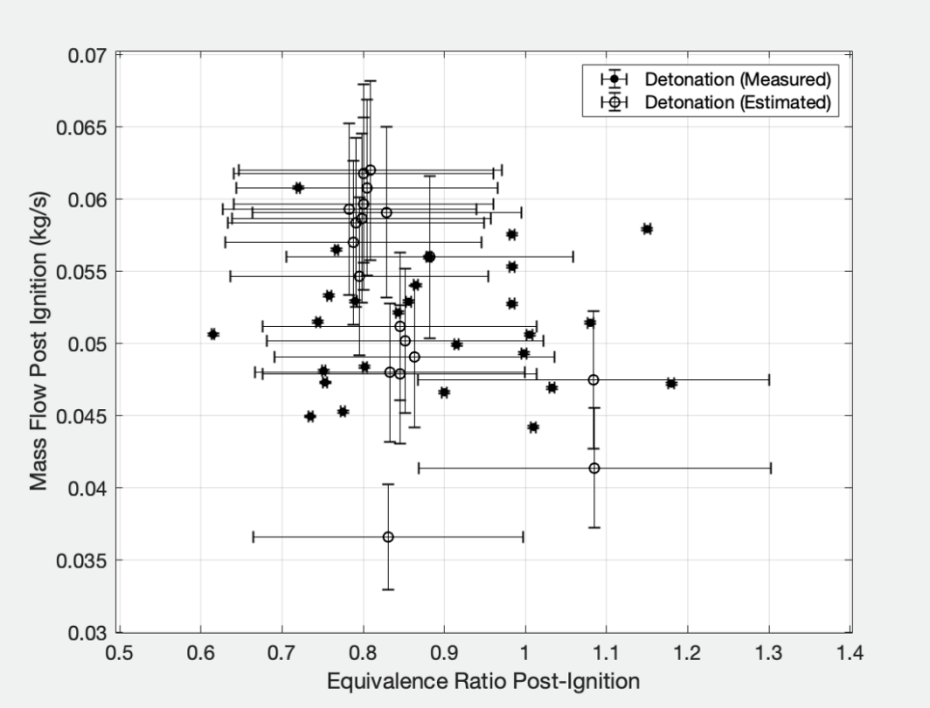

[2]

Figure 17. Fiorino's Operating Map Using Estimated and Measured Values

approximately 14 kHz, well shy of the design objective 20 kHz.

Table 4. Observed Wave Modes and Corresponding Score Based on Detonation Stability. Higher Values are Less Unstable, Score of 10 is Stable

[2]

Mode Description	Score
Stable single wave mode	10
Single wave mode with limited counter rotation and clapping. Potential for wave direction reversal.	9
Single wave mode with intermittent counter rotation and clapping. Potential for wave direction reversal.	8
Single-wave galloping mode (wave varies frequency within 5 rotations)	7
Alternating transition between single wave mode and counter rotating two wave mode. Potential for clapping.	6
Dominant clapping mode with intermittent single wave rotations	5
Pure clapping mode	4
Continuous transitions between, counter rotating/clapping/galloping behavior. No deflagration	3
1 wave mode that transitions to deflagration then transitions back to detonation in sequence (Repeated DDT events)	2
No dominant mode with intermittent direction reversal/clapping/counter rotating waves and transitions to deflagration	1
Pure deflagrative mode	0

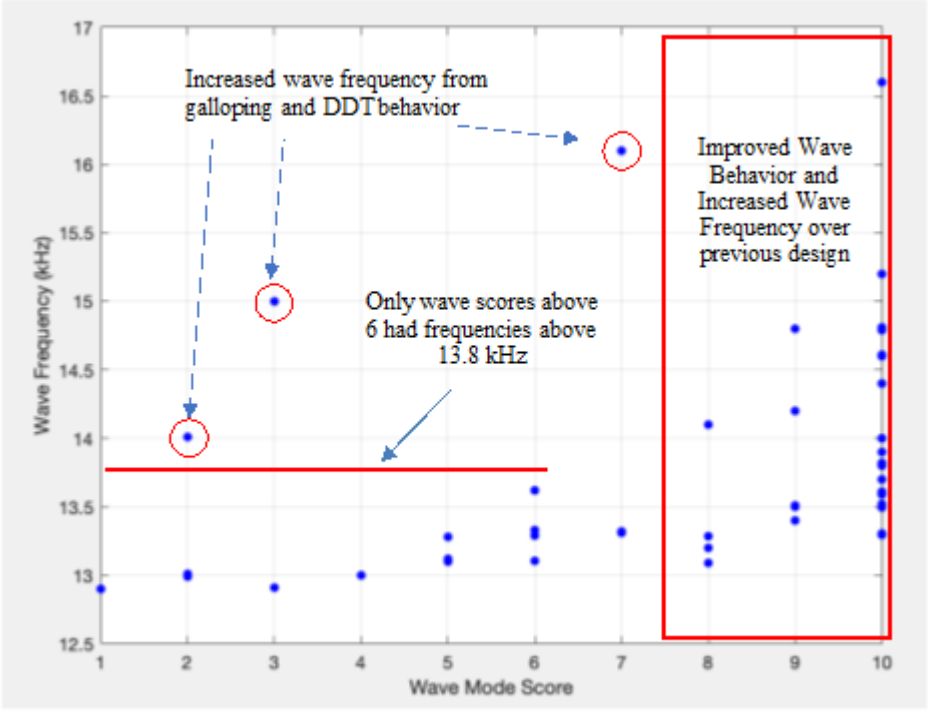

[2]

Figure 18. Wave Speed versus Wave Mode. Outlier Points are Highlighted

2.6 Optical Access

Visualization of detonation waves is vital to the understanding of RDEs and identifying parameters that influence the operation and performance of an RDE [25]. Some of these parameters include fill height, cell size, mixing time, detonation wave mode, and other detailed parameters found in Section 2.3. Additionally, visualization of reactions flowing from injection geometries have potential to analyze their performance when mixing the fuel and oxidizer. Experiments done by Rankin et al. demonstrate some of these advantages of optical access into a RDE. Utilizing a quartz tube, which is transparent and highly resistant to extreme temperatures and pressures, as an outer body, the detonations inside the chamber were able to be visualized and analyzed. Figure 19 shows the schematic of the traditional RDE used (bottom) and the changes made to install the optical access with the quartz outer body [25]. A top plate with screws was utilized to ensure the quartz tube remained attach to the configuration during detonation. The drawings for this optically accessible RDE were used as a basis for the RDE utilized in the research for this current paper.

Similar to the current research, the optically accessible RDE was intended to allow for the creation of images that help evaluate the effects of air mass flow rate, equivalence ratio, and fuel injection scheme on the performance of the detonation wave mode and stability in the RDE. This optically accessible RDE during operation is pictured in Figure 20. The images were captured using a high-speed camera Photron SA-5 CMOS while using a LaVision IRO UV intensifier [25]. High-speed cameras are necessary to capture the detonation waves that move on the order of thousands of meters per second.

Results from the testing of various injection schemes with this optically accessible RDE are shown in Figure 21. These show instantaneous (Columns 1-3) and phase-averaged (Column 4) images of the OH* chemiluminescence for the three equivalence

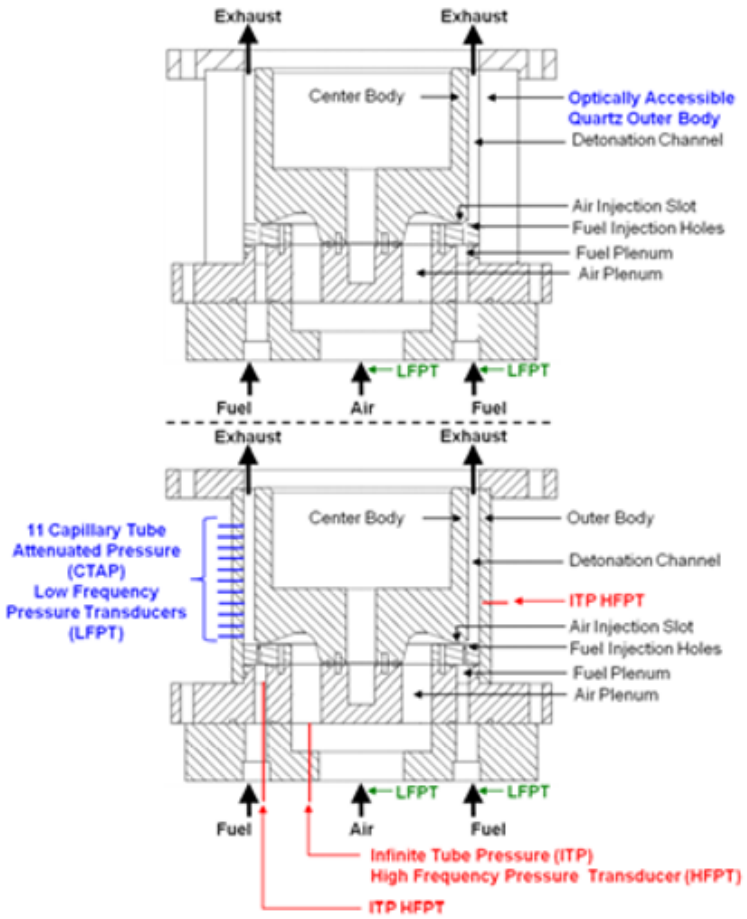

[25]

Figure 19. Schematic of the Optically Accessible (top) and Non-Optically Accessible (bottom) RDE

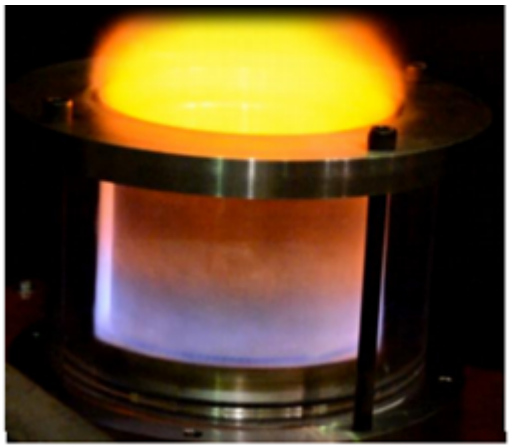

[25]

Figure 20. Photograph of Optically Accessible RDE During Operation

ratios while keeping a uniform air mass flow rate and fuel injection scheme between each case. In these photographs black and white regions represent low and high OH* chemiluminescence emissions, respectively [25]. The instantaneous images are randomly selected from a group of images where the detonation is near the image centerline. The phase-averaged images are normalized by the maximum phase-averaged intensity for the given condition, allowing for the size and shape of the detonation wave to be compared [25]. When necessary, images shown have been flipped horizontally to allow for comparison with waves travelling in the same direction.

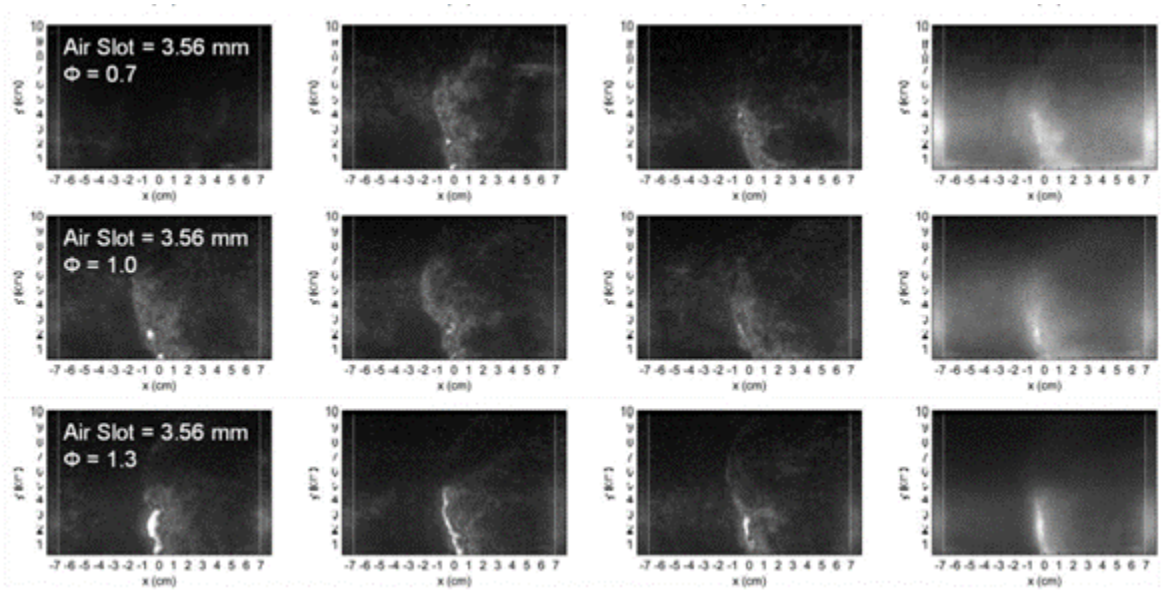

[25]

Figure 21. Instantaneous (Columns 1,2,3) and Phase-Averaged (Column 4) Images of OH* Chemiluminescence in RDE for Three Equivalence Ratios

It is seen for the fuel lean case ($\phi = 0.7$) in Figure 21 that there are not consistent detonations while at stoichiometric conditions ($\phi = 1.0$) there are. The fuel rich case ($\phi = 1.3$) shows a consistent transition between one and two detonations as is indicated by the height of the detonation wave which is twice the other waves for the fuel rich case. Although determining if a test run resulted in a detonation or not is plain to see, determining the height of the detonation wave would be impossible without the optical access.

Using a similar configuration as Rankin et al., Naples et al. tested an optically accessible RDE to generate a picture of a detonation wave and its flowfield structure [26]. Previously pressure measurements were used as a basic understanding of a flowfield, but optical measurements provide a more complete picture of a detonation. Chemiluminescence was once again used to see the basic structure of the detonation, and ethylene was added to the reactants, hydrogen and air, to increase the light emission. The flowfield was visualized in 2D as seen in Figure 22. To do so, the RDE image had to be "unwrapped" because the photo taken was of a curved/circular quartz outer body [26]. Two things were done to achieve this. First, the videoframe had to be corrected for refraction effects because the quartz outer body was thick. Second, a pixel's horizontal distance from the centerline was set equal to its arc length from the centerline. This resulted in additional pixels which were simply averaged out with the surrounding pixels.

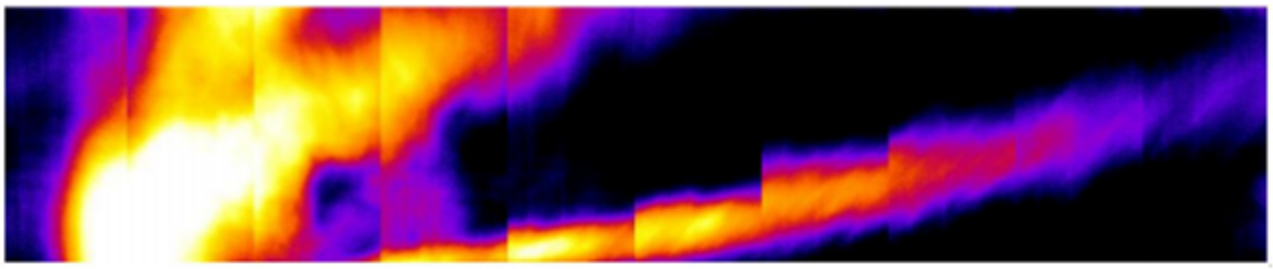

[26]

Figure 22. 2D flowfield of 360 view of RDE

To better describe the flowfield, angles of important detonation structures were analyzed as seen in Figure 23. Naples et al. describes the structures as follows: A – oblique shock wave, B – shear layer between gases of different detonation cycles, C – detonation wave, D – contact region between the combustion reactants and fresh products [26]. The oblique shock angle (α), shear layer angle (β), detonation wave angle (ε), and the contact surface angle (θ) in addition to the detonation wave height were identified in Figure 24. Detonation wave speed, equivalence ratio and mass flow

rate were also recorded along with an error measurement for each parameter and angle. These error measurements account for the quartz light refraction, the 3D to 2D transformation, human error, and any other potential sources of error. All the previously mentioned parameters help characterized the flowfield of the detonation for each run.

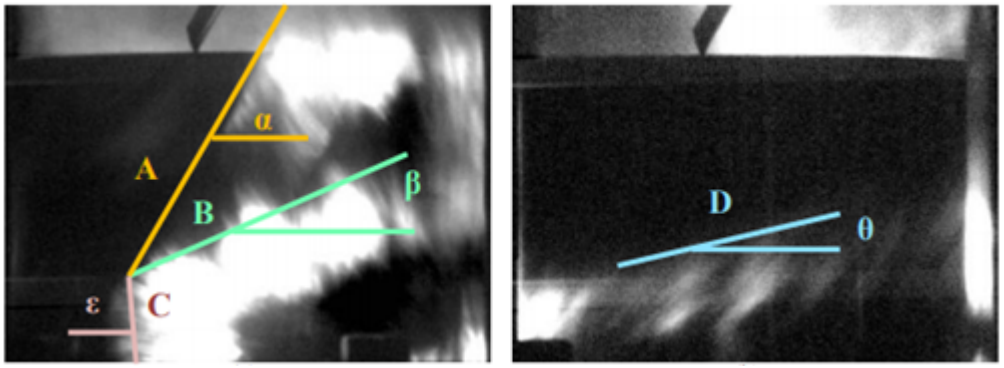

[26]

Figure 23. Light Intensity of Detonation Wave with Labeled Structures

	Run 1	Run 2	Run 3
Total Flow (kg/s)	1.23 ± 0.04	1.36 ± 0.04	1.55 ± 0.04
Equivalence Ratio	1.26 ± 0.03	1.26 ± 0.03	1.20 ± 0.03
Wavespeed (m/s)	1730 ± 165	1768 ± 192	1752 ± 168
α (°)	57 ± 16	55 ± 13	62 ± 15
β (°)	29 ± 15	29 ± 13	23 ± 14
θ (°)	14 ± 9	13 ± 8	13 ± 8
ε (°)	88 ± 9	84 ± 10	85 ± 14
h (mm)	49 ± 19	46 ± 16	38 ± 16

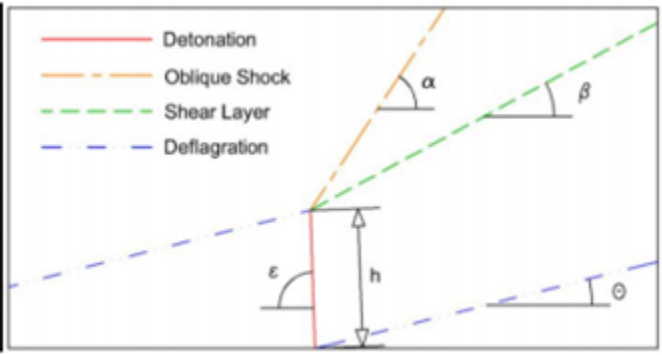

[26]

Figure 24. Detonation Wave with Labeled Structures and Angles

Figure 25 plots the values and error bars for the angles shown in Figure 24 along with measurements taken from the 2D average intensity frames found in Figure 22 (denoted by black squares). The results from both measurements show minimal trends, however it is seen that an increase in mass flow rate results in an increase in θ. This result is expected since a higher mass flow rate usually results in larger fill heights since the channel is filled quicker [26]. Although the results were not definitive, this

ability to model trends of the changes in detonation structure as different parameters are changed shows the potential of optical access in an RDE.

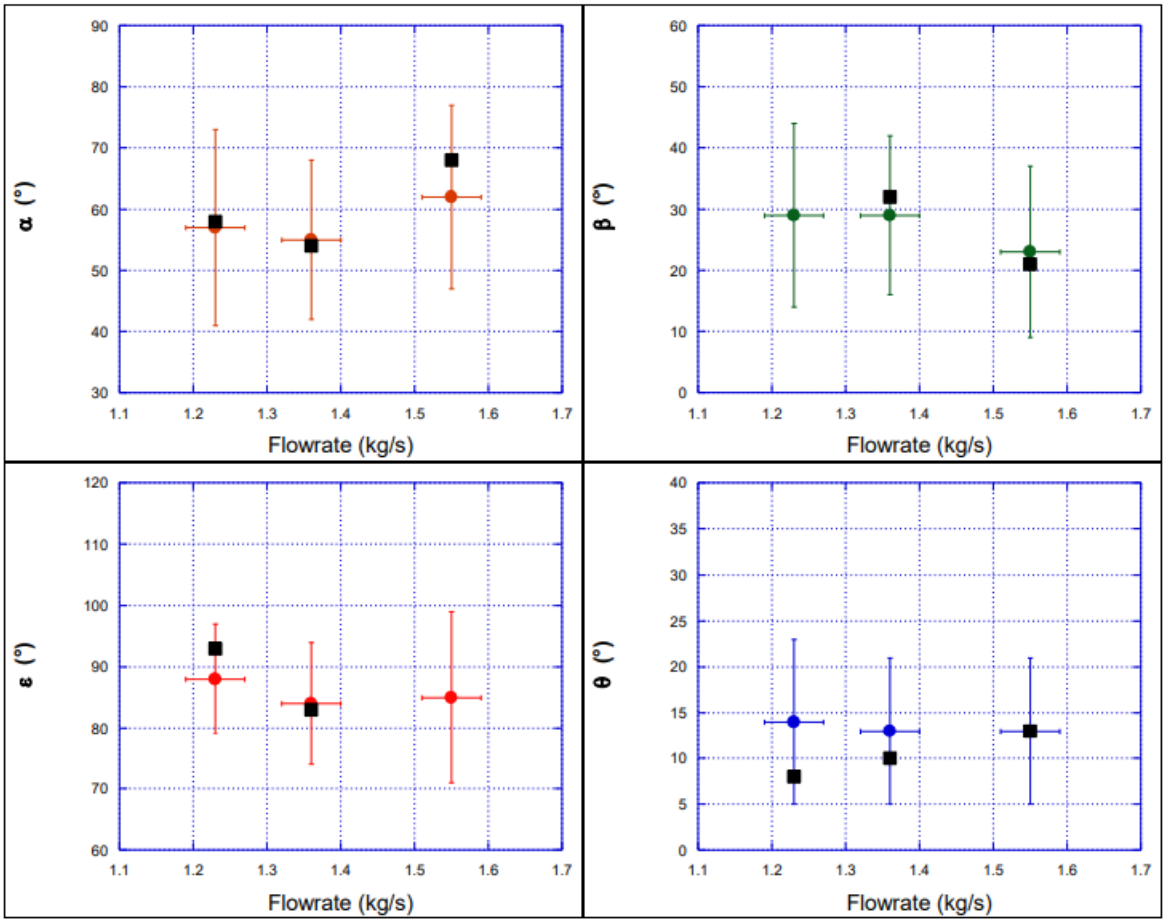

[26]

Figure 25. Plots of Measured Angles with Error Bars

Other more unique configurations of optically accessible RDEs exist including the "Racetrack" RDE developed by Unruh et al [27]. This oblong shape allowed for the continuous propagation of a detonation but also provided optical access within a linear section of the combustor. The cross-section of this RDE is pictured in Figure 26. The RDE is designed with two windows that provide optical access completely through one of the linear sections of the "racetrack" allowing for direct imaging of the detonation wave and injector spray interactions.

The center of this RDE contained a hollow cavity for placement of optical and

pressure instruments inside the combustor channel walls. The windows and cavity of the RDE are pictured on the left and right sides of Figure 27, respectively. The dimensions of this RDE were based off Bykovskii et al.'s methods for optimizing the size of an RDE using the cell size [27][16]. Cell size was estimated using Gavrikov et al.'s model derived by empirical data. This model can be found in Equation 8 where λ is the cell size, δ is the characteristic reaction zone width, and X and Y are values calculated in Equation 9 using coefficients outlined in Table 5 [28]. Parameters in Equation 9 include activation energy (E_a), universal gas constant (R), post shock temperature (T_{ps}) and the von Neumann temperature (T_{vn}). This RDE is another example of the many implementations of optical access into an RDE. It has been built and is ready for testing.

$$\log \frac{\lambda}{\delta} = Y(aY-b)+X[cY-d+(e-fY)Y]+g\ln Y+h\ln X+Y(\frac{i}{X}-\frac{kY}{X^m})-j \quad (8)$$

$$X=\frac{E_a}{RT_{ps}}, Y=\frac{T_{vn}}{T_0} \quad (9)$$

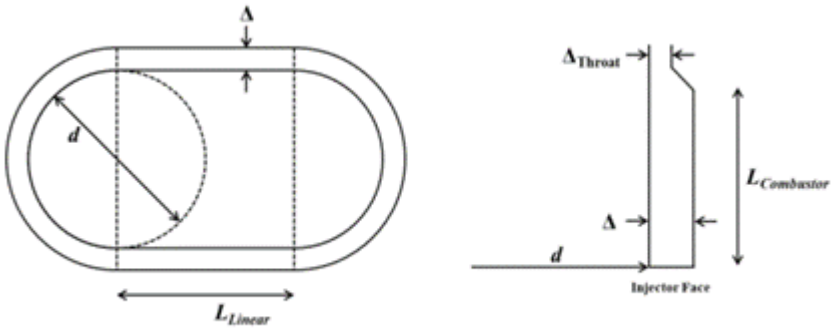

[27]

Figure 26. "Racetrack" Channel Key Dimensions

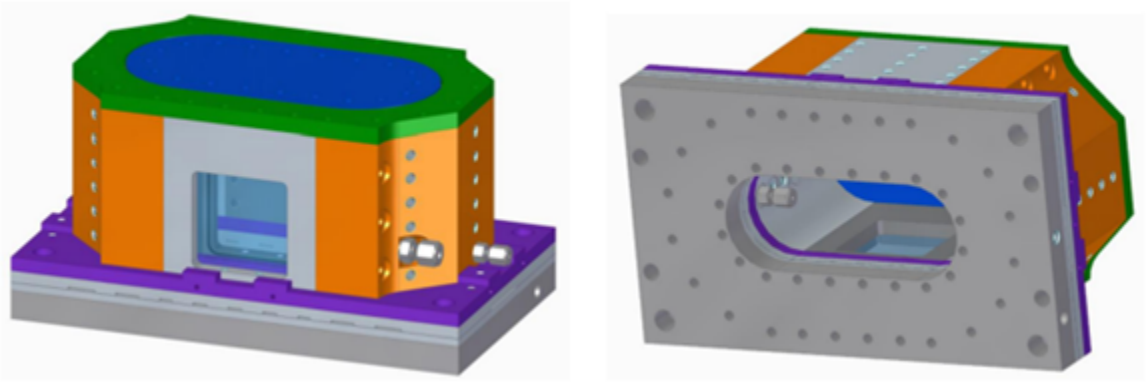

[27]

Figure 27. "Racetrack" Engine View Showing Channel Windows (left) and Central Cavity (right)

Table 5. Coefficients for Equation 8

Coefficient	Value
a	-0.007843787493
b	0.1777662961
c	0.02371845901
d	1.477047968
e	0.1545112957
f	0.01547021569
g	-1.446582357
h	8.730494354
i	4.599907939
j	7.443410379
k	0.4058325462
m	1.453392165

[27]

III. Solution Methodology

This research was intended to compare the performance of various injection schemes and their influence on detonation waves in the Micro-RDE. Additional goals included gaining optical access into the small-scale detonation engine while improving the operability and survivability of the engine. The design and implementation of the changes outlined in this chapter were driven by these objectives. An overview of the facility where all iterations of the small-scale engine were designed, changed and tested can be found in Section 3.1. Section 3.2 gives an in depth review of the original Micro-RDE design from Dechert[1] and the previous modifications made to the RDE by Fiorino[2]. The use of a different flow control system intended to improve the operability of the engine is covered in Section 3.3 while other design changes made for this research, which include the incorporation of an optical outerbody and the testing of injection geometries, are discussed in Section 3.4. The instrumentation of the RDE such as pressure/temperature sensors and the high speed camera is documented in Section 3.5.

3.1 Detonation Engine Research Facility

All designs of the Micro-RDE, including the previous designs by Dechert and Fiorino, were tested in the Air Force Research Lab's (AFRL) Detonation Engine Research Facility (DERF). The DERF contained an explosion proof bay that was ideal for housing RDE operations. This bay allowed for the supply of various fuels and oxidizers to locations throughout the test cell and contained bay door interlocks that could turn off all valves that opened these supply lines. This enabled multiple research projects to be conducted simultaneously while providing testing safety and minimizing accident risks. Next to the bay and protected by 69 cm of concrete wall

was a control room that allowed for remote operation and observation of the test cell. Data acquisition systems were housed here and used to monitor parameters such as temperature, pressure, and high-speed imaging.

For this research gaseous ethylene and nitrous oxide were used as the fuel and oxidizer, respectively. Both reactants were supplied from high pressure sources on opposite sides of the DERF bay for safety purposes. The reactants were brought to a desired pressure upon reaching final valves which opened and closed to mark the start and end of a test. These valves were controlled by a Laboratory Virtual Instrument Engineering Workbench (LabVIEW) program from inside of the control room. Nitrogen, supplied by high and low pressure bottles within the bay, was used as the inert working fluid to actuate all valves in the Micro-RDE system.

Additionally, oxygen and hydrogen were used as reactants for the pre-detonator device that provided the heat necessary to detonate in the RDE. The oxygen was housed adjacent to the nitrous oxide, while the hydrogen was supplied from high pressure bottles outside of the bay. Reactants were stored in separate locations as a safety precaution for any incidents in the bay and prevent the fuel and oxidizer from mixing at undesired times (providing two of the three components necessary for combustion). Further precautions were built into the bay system such that valves could not open unless the bay door was closed signaling that all personnel had already exited the bay and was safely positioned in the control room.

Tests were ran from inside the control room where the user used the LabView program to send signals to a National Instruments NI-cDAQ9185 (DAQ) chassis which controlled valves and monitored readings from sensors positioned throughout the bay. Signals were sent via an ethernet cable to the chassis which held three data acquisition and control boards, each controlling a specific portion of the RDE configuration. Board one, an NI-9214, corresponded to channels gathering temperature data and

board two, an NI-9215, corresponded to pressure readings. Each pressure transducer and thermocouple corresponded to a specific channel in the respective control boards in the chassis. The channels of the pressure transducers and thermocouples are further discussed in Section 3.5.1. Board three, an NI-9923, was used to run the control sequence by operating the fuel and oxidizer valves and triggering the spark. Upon completing each test run, the measured data from each board was transferred to the DAQ and then logged using LabView software, where it was outputted to a .txt file after every run for user analysis.

3.2 Previous RDE Design

Since it's original design, the Micro-RDE has undergone several changes to produce a stable detonation wave at a design frequency of 20 kHz. The methodology behind the original design created by Dechert is discussed in Section 3.2.1 along with additional changes that he made to further optimize the RDE. Modifications made by Fiorino to Dechert's final design are outlined in Section 3.2.2, which include changes to the ignition mechanism, injection scheme, and centerbody.

3.2.1 Dechert's Design

Dechert et al. [1] constructed the first iteration of the Micro-RDE using the sizing guidelines outlined by Bykovskii et al. [16]. The RDE itself was built using the five following parts (as seen in Figure 28): a connection plate (red), an oxidizer manifold (orange), a fuel manifold (green), an outerbody (dark blue), and a centerbody (light blue). These parts created the dimensions of the RDE where the channel gap (Δ) = 2 mm, the channel length (l_c) = 30 mm, and the channel diameter (d_c) = 28 mm, as seen in Table 3 in Section 2.5.1. Fuel and oxidizer supply lines were connected to the RDE via the connection plate. Upon entering the engine, fuel and oxidizer were

routed into their respective plenums to be injected for mixing and consumption in the detonation channel. The product gases traveled the remaining length of the channel and were exhausted from the engine.

The injection geometry utilized in this original design of the Micro-RDE was a 90-degree Jets in Crossflow (JIC) scheme positioned 2 mm into the detonation channel. This scheme is highlighted in the right image of Figure 28. The fuel and oxidizer, ethylene and gaseous nitrous oxide, were both injected by 24 injection holes from their respective manifold. The diameters of the injection holes were 0.40 mm and 0.11 mm for the fuel and oxidizer, respectively. These holes were designed to choke the mass flow at rates between 0.025 kg/s and 0.075 kg/s without overly back pressuring the supply lines. The gaseous nitrous oxide was supplied from the three oxidizer supply lines into the oxidizer plenum (inside the connection plate) from which it was injected through the oxidizer manifold. The ethylene was supplied from the single fuel supply line in the middle of the RDE directly into the fuel plenum from which it was injected by the fuel manifold [1].

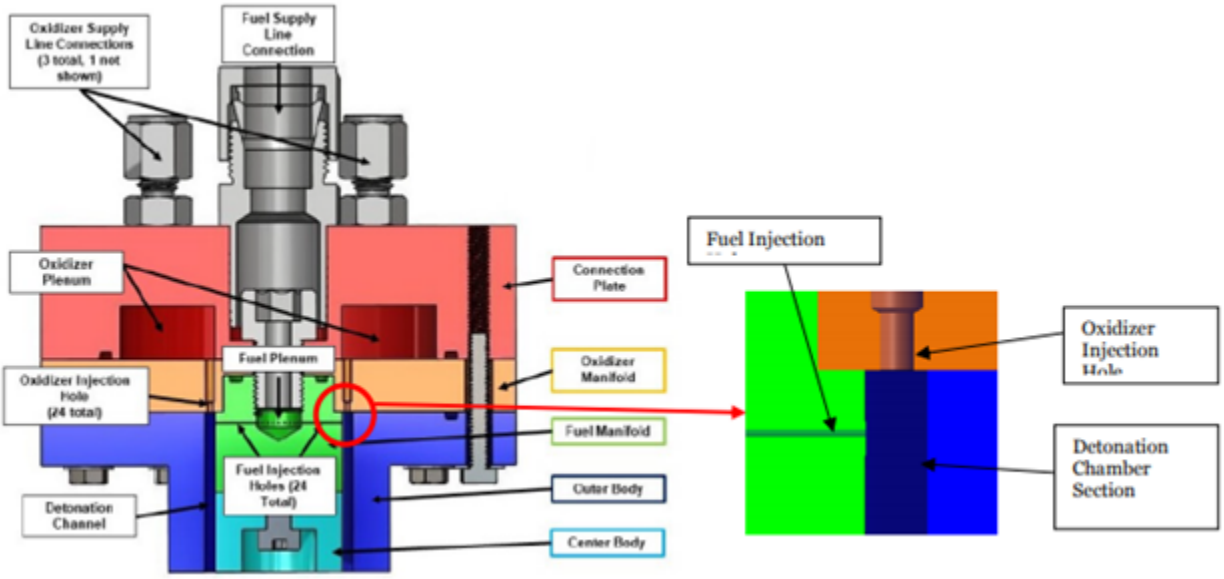

[2]

Figure 28. Cross-Section View of Dechert's RDE w/ Injection Geometry Highlighted

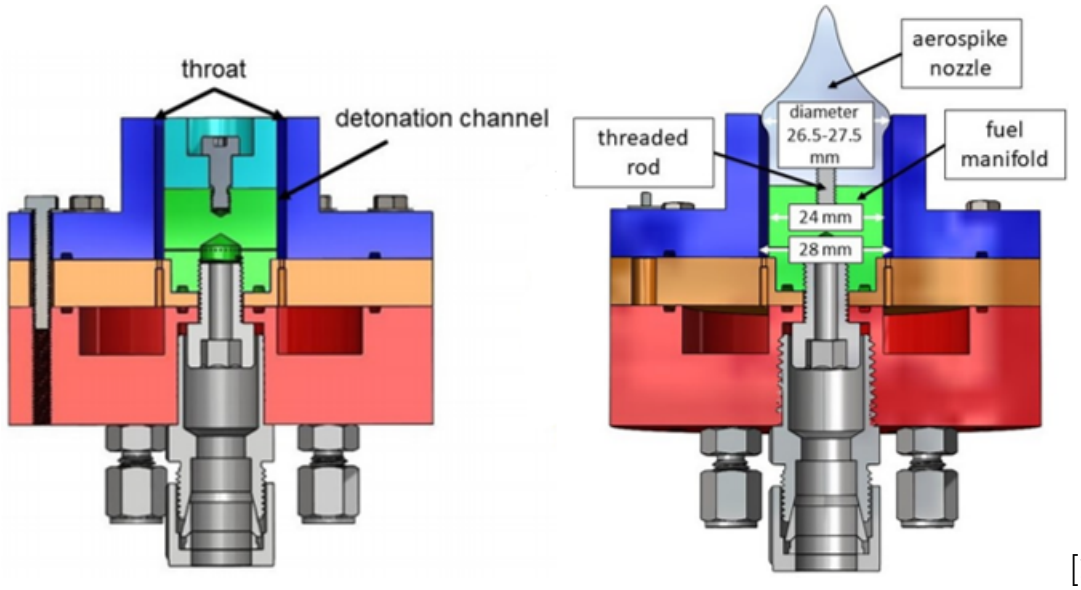

[1]

Figure 29. Washer/Backplate Centerbody (left) and Aerospike Nozzle Centerbody (right)

The centerbody, attached to the fuel manifold, was initially comprised of a washer/backplate configuration. The backplate was implemented by a washer fastened to the centerbody and attempted to increase flow constriction and the static pressure in the detonation chamber by decreasing the exit area of the channel [1]. Due to its inability to sufficiently reach and hold an adequate pre-detonation static pressure, Dechert replaced the washer/backplate centerbody configuration with an aerospike nozzle [1]. This change to the centerbody is shown in Figure 29. The addition of the aerospike nozzle allowed for an additional decrease in the exit area of the channel without compromising the area of the detonation channel where mixing would occur and the detonation wave would propagate. Aerospike nozzle diameters that created channel exit channel gaps between 0.50 mm and 0.75 mm were utilized to control the channel pressure by varying this exit area of the combusted products.

To meter the flow of the reactants Dechert used MCRQ High Pressure Mass/Gas Flow Controllers from Alicat Scientific. A 500 and 2000 Standard Liter Per Minute (SLPM) controller were used to meter the fuel and oxidizer, respectively. The 500

SLPM controller was chosen for the ethylene line because of its ability to control the desired mass flow range 1.26 g/s to 10.31 g/s. The 2000 SLPM controller, which was calibrated to handle flows up to 2500 SLPM, was chosen for the nitrous oxide line because of its ability to control the desired mass flow range 21.56 g/s to 71.22 g/s. These desired mass flow rates of ethylene and nitrous oxide allowed for mass flow rates from 25 g/s to 75 g/s to be tested at equivalence ratios between 0.5 to 1.5. Both controllers were calibrated and tuned by the manufacturer according to the specific gas they'd meter [1].

To ignite the reactants, an NGK 5869 ER9EH spark plug was utilized and situated approximately 21 mm above the injection holes. This spark plug method required an opening directly into the detonation chamber which was provided through a 1/4" threaded hole. The placement of spark plugs into the detonation chamber was found to be necessary when achieving a detonation in these first iterations of the Micro-RDE [1]. The spark plug was fired using a 5ms, 5V signal to a 40 kV ignitor coil [1]. The spark plug and Alicat controllers are pictured in the control system layout in Figure 30. Also pictured are last chance valves, used for safety purposes, which ensure reactants don't leak into the RDE except when testing.

This design produced wave frequencies between 11.4 and 14 kHz which correspond to wave speeds from 1020 to 1230 m/s using the 28 mm channel diameter. The speeds recorded were significantly lower than the expected CJ speed (2080 – 2291 m/s), and the detonations were determined to be unstable. Improper mixing was hypothesized to be the cause of these wave speeds at such low magnitudes relative to their CJ velocity [1]. This stemmed from the location of the mixing process which took place in the detonation chamber. The point of intersection inside the detonation chamber meant reactants could easily be diluted by recirculation products and/or might have less time to mix before each wave passed. Further decline in mixing quality could

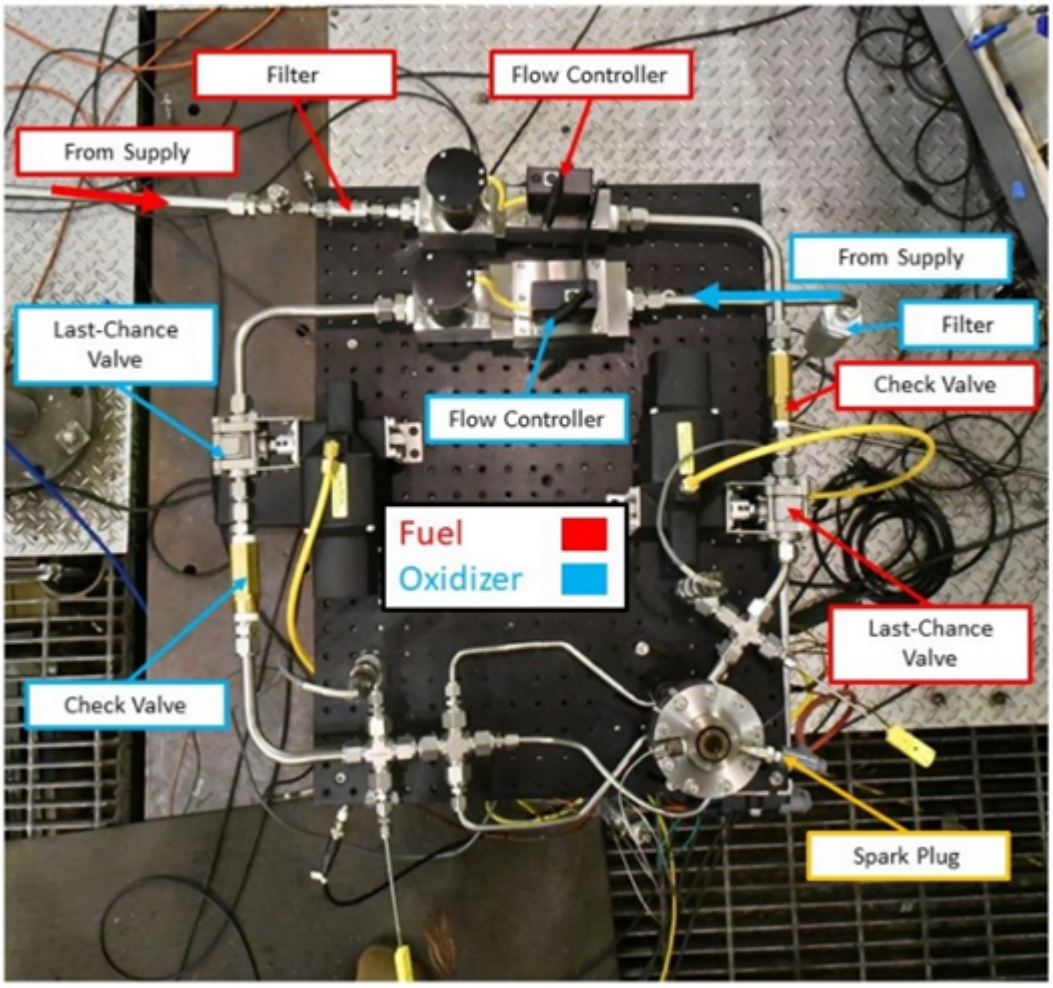

[1]

Figure 30. Dechert's Micro-RDE Control System Layout

have also resulted from the improper alignment of the the fuel and oxidizer injectors during assembly. Had they been misaligned during some runs, there would not have been a point of crossflow between the fuel and oxidizer as they were injected into the detonation channel. Thus, a new injection scheme was needed to ensure better mixing which would consequently improve the detonation wave's stability.

3.2.2 Fiorino's Design

To improve the operability of the RDE and its wave stability, Fiorino made certain modifications to Dechert's Micro-RDE beginning with changes to the injection scheme

[2]. Figure 31 shows the modifications made to the original JIC scheme from Dechert by Fiorino. The location of the point of cross flow between the fuel and oxidizer was moved from inside the detonation chamber to inside each oxidizer hole. To do this, the 24 injection holes were placed within an oxidizer injector about 1 mm from the detonation channel. The angle of cross flow between the reactants was maintained at 90 degrees. Thus, the mixing zone was set to begin earlier than with the previous injection scheme and allowed for partially pre-mixing of the reactants prior to arriving at the detonation channel. Additionally, this gave the reactants a space to mix without the interference of a passing detonation wave or recirculating combustion reactants. This new injection scheme showed potential for enhanced mixing quality because of its larger mixing zone and allowance for partial pre-mixing.

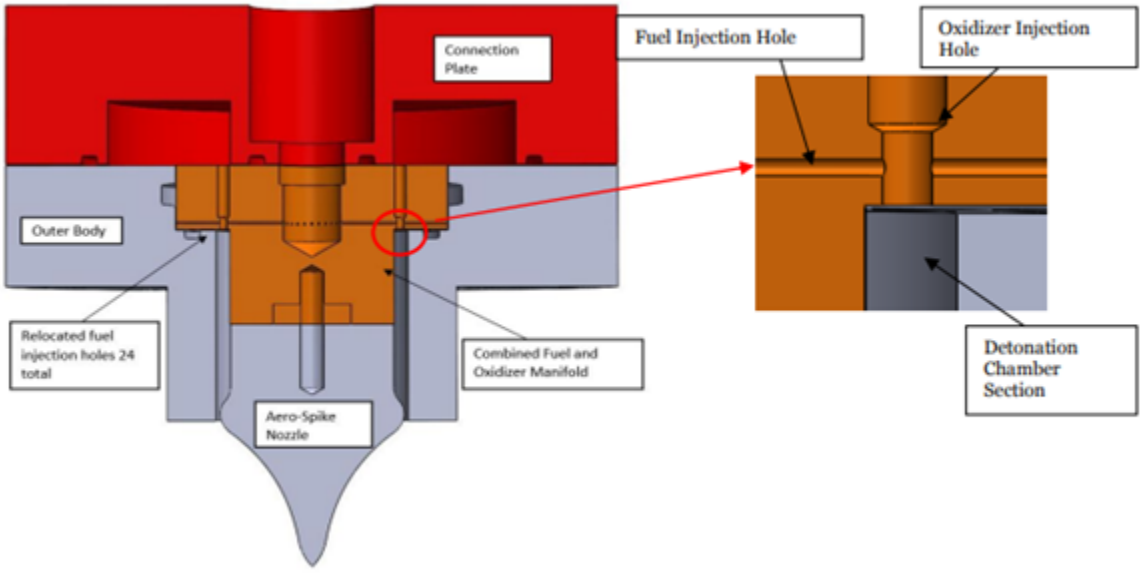

[2]

Figure 31. Cross-Section View Highlighting Relocated Fuel Injection Holes Adapted from Fiorino

To create the new injection scheme Fiorino et al. designed the fuel and oxidizer manifolds into a single new interface. The outerbody of the RDE was modified to accommodate and fit around this new part. The 0.40 mm fuel injection holes were

machined into the combination of the two manifolds this creating the desired JIC scheme pictured in Figure 31. However, the holes were drilled from the outside in, leaving holes on the manifold that were not intended to feed reactants to the RDE and could potentially have lead to leaks during operation of the RDE. To prevent this, two PTFE O-rings were added to the new manifold to seal off the fuel and oxidizer from entering the oxidizer plenum. Additionally, because the fuel holes were machined through each oxidizer hole, the possibility of the misalignment of injector holes during assembly found in Dechert's design was removed [2]. This new design that offered partial pre-mixing, perfect alignment of injectors, and the confinement of the reactants to mix undisturbed was believed to improve the quality of the local mixing. This increase in mixing quality helped produce a more stable wave that operated closer to the designed CJ velocity [2].

Initial tests of Fiorino's Micro-RDE design used Dechert's spark plug configuration as an ignition mechanism. However, the placement of the spark plug in the chamber, which was deemed necessary for detonation, resulted in a protrusion in the detonation chamber and caused significant damage to the spark plug after a single detonation [2]. Thus, frequent spark plug removal and replacement were required between tests. Figure 32 shows a used spark plug after a detonation next to an unused new spark plug to reveal the significant erosion.

The erosion to the RDE configuration caused by the protrusion into the chamber was not limited to the spark plug. Erosion to the outerbody and aerospike nozzle were consistently found at the quarter inch entry hole of the spark plug [2]. An example of this erosion can be seen in Figure 33. This damage to the outerbody and nozzle proved problematic because these parts were not as easily replaceable as the spark plug. Additionally, erosion to the outerbody and nozzle could alter the designed dimensions of the Micro-RDE, changing important parameters such as

[2]

Figure 32. Erosion of Spark Plug After One Detonation. Eroded Spark Plug (left), New Spark Plug (right)

channel diameter and channel length. These parameters were calculated based on the design frequency 20kHz, so changes to these could reduce the likelihood for a stable detonation at this frequency.

To reduce erosion and improve survivability, more recent designs of the Micro-RDE replaced the spark plug with a pre-detonation device as an ignition mechanism [2]. A pre-detonation device, also called a "pre-det", is a Pulsed Detonation Combustor that creates a single detonation using deflagration to detonation transition (DDT). It is often used to provide the heat to initiate a detonation in another device, and served this purpose in the Micro-RDE as seen in Figure 34. The advantage of the pre-detonation device stemmed from the smaller access hole and flushed entry into the channel that it offered, as opposed to the protruding spark plug. The pre-det used to run the Micro-RDE was designed by Innovative Scientific Solutions Inc., and the schematic can be seen in Figure 34. To operate this pre-det, hydrogen and oxygen

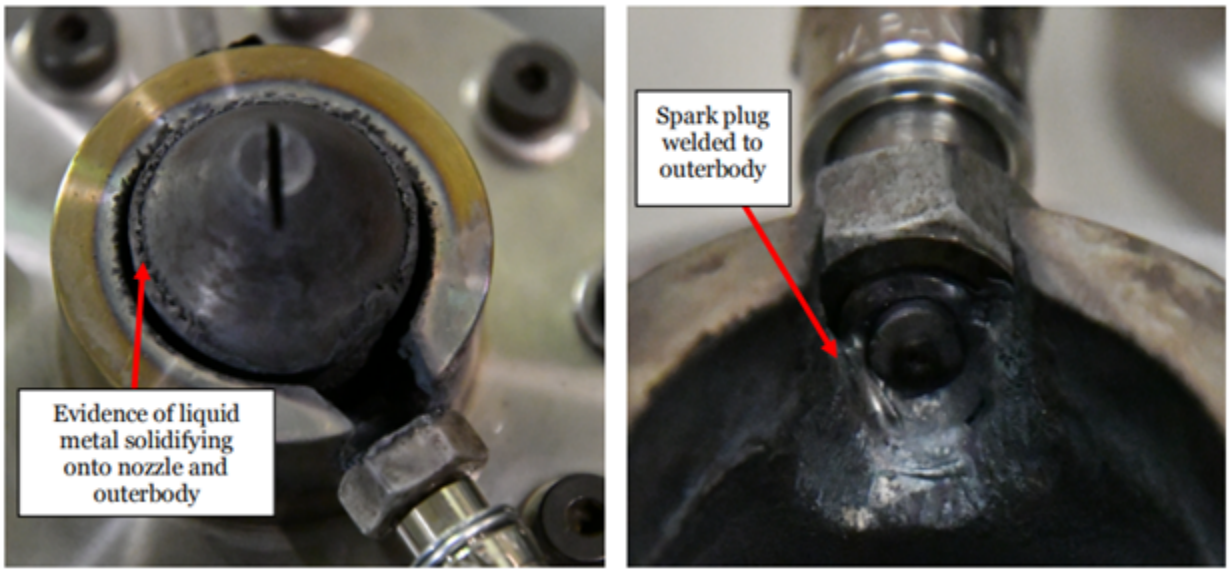

[2]

Figure 33. Outerbody and Aerospike Nozzle Erosion Damage from Entry Hole of Spark Plug

were used as the fuel and oxidizer and were injected at an equivalence ratio of two. Each reactant gas was injected at 1.38 MPa (200 psi) and then ignited by a spark plug, thus resulting in a detonation. The detonation traveled through a tube and into the detonation chamber to ignite the reactants of the Micro-RDE. This detonation tube was brazed into the outerbody of the Micro-RDE to ensure it would be held in place throughout detonation events.

Initially, Fiorino et al. placed the position of the pre-det 21 mm above the injection holes to be consistent with Dechert et al.'s position of the spark plug [2]. Further iterations on the location of the pre-det were made to improve the ignition mechanism's susceptibility to damage. The pre-det was moved to 5.5 mm above the injectors (well within the estimated fill height of 12 mm), where it would experience less heating and would be cooled by the flowing reactants leaving the injector. The lower position of the pre-det is shown in Figure 35. These changes allowed for the improved survivability of the ignition mechanism and contributed to the reduction of erosion on the Micro-RDE outerbody as a whole [2].

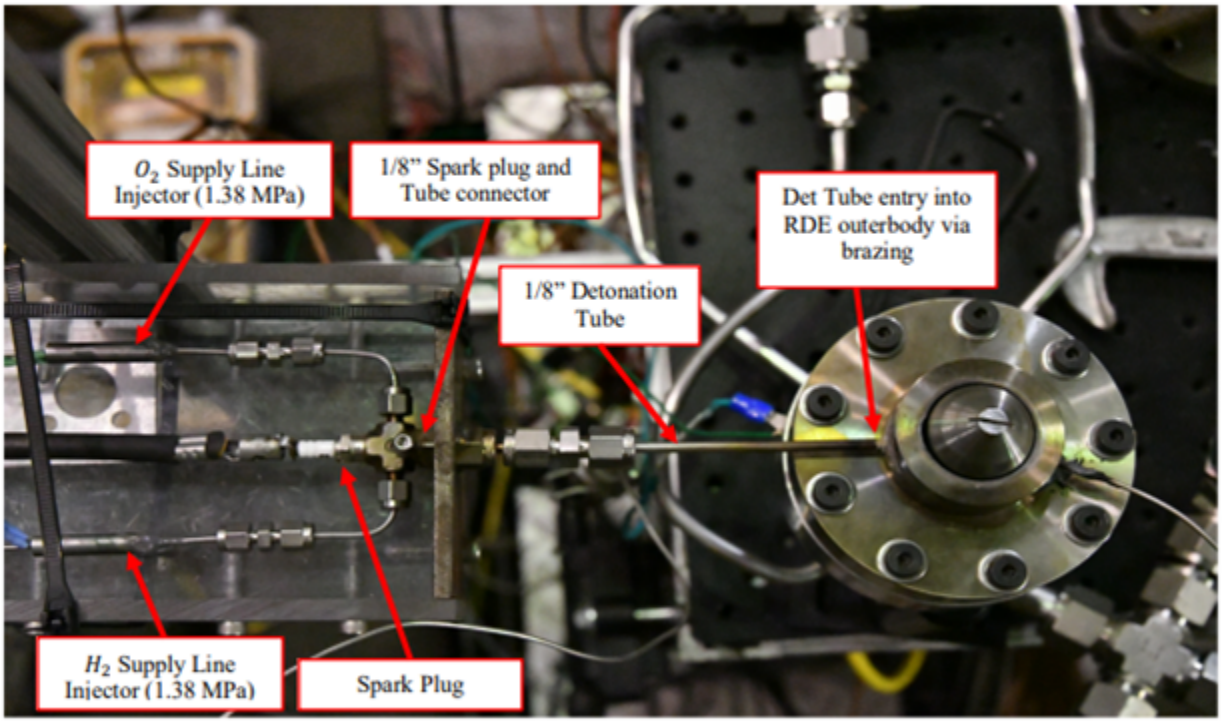

[2]

Figure 34. Pre-Detonator Device Using H_2 and O_2 Mixture at $\phi = 2$ Integrated into Micro-RDE Outerbody via Detonation Tube.

To further reduce erosion, new outerbodies out of Inconel 625 were machined by the University of Dayton Research Institute (UDRI). Fiorino hypothesized that chamber temperatures in the Micro-RDE reach close to 4000 K [2]. While there was no direct measurement of this temperature, this warranted that the selection of materials subjected to those extreme conditions be put under careful consideration before using them on the RDE. 304 Stainless Steel, although it has a higher melting point of 1725 K, is vulnerable to oxidation at high temperatures which is believed to be the cause of erosion on the Micro-RDE outerbody and aerospike nozzle in previous testing [29]. Inconel 625, despite its lower melting point of 1625 K, is highly resistant to oxidation at high temperatures and thus made it the optimum choice for the new material of the RDE [30]. An additional advantage of Inconel 625, was its ability to maintain a nominal tensile strength of 280 MPa at 1170 K as opposed to 304 Stainless

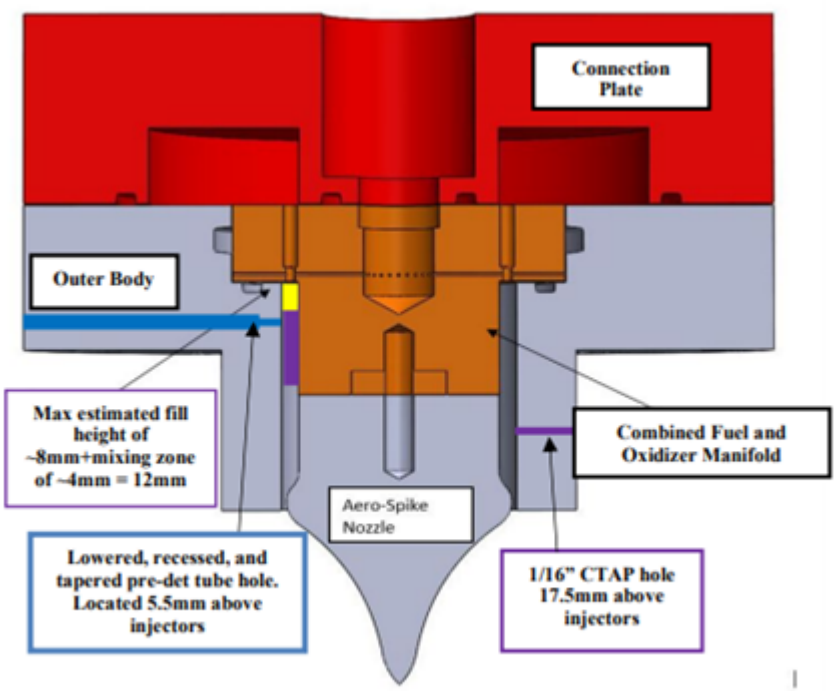

[2]

Figure 35. New Lowered Position of the Pre-Det Hole Now Located 5.5 mm Above Injectors

Steel's ability to maintain a nominal strength of 75 MPa at 1170 K [29, 30].

Issues of erosion in Fiorino's Micro-RDE were not limited to the outerbody and the bell of the aerospike nozzle. The connection between the nozzle and the manifold also saw problems of erosion in addition to problems of attachment. The nozzle was previously mated to the injection scheme manifold as shown in Figure 36. A threaded rod protruding from the manifold was used to attach the nozzle to the manifold and ensure its proper alignment in the detonation channel while preventing the nozzle from blowing off during detonation events. The rod, 12.5 mm long, was threaded into both the manifold and the nozzle which resulted in approximately half ($\sim$ 6.25 mm) of the threads in the manifold and the other half ($\sim$ 6.25 mm) in the nozzle. This proved to be insufficient in consistently holding the nozzle in the detonation chamber, and many tests resulted in the nozzle's complete detachment from the manifold during the detonation events and its ejection from the Micro-RDE.

Additional issues with this configuration stemmed from the small space between the aero-spike nozzle and the manifold. Held together by the threaded rod, it was impossible for the two separate parts to create an interface that was completely flushed with no discontinuities. Fiorino hypothesized that the discontinuity, although small, was enough to create a recirculation zone between the two parts which became the anchoring location for the detonation [2]. This resulted in extreme erosion at the nozzle attachment point as seen in Figure 37, which shows an aerospike nozzle after a single detonation. While this case was an extreme, in general it did not take many detonations for this erosion to vastly increase the channel gap inside the detonation channel and render the eroded nozzles unfit for future testing.

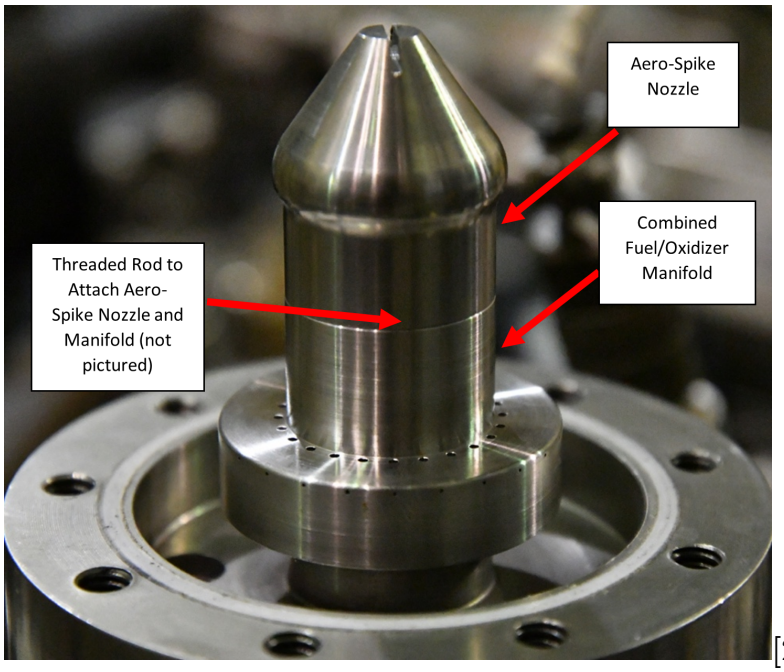

[2]

Figure 36. Cross-Section View Highlighting Aero-Spike Nozzle Attached to JIC Manifold, adapted from Fiorino

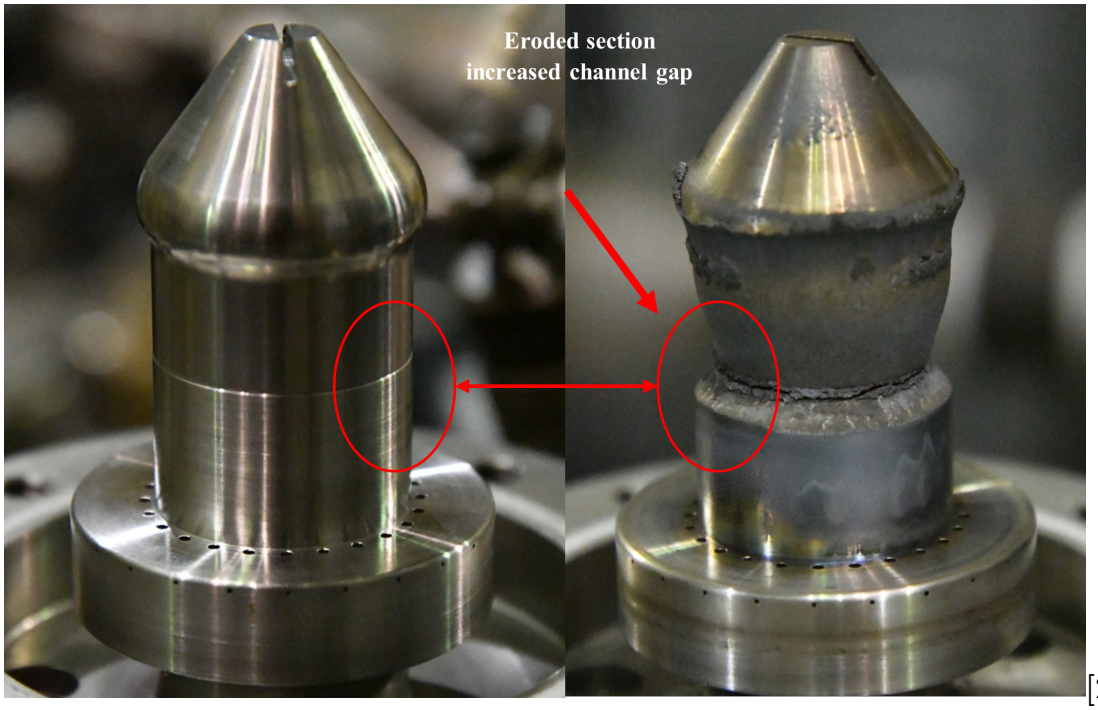

[2]

Figure 37. Fuel/Ox Manifold and Nozzle Pretest (left) and Eroded (right) after a Single Detonation

3.3 Mass Flow Control

Previous designs of the Micro-RDE proved to have difficulty with metering mass flow reliably during testing. To produce more stable and reliable mass flow, the Alicat controllers were replaced with sonic nozzles as the flow control system. An overview of sonic nozzles and their use in the RDE is found in Section 3.3.2. Because sonic nozzles do not possess a built in data logging system like the Alicats, other methods were used to gather data and calculate mass flow for a given test. These methods are outlined in Section 3.3.3. Lastly, Section 3.3.4 discusses the results of testing with the sonic nozzles and how they improved the stability of the flow after the detonation.

3.3.1 Issues with Alicat Controllers

Mass flow control proved to have issues in Fiorino's Micro-RDE configuration. To meter the reactant flow Fiorino used the same 500 and 2000 Standard Liter Per Minute

(SLPM) flow controllers from Alicat Scientific that were previously used by Dechert. Fiorino found that testing with these controllers brought up two major issues: 1) the rate at which data was sampled was inconsistent and 2) the flow controllers did not compensate for the backpressure from the detonations in the chamber so the detonation mass flows were always lower than requested [2]. Equation 10 solves for the mass flow across an injector, and when calculating this flow rate, it was believed that the flow was choked across the injector ($M = 1$). However, during detonations, the elevated pressure in the channel caused the controller to unchoke. Therefore, the mass flow rate calculated from Equation 10 using $M = 1$ was only accurate for flow prior to the detonation. Table 6 shows the measured SLPMs from the Alicat controllers and the estimated SLPMs from Equation 10 prior to the detonation (assuming $M = 1$). The estimated values were always within 5% of the measured values showing the accuracy of the estimation prior to detonation [2].

$$\dot{m}_{inj} = \frac{C_D A_{inj} P_T}{\sqrt{T_T}} \sqrt{\frac{\gamma_{gas}}{R_{specific}}} (1 + \frac{\gamma_{gas} - 1}{2} M_{inj}^2)^{\frac{-(\gamma_{gas}+1)}{2(\gamma_{gas}-1)}} \tag{10}$$

Table 6. Comparison of Cold Flow Measurements from Alicat Devices and their Corresponding Estimates from Equation 10

[2]

	Alicat Ox Measurement (SLPM)	**Alicat Fuel Measurement (SLPM)**	**Est. Ox C_D=0.70 (SLPM)**	**Est. Fuel C_D=0.70 (SLPM)**	**Percent Error (Ox)**	**Percent Error (Fuel)**
Case 1	1237	279.7	1277	279.8	± 3.23%	± 0.04%
Case 2	1520	275.1	1496	282	± 1.58%	± 2.51%
Case 3	1775	333.4	1792	348.5	± 1.00%	± 4.33%

While the Alicat controllers metered the flow well prior to detonation, they could not adequately adjust the flow during a detonation. During the detonation, it was found that there was ~ 0.20 MPa pressure differential across the controllers [2]. When adjusting mass flow, the Alicats should have opened more when the pressure differential across the controller was small and closed more when it was large. Discussions

with Alicat technicians revealed that a 0.17 kPa pressure differential would result in a 99% duty cycle for the upstream pressures that were being requested ($\sim$ 1.9 MPa). Since the controllers could not respond adequately this resulted in significant drops in mass flow after the detonation began.

Figure 38 shows this phenomenon where [A] denotes where the detonation begins and the mass flow decreases. This decrease in mass flow rate resulted in detonation mass flows that were much lower than what was requested and therefore specific test points of mass flow rate and equivalence ratio could not be tested reliably [2]. This presented a challenge to characterizing the operating space of the Micro-RDE since desired conditions could not be reached consistently. Figure 39 shows the requested, measured, and estimated mass flow rates before and after the detonation. As discussed, the mass flow rates before the detonation were more reliable than those after the detonation.

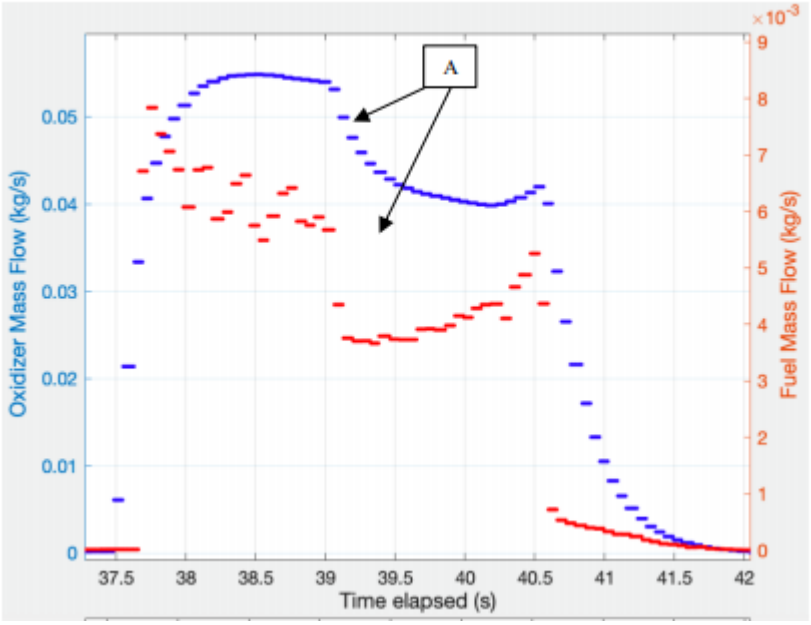

[2]

Figure 38. Example Mass Flow Time History. [A] Shows Flow Rate Drop Due to Detonation Beginning, adapted from Fiorino

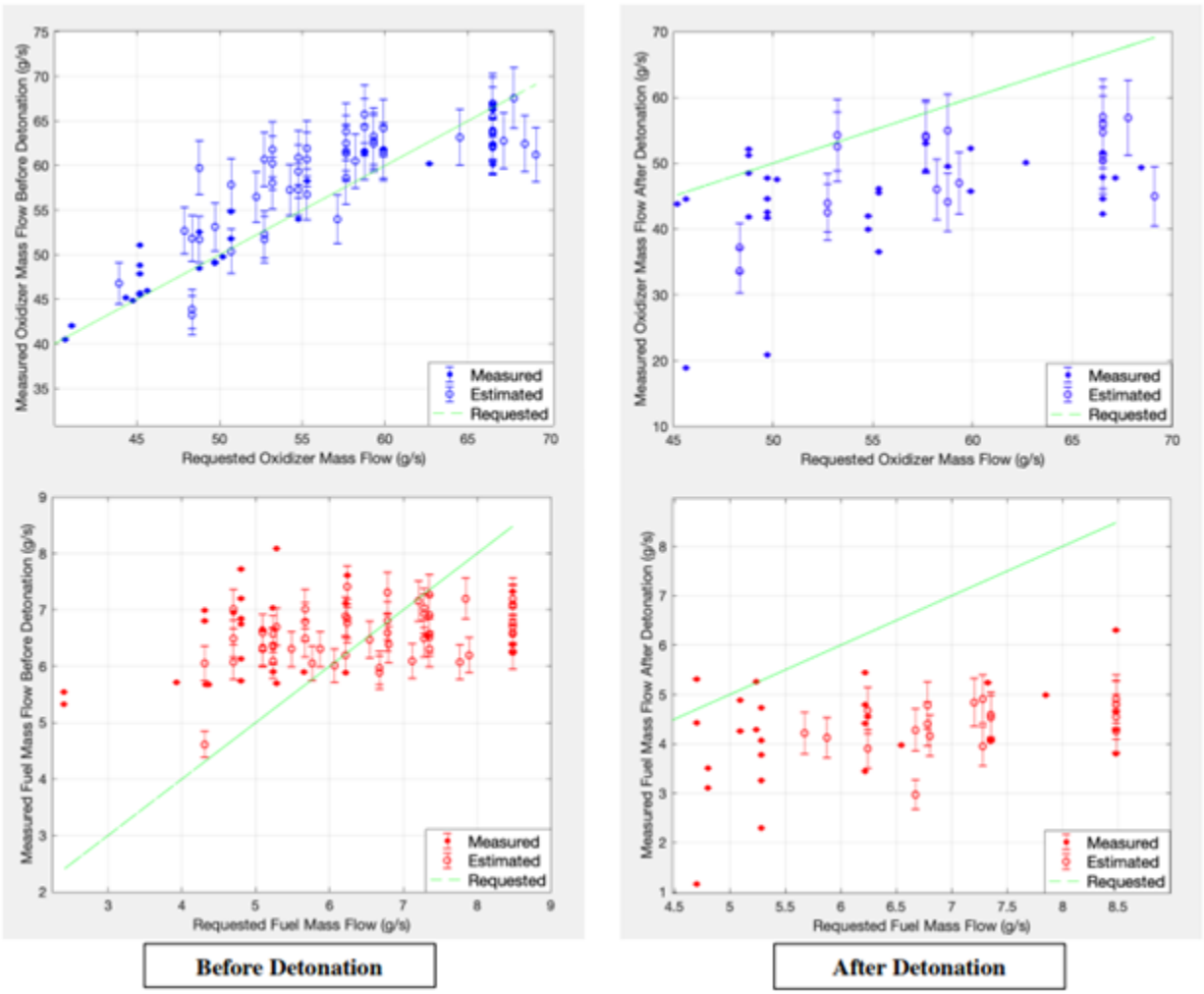

[2]

Figure 39. Observed Mass Flows versus Requested Mass Flows Before and After Detonation

3.3.2 Sonic Nozzles

To improve the reliability of the requested mass flow rates before and after the detonation, the Alicat controllers were replaced with sonic nozzles. Sonic nozzles are another method of metering flow and are widely used in the aerospace industry. These are operated by pressurizing the nozzle inlet with the desired gas which accelerates through the nozzle and reaches a "choked" or sonic state where the flow reaches a speed of Mach 1. Figure 40 shows the general schematic of a sonic nozzle where P1 is the inlet pressure, P2 is the pressure at the throat, and P3 is the exit pressure.

The choked state is revealed by a pressure ratio of the inlet to the outlet (P1:P3) of 1.2:1 or greater [31]. The main advantage of a sonic nozzle is it is unaffected by downstream disturbances in pressure. Differences in pressure downstream of the nozzle cannot move upstream past the throat of the nozzle since the velocity at the throat is at the speed of sound and therefore propagating downstream faster than the pressure disturbances can move upstream. Thus, the flow through the nozzle is unaffected. This advantage of keeping a constant sonic condition at the throat promised a better pressure recovery after experiencing disturbances in pressure downstream of the controllers due to detonations. This would allow for stabilized mass flow at the desired conditions before and after a detonation.

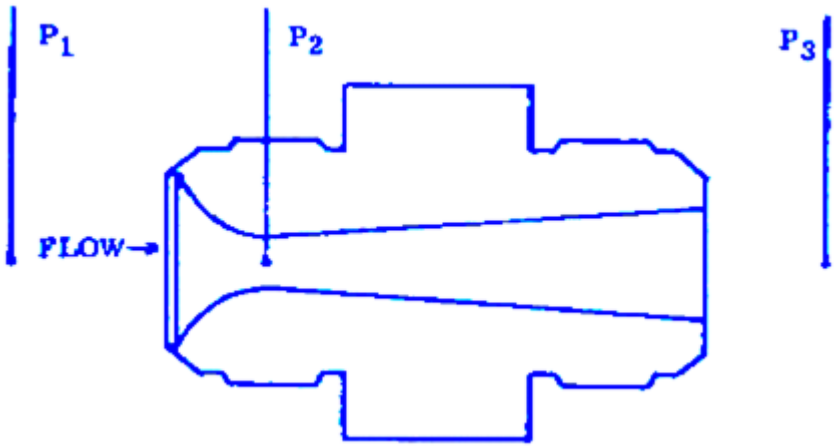

[31]

Figure 40. General Schematic of a Sonic Nozzle

While sonic nozzles provide this constant sonic condition, they must be sized according to the inlet pressure to properly choke the flow. Lower mass flow rates (and inlet pressures) require smaller nozzle diameters to be choked, while higher mass flow rates require larger nozzle diameters to reach the choked condition. Equation 11, the Universal Flow Function, was used to calculate the area of the nozzles necessary to choke the flow to output at the desired mass flow ranges, from 25 kg/s to 75 kg/s at equivalence ratios between 0.5 and 1.5. In said equation, A_{SN} is denoted as the area

of the desired sonic nozzle, while $\dot{m}$ is the desired mass flow rate through the nozzle. P_0 and T_0 represent the inlet pressure and temperature, respectively, and T_0 was kept at a constant 290 K assuming ambient conditions. P_0 was allowed to vary between 2.07 MPa and 3.45 MPa (300 psi and 500 psi) to ensure that the gases, specifically ethylene, didn't liquidize at the higher pressure limit and that the inlet pressure at the lower limit was sufficient to keep the nozzles choked. If the inlet pressure was out of these pressure bounds for a given mass flow rate than a different nozzle had to be utilized. R and γ are the specific gas constant and the ratio of specific heat for the desired gas flowing through the nozzle.

Ethylene and nitrous oxide were used as the reactants in the Micro-RDE, which correspond to a $\gamma = 1.24$ and $R = 296.4$ J/kgK for ethylene, and a $\gamma = 1.27$ and $R = 188.9$ J/kgK for nitrous oxide, still assuming an ambient temperature of 290 K. These values were found from [32]. Lastly, M, the Mach number, was assumed to be one to ensure the sonic condition was reached. As nozzle sizes are sold in terms of their diameter, Equation 12 solves for the diameter of the nozzle using the area found in Equation 11.

$$\frac{\dot{m}}{A_{SN}} \frac{\sqrt{T_0 R}}{P_0} = M\sqrt{\gamma}(1 + \frac{\gamma - 1}{2} M^2)^{\frac{-(\gamma+1)}{2(\gamma-1)}} \tag{11}$$

$$D_{SN} = 2\sqrt{\frac{A_{SN}}{\pi}} \tag{12}$$

This resulted in the use of four nozzles throughout the duration of testing on the Micro-RDE. The nozzles and their diameters can be seen in Table 7. The sonic nozzles used were engineered by and purchased from Flow-Dyne Engineering, Inc. All nozzles contained the following properties: made of 303 stainless steel, used A/N aircraft type connectors with a 37 degree flare, a height of 25.4 mm and a length of

63.5 mm. This allowed for continuity between the nozzles, aside from their various nozzle diameters, which allowed for relatively easy replacement seeing that all nozzles had the same outer dimensions. Additionally, all nozzles received a standard NIST Air Calibration by Flow Dyne Inc. before operation, which translated to mass flow data produced with an accuracy tolerance of less than 1 %.

When installing the nozzles, a Seco Seals Inc. 7C16 copper sealant was placed on each side to ensure flow in the tubes did not escape either end of the nozzle. Pressure transducers were situated upstream and downstream of the nozzle to measure the inlet and outlet pressures and confirm that the flow was choking properly (see Section 3.5). Bends or turns in the tubing directly before or after the flow crosses the sonic nozzle can cause the flow to unchoke or not choke at all. To properly choke flow across a sonic nozzle, a general rule of thumb is that there must be no bends in the tube within ten times the tube diameter upstream of the nozzle and five times the tube diameter downstream of the nozzle. These guidelines were followed in the installation of the sonic nozzles. Last Chance valves were positioned downstream of the sonic nozzle and were opened at the beginning of the run and closed at the end. Once the last chance valves were opened, the pressure across the nozzle was choked. The pressure was unchoked when the valves were closed at the end of the run. Figure 41 shows the layout of the RDE control system.

Table 7. Sonic Nozzle Diameters Used

Nozzle Diameter (mm)
1.12 (0.044 in)
1.37 (0.054 in)
2.67 (0.105 in)
3.18 (0.125 in)

Providing the right inlet pressure to the sonic nozzle was vital in ensuring the flow across the nozzle was choked. To do so, a Type 500X (E-I)/P Transducer pres-

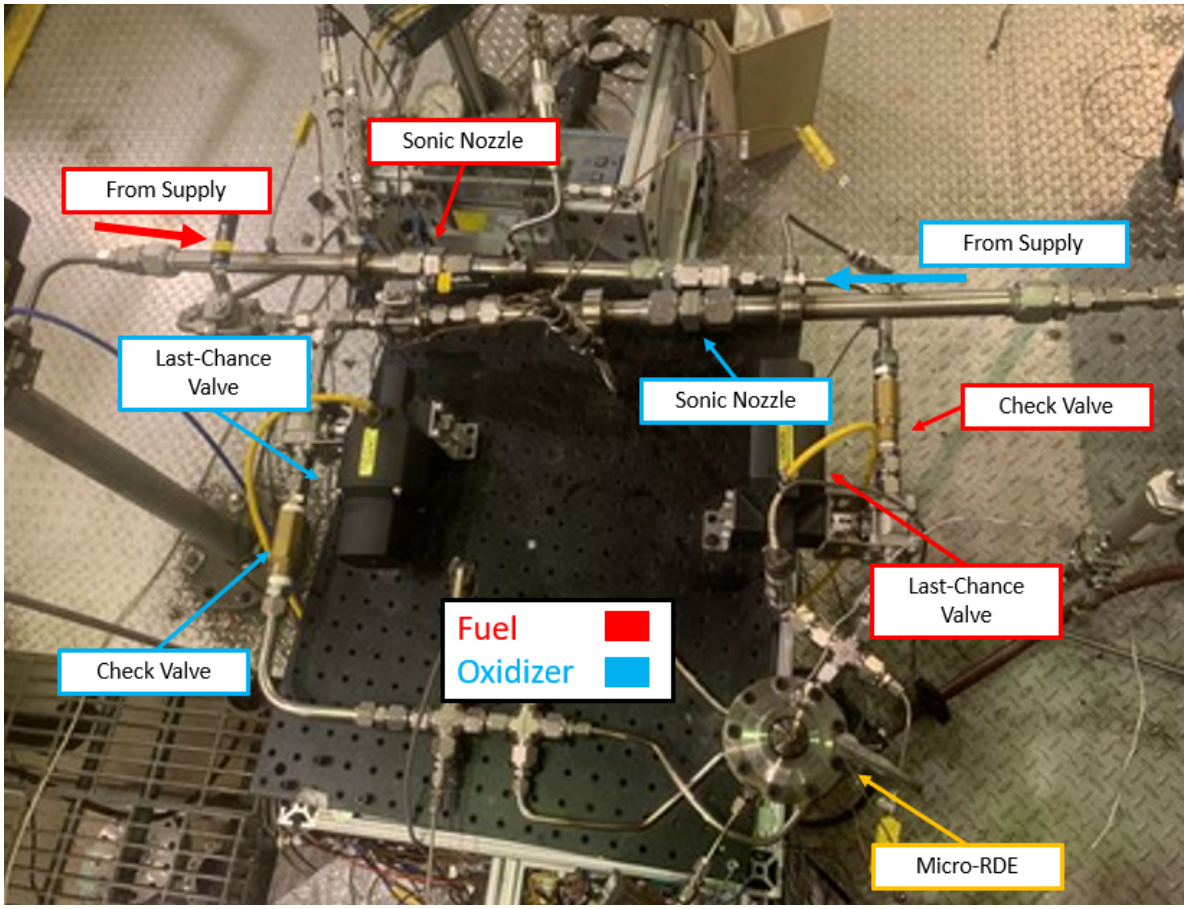

Figure 41. RDE Control System Layout with Sonic Nozzles

sure controller from Control Air Inc. was used on both the fuel and oxidizer side to pressurize the reactants before reaching the nozzle. An I/P Transducer, which used current as an input to control the pressure, was used on the oxidizer side while an E/P transducer, which used voltage as an input, was used on the fuel side. The controllers are the same, however one responds to changes in mA while the other responds to changes in V. A KNACRO voltage to current module converter was installed on the oxidizer side such that the pressure across both controllers can, in principle, be regulated by a voltage input.

To regulate the inlet pressure to the sonic nozzle, and thus input the desired mass flow rate for a specific run, a LabView program was operated from inside the

facility control room. A screenshot of this function on the program can be seen in Figure 42. This program allowed for the mass flow rate of the fuel and oxidizer to be inputted and manipulated separately to achieve the desired total mass flow rate and equivalence ratio. Discharge coefficient, assumed to be constant at 0.99 because of the NIST calibration, was inputted at the top of the program for both the fuel and oxidizer side. Mass flow rates for the respective reactants could be inputted in terms of kg/s along with the specific gas constants and ratio of specific heats that were previously mentioned.

Additionally, the diameter of the injectors, and the amount of injector holes, were inputted next to the diameter of the sonic nozzle. These values changed as the various injection schemes were tested. Using Equation 13, the ratio of the areas of the sonic nozzles to the injectors was calculated. If this ratio was less than 0.7, the indicator light would turn red indicating that the nozzle diameter was too large for the given configuration. This was created as a warning to the user to ensure that the flow was choked across the nozzle instead of at the injectors which could occur if the area ratio between the injectors and nozzle was too small. Choking at the injectors instead of the nozzle could produce undesired mass flows and insufficient pressure recovery after a detonation. If the area ratio was greater than 0.7, the indicator light labeled A_{SN}/A_{inj} would become green as seen in Figure 42, indicating the nozzle diameter was small enough to ensure the sonic condition was reached.

Using Equations 14 and 15, the inlet pressure required (in psi) to choke the flow across the nozzle and produce the desired mass flow rate was calculated. To reach that pressure, a voltage signal was adjusted from inside the control room and sent to the pressure controller which varied the actual pressure of the reactants. Voltage was manually adjusted by the user until the actual pressure was within 5 % of the pressure required to produce the desired mass flow rate. Due to the numerous bends

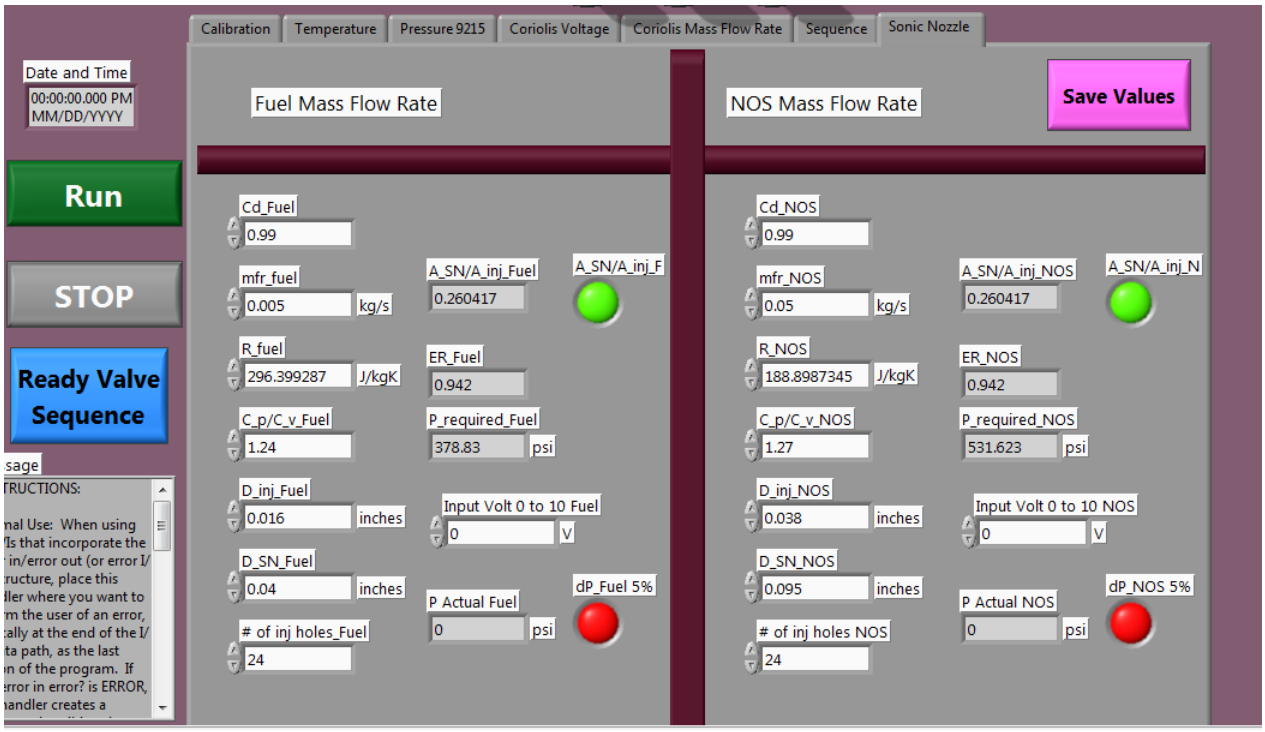

Figure 42. Labview Program for Mass Flow Control using Sonic Nozzles

between the fuel and oxidizer supplies and their respective sonic nozzles, the actual pressure was often set at the higher end of the "within 5 % range" to compensate for the consistent 68.9 - 103.4 kPa losses seen in the tubing leading up to the sonic nozzle inlet. The voltage was allowed to be adjusted to between 0 and 10 V, and the actual pressure was responsive to changes in voltage as low as 0.1 V. Once within the 5 % range of the pressure required, the bottom indicator light labeled dP 5 % (and currently red) in Figure 42 would turn green revealing the test point was ready to be ran. The actual pressure was measured from pressure transducers discussed in more detail in Section 3.5.1.

$$\frac{A_{SN}}{A_{inj}} = \frac{\pi(\frac{D_{SN}}{2})^2}{\pi(\frac{D_{inj}}{2})^2 * num_{injholes}} \tag{13}$$

$$P_{required} = \frac{0.00014504 * \dot{m}_{fuel} * \sqrt{(T_T - 32)(5/9) + 273.15} * MFP}{C_d * (\pi(\frac{D_{SN}}{2})^2) * (.0254^2)} \tag{14}$$

$$MFP = [\sqrt{\frac{\gamma}{R}} * (1 + \frac{\gamma - 1}{2})^{\frac{-(\gamma+1)}{2(\gamma-1)}}]^{-1} \tag{15}$$

3.3.3 Data Acquisition

Data logging was important in this experiment because it allowed the user to monitor the mass flow rate histories during a test run. To monitor the mass flow rate, pressure and temperature data were taken at points throughout the experiment. Pressure transducers were situated 7.6 cm upstream and downstream of the sonic nozzles to monitor the inlet and exit pressure across the nozzles. A thermocouple was placed upstream of the nozzles to measure the inlet temperature. The pressure transducers and thermocouples were situated around the nozzles on both the fuel and oxidizer side. Figure 43 shows the position of the pressure transducers and thermocouples with relation to the sonic nozzles. Data measurements were taken every millisecond via a National Instruments NI-cDAQ9185 (DAQ) chassis and were sent to the LabView program in the control room from which they were outputted to a .txt file at the end of every test run.

3.3.4 Flow Control Improvements

Using the data from the .txt files created via the data acquisition methods and Equation 10, the mass flow rate of the reactants throughout the duration of the test was able to be calculated. This data revealed that the use of sonic nozzles to meter mass flow into the Micro-RDE improved the stabilization of the flow during detonation conditions. Figure 44 shows a plot of the mass flow histories of a test run that resulted in a detonation using the sonic nozzle configuration. This test point was

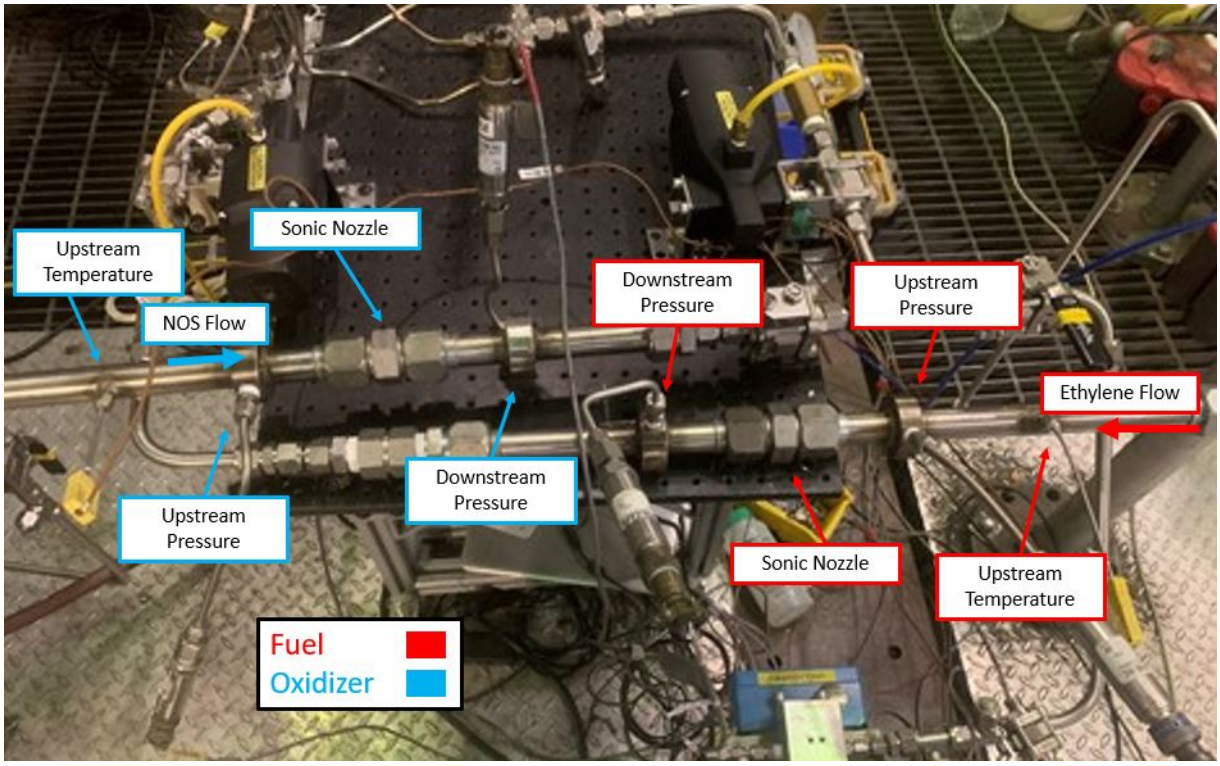

Figure 43. Position of Pressure Transducers and Thermocouples in relation to Sonic Nozzles

ran using the same injection scheme and nozzle size Fiorino used when highlighting the issues of the Alicat controllers. On the plot, the left axis represents the flow rate of the oxidizer while the right axis represents the flow rate of the fuel, both changing as time progresses from left to right. [A] and [F] show the regions before and after the test run, respectively.

It is important to note that the mass flow rate was calculated based off of pressure data, therefore as long as there was pressure in the lines there appeared to be mass flowing. To decipher between the apparent mass flow being recorded and the mass flow rates recorded during the run, the user had to search for abrupt drops in mass flow followed by an abrupt increase in mass flow, representing the beginning and end of the test run respectively. At the beginning of the run valves into the RDE were opened, causing the flow at the sonic nozzle to choke and drop in pressure.

This pressure drop across the nozzle equates to the apparent drop in mass flow rate denoted by [B]. At the end of every run the valves were closed, which caused the flow to unchoke and the pressure at the sonic nozzle (and the apparent mass flow) to increase. This is represented by [E] in the plot. Thus, the actual mass flow rates of the test run can be seen in between these regions.

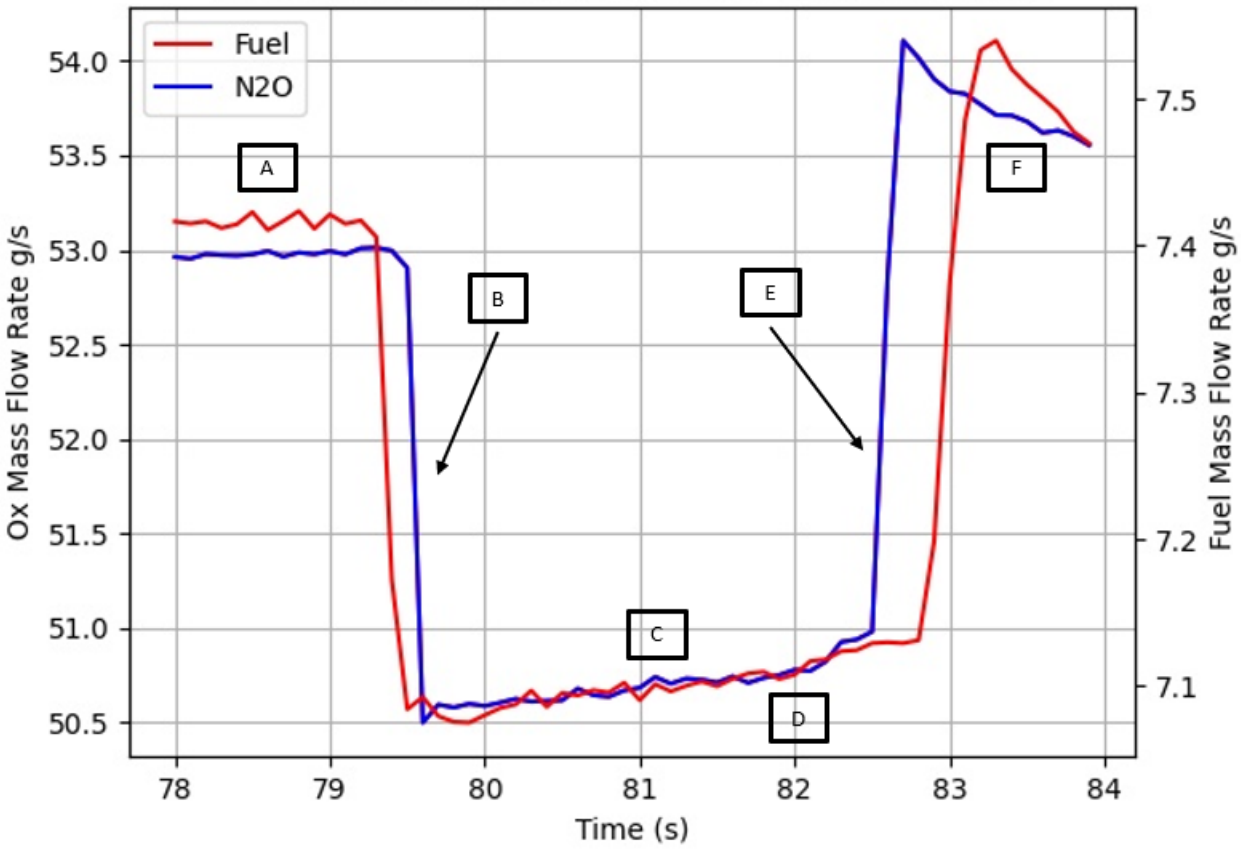

Figure 44. Mass Flow Time History in kg/s for a Run with a Detonation

Region [C] represents the entire duration of the test run from time t = $\sim$ 79.5 s to time t = $\sim$ 82.75 s. As seen in the plot, the mass flow rate of the fuel and oxidizer vary on the order of 0.01 g/s and 0.1 g/s respectively, showing stable flow during the entirety of the run. Point [D] denotes the beginning of the detonation in this run where there was seen to be a huge spike in the RDE chamber pressure. Mass flow rate was unaffected by the sudden increase in pressure that came with the detonation

event showing increased stability of the mass flow. This ability to have stable mass flow during detonation conditions, as opposed to the instability by the Alicats seen in Figure 38, reveals that the change to sonic nozzles increased the accuracy of flow control in the Micro-RDE thus increasing its overall operability.

In addition to solving the previous issue of unstable mass flow, the use of sonic nozzles also reduced the gap between the requested mass flow and the observed mass flow in the Micro-RDE. Fiorino's use of the Alicat controllers resulted in a 3.5 % and 18.4 % average percent difference in the oxidizer flow before and after a detonation, and an average 31 % and 32 % percent difference for fuel flows before and after detonations [2]. After replacing the Alicat system with the sonic nozzles, the same mass flow rates tested by Fiorino (25 g/s - 75 g/s for oxidizer) were tested using the same injection scheme he used (partially-premixed JIC) to properly compare the performance of the different flow meter systems. For direct comparison to Fiorino's results, the percent difference between the requested and observed mass flow rates for each test case was calculated using Equation 16. The percent difference for these test cases ran with the sonic nozzles can be seen in Figures 45 and 46, where for the majority of the points the percent difference for both the fuel and oxidizer fell below 5 %, averaging 2.81 % for the oxidizer and 2.71 % for the fuel. Typically the observed mass flow rate was slightly greater than the requested mass flow rate due to overcompensation of the losses in the lines by the user. Because the flow was shown to be stable, as seen in Figure 44, it was assumed that the percent difference for the reactants was the same before and after the detonation. Mass flow in the Micro-RDE was now sufficiently stable and accurate for other testing to continue.

$$\%Difference = \frac{Observed - Requested}{Requested} * 100\% \tag{16}$$

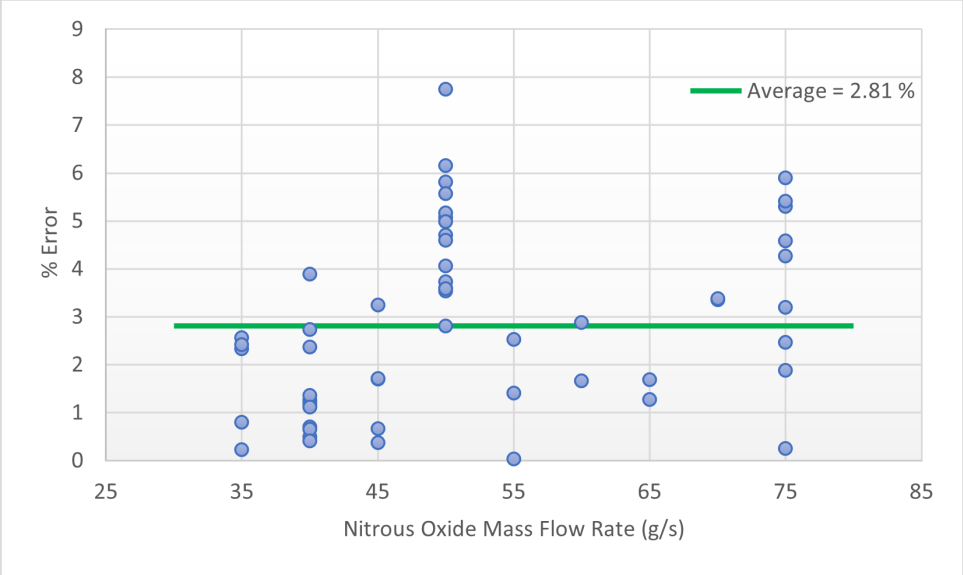

Figure 45. Percent Error between Requested and Observed Mass Flow Rates for Nitrous Oxide

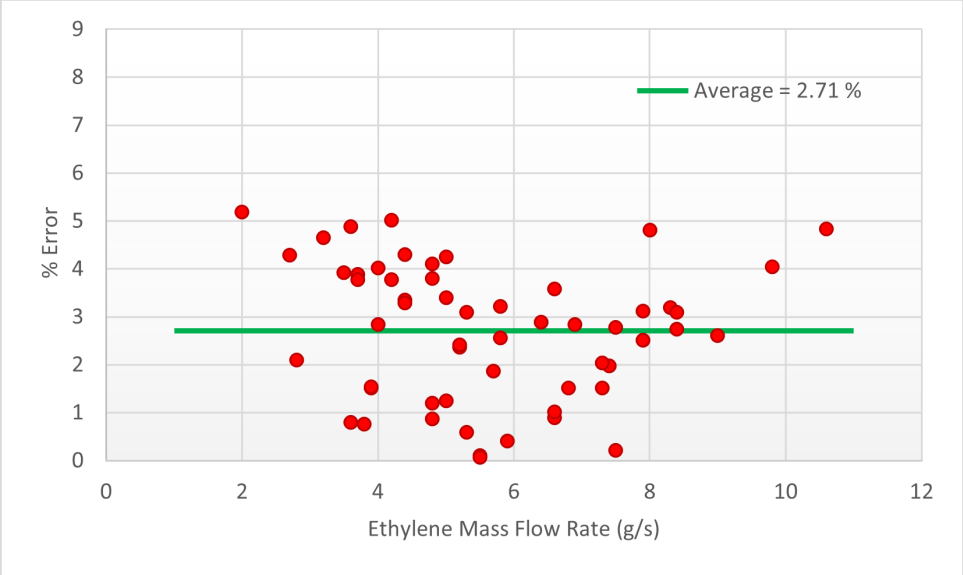

Figure 46. Percent Error between Requested and Observed Mass Flow Rates for Ethylene

3.4 New RDE Design Changes: Injection, Erosion and Optical Access

Building upon the previous work, this research aimed to further improve the survivability in the RDE, compare the individual designs of injection geometries, and gain optical access into the engine. Changes to the centerbody and material designed

to reduce erosion are covered in Section 3.4.1. The various injection geometries tested and their designs are found in Section 3.4.2 while the new Micro-RDE design that allows optical access into the detonation chamber is found in Section 3.4.3.

3.4.1 New Centerbody Design

Changes to Fiorino's design of the aerospike nozzle were made to reduce erosion and decrease the need for constant replacement. New aerospike nozzles were engineered out of Inconel 625 to reduce erosion. Inconel 625's stronger tensile strength at extreme temperatures made it the ideal choice of material when compared to the original material of the nozzles, 304 Stainless Steel. Additionally, to prevent the creation of a recirculation zone on the nozzle, the interface between the nozzle and manifold was moved to be flush with the injectors instead of its previous position, 15 mm above the injectors. This resulted in the creation of two new parts: a manifold without a centerbody and an elongated aerospike nozzle. These parts are shown separately and attached in Figure 47. For direct comparison, Figure 48 shows the old configuration of the aerospike nozzle next to the new. It is important to note that this figure shows the old configuration using the Plain JIC injectors while the new configuration uses the Partially-Premixed JIC because all the old configurations with the premixed geometry were eroded during testing by Fiorino.

To attach the two parts a 10 mm threaded rod was machined directly into the manifold, protruding from the side of the injected reactants. This longer rod was designed to allow for more threads to properly attach the two parts and prevent further ejected nozzles. Multiple sizes of nozzles were created to vary the exit area of the detonation chamber in the Micro-RDE. These nozzles created a 0.50, 0.625, and 0.75 mm diameter gap between the nozzle and outerbody. This equated to area ratios of $\epsilon = 0.26$, 0.33, and 0.39 where ϵ was the ratio of the nozzle throat area to

the channel area.

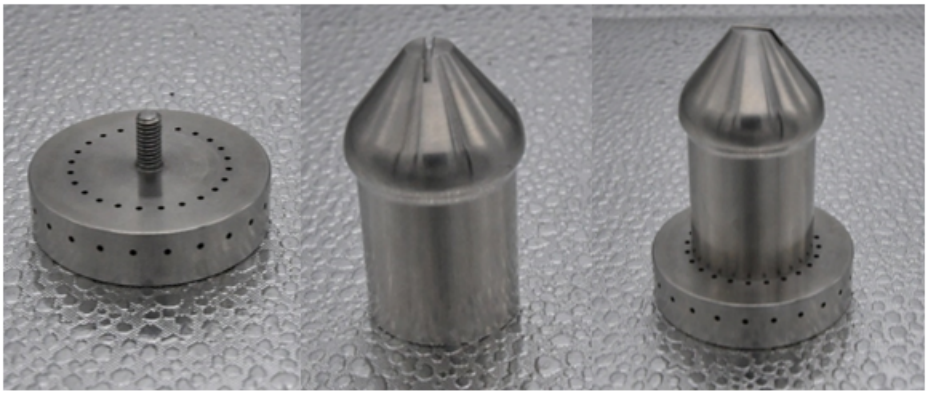

Figure 47. Modified Manifold (left) and Aero-Spike Nozzle (middle) Separate and Attached (right)

Figure 48. Old Centerbody Configuration by Fiorino (left) and New Centerbody Configuration (right)

Tests ran with the newer nozzle design revealed an increased resistance to erosion and no nozzles were ejected during testing with this configuration. Figure 49 shows a nozzle with the new design after experiencing twelve detonations. As pictured, there was little erosion to the nozzle even after multiple detonations, showing the improved heat resistance of the Inconel 625 material. Additionally, the movement of the point of connection between the nozzle and manifold proved to remove the recirculation

zone that was prevalent in detonations on the previous design. Although there was still a discontinuity between the nozzle and the manifold, its position was below the detonation, and therefore not susceptible to the high temperatures. This mitigated the possibility for any recirculation issues at that position.

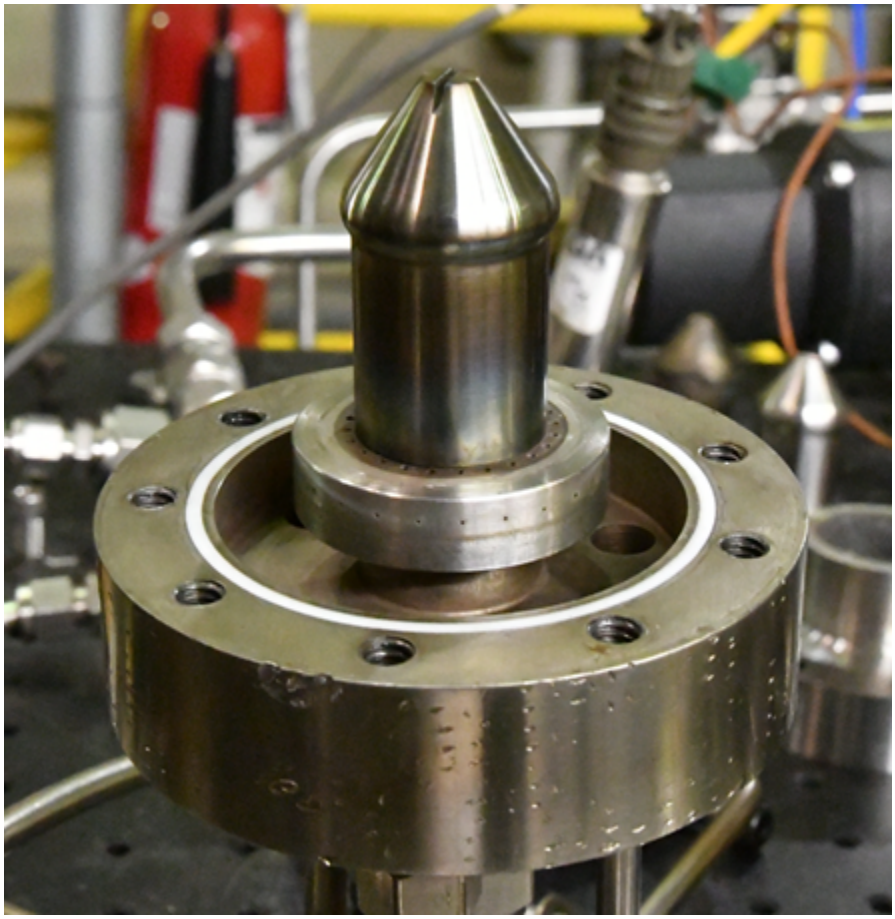

Figure 49. New Fuel/Ox Manifold and Nozzle After Twelve Detonations

3.4.2 Additional Injection Scheme Designs

Various injection schemes were tested on the Micro-RDE in this research. When testing the injection schemes, all other components of the RDE were kept constant including the mass flow rates tested and the aerospike nozzle size that created a 0.75 mm channel gap ($\epsilon = 0.39$). In some cases, the addition of a different injection

schemes warranted the use of a different outerbody. The injection scheme design and any potential changes to the outerbody while incorporating the said injection scheme are as follows.

3.4.2.1 Plain JIC

In a Jets-in-Crossflow (JIC) injection scheme, oxidizer and fuel are injected into the detonation channel 90 degrees from each other and intersect at what is called the point of crossflow. In a traditional JIC scheme, this point of crossflow is inside the detonation channel. The version of the JIC that is used on the Micro-RDE also keeps the point of crossflow inside the detonation chamber, hence the name "Plain JIC". This injection geometry is identical to the geometry utilized by Dechert, and can be seen in Figure 50. Like Dechert's design, in this design the oxidizer is injected axially and the fuel is injected radially using a separate oxidizer and fuel manifold. However, in this design the diameters of the injectors were 0.40 mm and 0.89 mm for the fuel and oxidizer, respectively. Comparing to Dechert's design, he had the same diameter for the fuel injectors, but a 1.09 mm diameter for the oxidizer injectors. Dechert also used 24 injectors for both fuel and oxidizer injectors, while this design used 24 injectors for the fuel, and 16 for the oxidizer. Thus the total area of the oxidizer injector holes was decreased by decreasing their individiual hole size and the number of injectors. Decreasing the area of the oxidizer injectors was intended to help retain pressure in the detonation chamber. For more information about the implementation of this injection scheme on the Micro-RDE, see Dechert [1].

3.4.2.2 Partially Premixed JIC

The other variation of the JIC injection scheme tested on the Micro-RDE was the Partially-Premixed JIC. This JIC scheme was designed by Fiorino and moves the

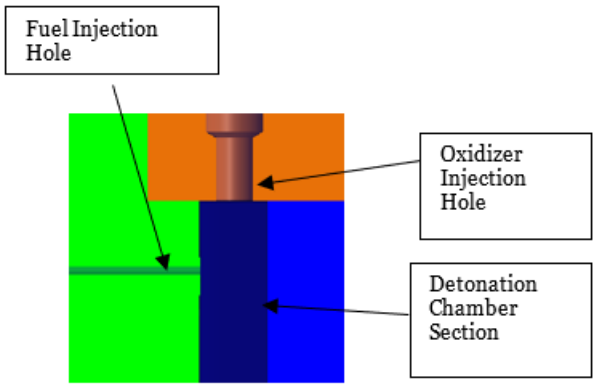

[2]

Figure 50. Plain Jets-in-Crossflow Injection Geometry, adapted from Fiorino

point of crossflow from inside the detonation chamber to 2 mm before the entrance as shown in Figure 51. This design uses fuel injectors with a 0.40 mm diameter and oxidizer injectors with a 0.96 mm diameter, having 24 injectors for each reactant. Like the Plain JIC, the oxidizer is injected axially and the fuel is injected radially. Unlike the Plain JIC, a combined fuel/oxidizer manifold was used to inject the reactants.

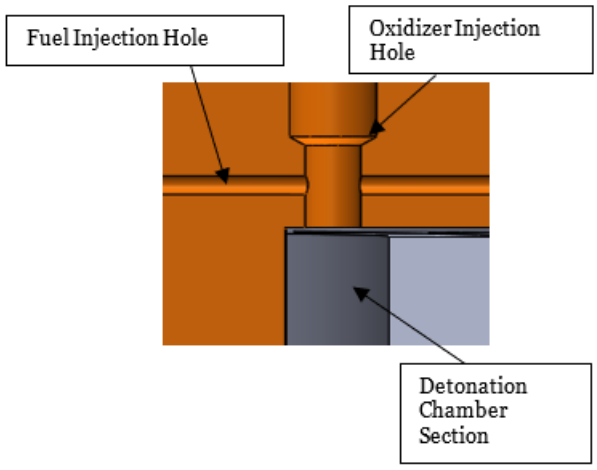

[2]

Figure 51. Partially Pre-mixed Jets-in-Crossflow Injection Geometry, adapted from Fiorino

3.4.2.3 Simplex

A variation of the simplex pressure swirl nozzle was designed by Nathan Snow and used as one of the injection schemes on the Micro-RDE. Traditional simplex injection geometries utilize liquid reactants in lieu of gaseous, but this simplex was designed with more and larger injector holes than typical to account for the use of gaseous nitrous oxide in this research. For direct comparison with the Plain JIC injection geometry, the injector holes had the same diameter and amount as those of the Plain for both the fuel and oxidizer (Fuel: 0.40 mm x 24, Ox: 0.89 mm x 16). Traditional simplex designs also create the swirling phenomenon for the fuel injected into the RDE, while the oxidizer is simply injected radially. As seen in Figure 52, Snow's design flips this, injecting the fuel radially while swirling the oxidizer. In this design small threaded screws were used as helical grooves to produce the radial flow in the swirl chamber. The centrifugal forces of this swirling flow were then intensified in the converging spin chamber upon which the flow was expected to be ejected through the discharge orifice and produce a spray cone. A separate fuel and oxidizer manifold were used to inject the reactants, with the oxidizer manifold being split into a top and bottom piece. The bottom piece possessed the helical posts and the top piece constructed the swirl chamber, spin chamber, and discharge orifice.

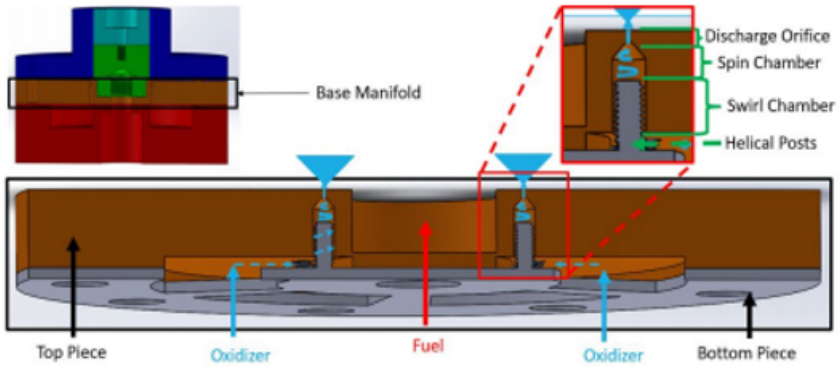

Figure 52. Simplex w/ Swirling Oxidizer Injection Geometry [courtesy of Nathan Snow]

3.4.2.4 Counter-jet

The last injection geometry tested in the Micro-RDE was the Counter-Jet. In this injection scheme, a separate fuel and oxidizer manifold were used. Both reactants were injected radially from their perspective manifold, but the oxidizer was injected towards the center of the RDE while the fuel was injected towards the outer radius. Assuming the injectors were properly aligned, this caused the stream of the fuel injected to directly collide with the stream of the injected oxidizer. A schematic of this injection scheme can be seen in Figure 53. The fuel was injected through 24 holes 0.40 mm in diameter and the oxidizer was injected through 24 holes 0.79 mm in diameter. It is important to note that because of the configuration of the outerbody, the pre-det hole had to be moved up to 20 mm above the connection plate. This was not ideal since all other injection schemes possessed predets positioned 5 mm above the injectors (positioned at the connection plate) to allow for adequate ignition time and prevent recirculation points, but this was necessary based on how the configuration was designed. Additionally, more tests were ran on this configuration where the injectors were intentionally offset by 7.5 degrees to compare with the results of tests ran when the injectors were directly aligned.

3.4.3 Incorporation of Optical Outerbody

A quartz tube was used to provide optical access into the chamber. The cylindrical quartz tube served as the outerbody for the detonation channel and was purchased from Quality Quartz Engineering with an inner diameter of 27.9 mm, an outer diameter of 41.9 mm, and a length of 31.75 mm. The installation of the quartz tube required different methods depending on whether the injection scheme utilized combined or separate fuel and oxidizer manifolds. For the combined fuel and oxidizer manifold, used by the Partially-Premixed JIC, the base of the RDE outerbody (Figure 54a) was

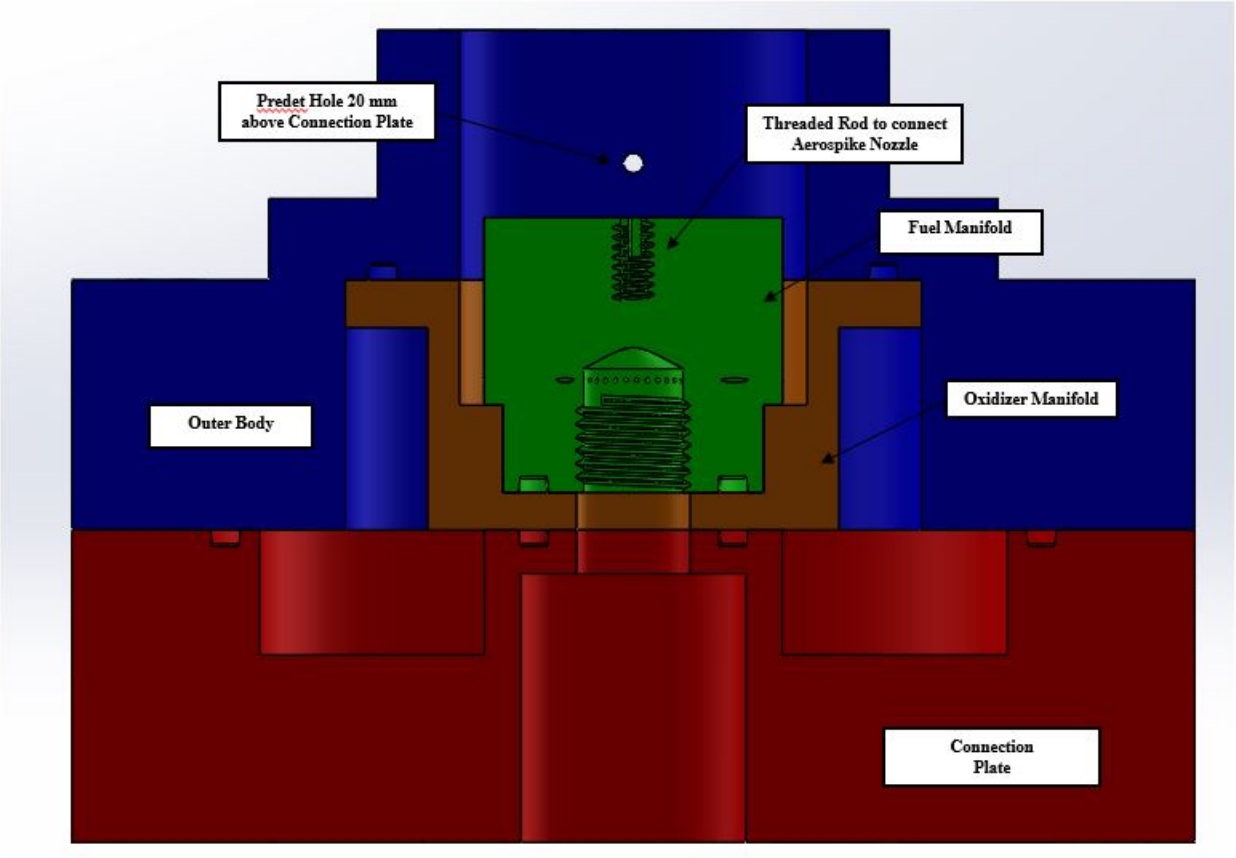

Figure 53. Counter-jet Injection Geometry [courtesy of Nathan Snow]

used to house the quartz tile. A 1 mm groove was machined into the outerbody base (Figure 54b) where the quartz could be placed during the run. Figure 54c shows the quartz positioned in the groove of the outerbody base to allow for optical access into the detonation chamber.

For the separated fuel and oxidizer manifolds, used by the Plain JIC and the Simplex, the 1 mm groove was machined into the oxidizer manifold as seen in Figure 55 such that the quartz tube was placed there during testing rather than the outerbody. Thus, no part of the original outerbody was used for this configuration. Because the outerbody connected the pre-detonator device to the detonation chamber, a new method for injecting heat energy from the pre-det device to ignite the reactants was needed. A 3.18 mm hole was drilled 2 mm into the oxidizer manifold to allow for

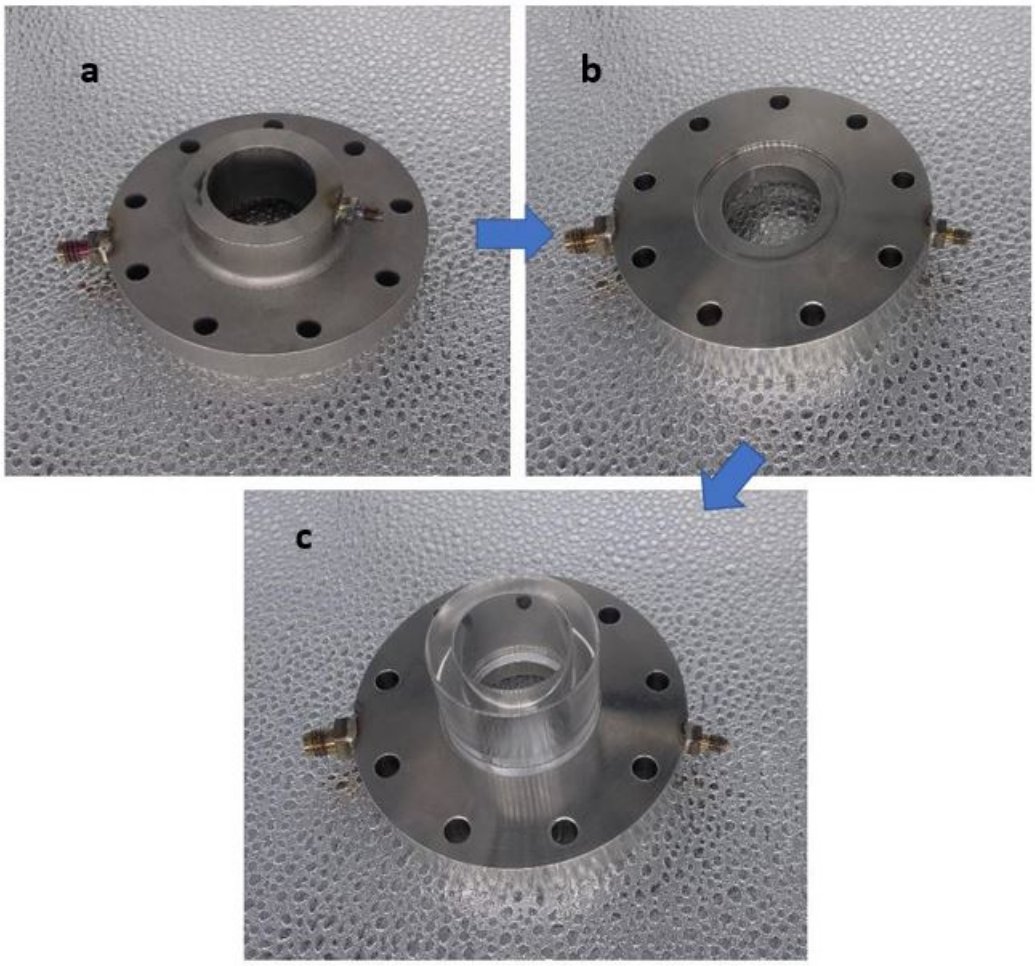

Figure 54. Process for Incorporating Optical Access into Partially-Premixed JIC: a) Original, b) Groove Cut into Outerbody Base, c) Optical with Quartz

connection to the pre-det device. From there, a 0.70 mm hole was further drilled radially into the oxidizer manifold,as seen in Figure 55, and then drilled axially upon reaching the point where reactants would be injected into the detonation chamber. The hole was drilled on the side of the reactants exiting the injection scheme, allowing for the heat energy to be injected into the chamber parallel to the flowing reactants.

For both optical configurations, a top plate with screws was used to ensure the quartz tube remained attached to the rig during testing (Figure 56). A 1 mm groove for the quartz tube was also machined in the metal top plate. This configuration is

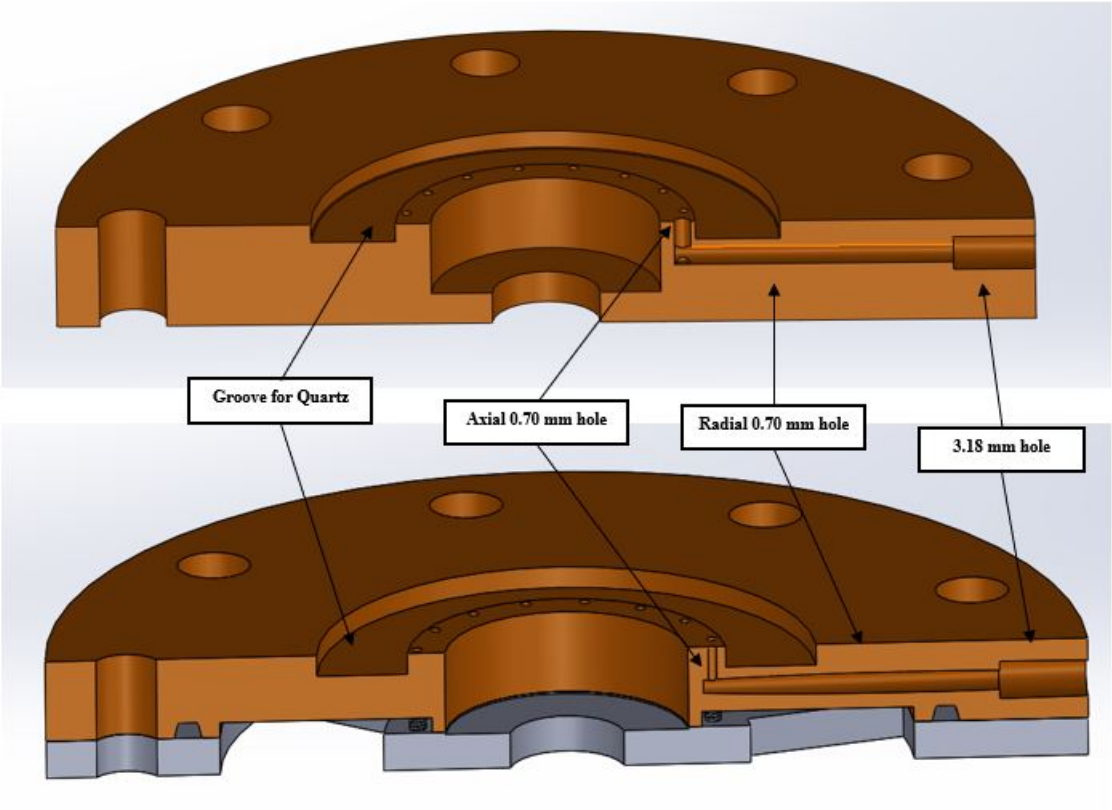

Figure 55. Optically Accessible Oxidizer Manifolds for Plain JIC (top) and Simplex (bottom)

similar to the optically accessible RDE tested by Rankin [25] (for more information see Section 2.6). Graphite gaskets were used to seal the flow between the quartz tube and the top and bottom metal pieces while also preventing contact between the hot metals and the quartz tiles. For some runs, additional silicone rings were used to provide extra cushion for the quartz, however this addition never became an official part of the optical configuration. To allow for visualization into the chamber, long screws to pin the quartz down to the RDE were positioned in every three slots to prevent the screws from being barriers in the way of the high-speed imagery. Springs were used on these screws to allow for the quartz tube to expand with the RDE during detonation conditions while still holding the quartz in place between the top plate and optical outerbody. Additional screws that weren't used to pin down the

quartz tile were placed in the remaining six slots to ensure the outerbody (or oxidizer manifold) was properly pinned down to the RDE base. Because the goal of this part of the research was purely to gain optical access, no pressure readings were taken in the RDE chamber for any optical configurations.

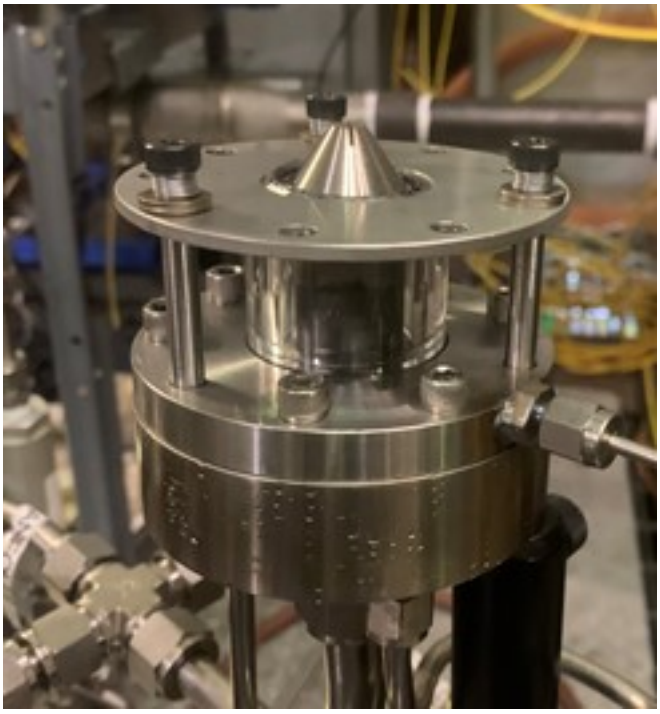

Figure 56. Optically Accessible Micro-RDE

3.5 Instrumentation

Pressure and temperature data were used to measure mass flow and used along side high-speed cameras to characterize the pre and post detonation conditions. The general setup of the instrumentation was based off of previous work by Dechert[1] and Fiorino[2] but additional changes were made to cater towards the new goals of the RDE system. The pressure and temperature instrumentation is outlined in Section 3.5.1 and the instrumentation of the high-speed imagery is outlined in Section 3.5.2. The data produced by this instrumentation was used to analyze the reliability of

the new mass flow controllers and also characterize the performance of the injection designs. Additional uses of the data included imaging of the detonation wave using the optical access into the detonation chamber.

3.5.1 Pressure and Temperature Readings

As documented by Dechert and Fiorino, a single pressure sensor was positioned in the oxidizer supply line, in the fuel supply line, and in the detonation channel. In addition to the original placement of these sensors shown in Figure 57, two pressure sensors were placed around the sonic nozzle, one upstream and one downstream, for both the oxidizer and fuel lines. The sensors placed in the oxidizer and fuel lines were placed directly between the respective last chance valves and the RDE. These sensors measured the instantaneous static pressure of the fuel and oxidizer before injection into the RDE. Both locations utilized high speed OMEGA PX429-500A5V pressure transducers which sampled data at 1000 Hz with an accuracy of $\pm$ 0.08 % over a range of pressures from 0 to 3.45 MPa [1]. The sensor inside the detonation channel was a high speed OMEGA PX429-250A5V pressure transducer which also sampled data at 1000 Hz, however its range of $\pm$ 0.08 % accuracy only spanned 0 to 1.7 MPa. These sensors and their specifications are discussed in more detail by Dechert [1].

New pressure transducers were added to the Micro-RDE configuration to ensure a choking condition was reached across the sonic nozzles. The position of these pressure transducers are seen to the left (downstream) and right (upstream) of the sonic nozzle in Figure 57. Upstream of the sonic nozzle on both the fuel and oxidizer lines was a PX429-1000A5V pressure transducer. This sensor sampled data at 1000 Hz with an accuracy of $\pm$ 0.08 % over a range of pressures from 0 to 6.89 MPa. Downstream of the sonic nozzle on both the fuel and oxidizer line was a PX429-1000G5V pressure transducer. This sensor sampled data with the same accuracy and over the same

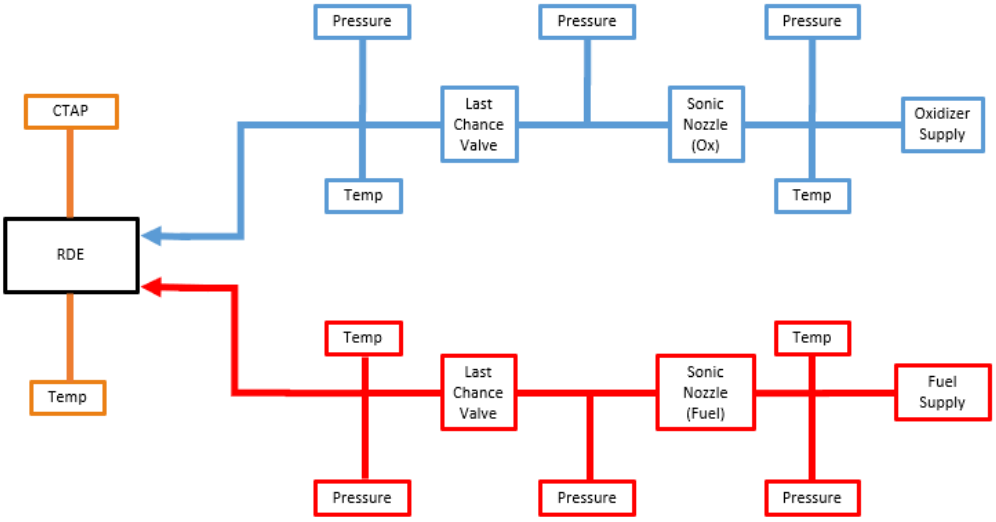

Figure 57. Schematic of Temperature and Pressure Instrumentation

range of pressures (± 0.08 % from 0 to 6.89 MPa) but at a frequency of 2000 Hz.

A Capillary Tube Average Pressure (CTAP) reading was connected by connecting the OMEGA PX429-250A5V pressure transducer to the detonation channel with a long tube. This long tube allowed for the high frequency pressure fluctuations from the detonation wave to be damped out before reaching the pressure transducer [2]. Thus, the pressure reading from the transducer represented the average static pressure in the channel rather than an instantaneous pressure. During pre-detonation conditions when there were no high frequency fluctuations, the average pressure reading was approximately equivalent to the instantaneous pressures in the channel.

Initially, the long tube from the pressure transducer was cold welded into the detonation channel using a JB Weld epoxy adhesive. Early tests using this configuration revealed that this adhesive could not consistently hold the CTAP inside the chamber during detonation conditions which resulted in many ejected CTAPs during testing. Thus, the CTAP was brazed into the outerbody of the RDE to prevent further removal from the detonation chamber during testing. The change from a cold welded

to a brazed CTAP can be seen in Figure 58.

Figure 58. CTAP configuration with JB Weld (left) and Braze (right)

All pressure transducers were powered by a 12 V power source as seen in Figure 59. The transducers returned a 0 – 5 V output signal to the NI-9215 control board module on the DAQ which interpreted the signal and converted it into a pressure reading. To distinguish between pressure readings, each pressure transducer corresponded to a specific channel on the control board. The channel number and the position of its associated pressure transducer can be seen in Table 8. These pressure readings were outputted to a .txt file at the end of every run for data analysis.

In the original configurations of Dechert and Fiorino, temperature data was gathered using K type Omega thermocouples positioned in the oxidizer and fuel lines. Additional K type thermocouples were added upstream of the sonic nozzles on the fuel and oxidizer lines to give temperature readings needed to calculate the pressure

Table 8. Channel and Pressure Transducer Position for NI-9215 Control Module

Channel	Pressure Transducer
1	Ox Plenum
2	Fuel Plenum
3	RDE Chamber (CTAP)
4	SN Ox Upstream
5	SN Ox Downstream
6	SN Fuel Upstream
7	SN Fuel Downstream

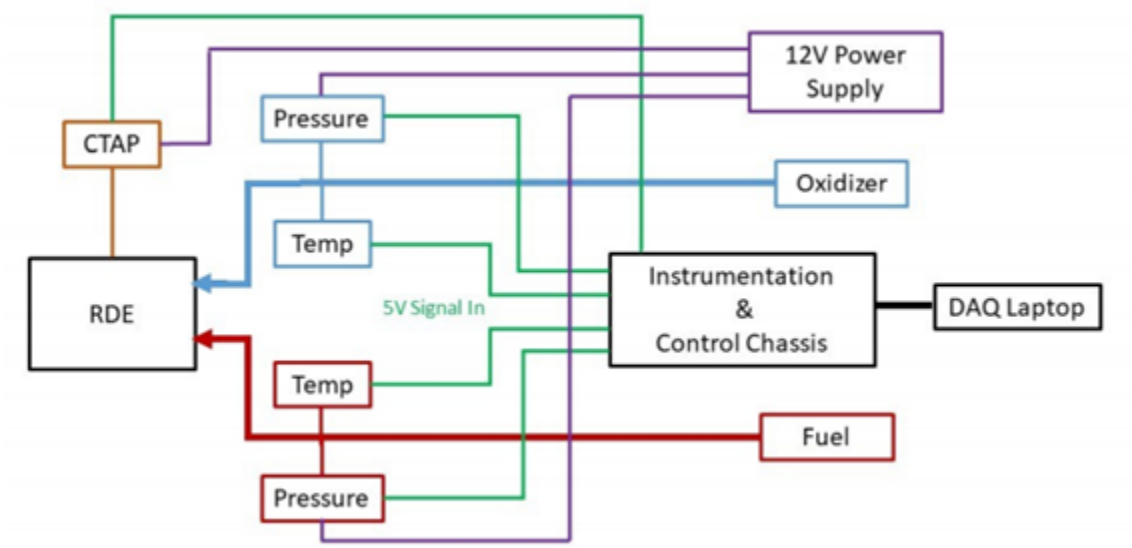

[1]

Figure 59. Schematic of Pressure and Temperature Readings from Control Chassis

required to choke across a nozzle in Equation 14. Another K type thermocouple was placed on the RDE outerbody to measure the temperature of the RDE itself before runs because detonations add temperature to the RDE which create more detonable conditions for the following run. All thermocouples measured temperature with the NI-9214 control board module on the DAQ. As with the pressure readings, temperature readings from different thermocouples corresponded with different channels on the control board. The channel number and the position of the associated thermocouple can be seen in Table 9. The NI-9214 control board module interpreted the voltage signal with an accuracy of $\pm$ 2K over a range of temperatures from 233 K to

343 K. This more than covered the anticipated temperature range of 250 – 300 K.

Table 9. Channel and Thermocouple Position for NI-9214 Control Module

Channel	Thermocouple
0	Ox Plenum
1	Fuel Plenum
4	RDE Outerbody
5	SN Ox Upstream
6	SN Fuel Upstream

3.5.2 High-Speed Imagery

Phantom v711 high-speed cameras were used to capture the footage of the propagating detonation wave to determine the detonation frequency. Two configurations were used to capture this footage. The first was the traditional setup used by Dechert and Fiorino to visualize the rotating detonation inside the channel from a top-down view as seen in Figure 60. This was used for the testing of various injection schemes without the optical access. A single camera was positioned away from the test stand but directed towards a mirror directly above the RDE. This setup allowed for visualization directly down the channel while protecting the camera from the hot exhaust that come with detonation conditions. The same 5V signal that triggered the spark for the ignition mechanism was used to trigger the camera recording to ensure video was taken at the correct time.

For the first configuration, the "top-down" camera was set to 79,000 frames per second at a resolution of 256 x 256 pixels. The resolution was increased from 128 x 128 pixels used by Dechert and Fiorino to prevent the channel from moving out of the frame should the RDE, or the table it was resting on, vibrate during detonations. At the frame rate of 79,000 fps, the position of the detonation wave could be oversampled approximately four times if the RDE operated at the design frequency, 20 kHz. Additionally, an exposure time of one microsecond was used during test runs. This

allowed for the detonation light, the brightest light during the run, to be visualized while filtering out other light such as deflagration or any other outside lighting around the RDE. In general, the camera settings were set and adjusted to the user's desire and could be changed based on visual preference.

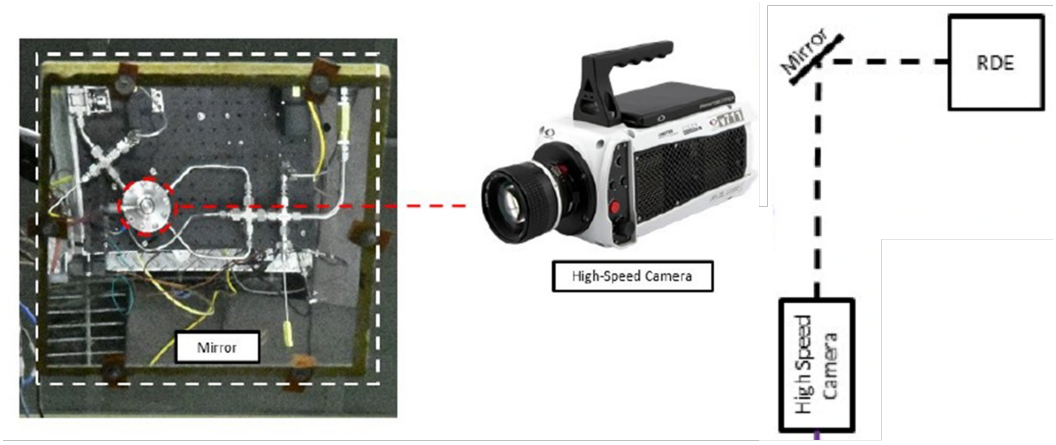

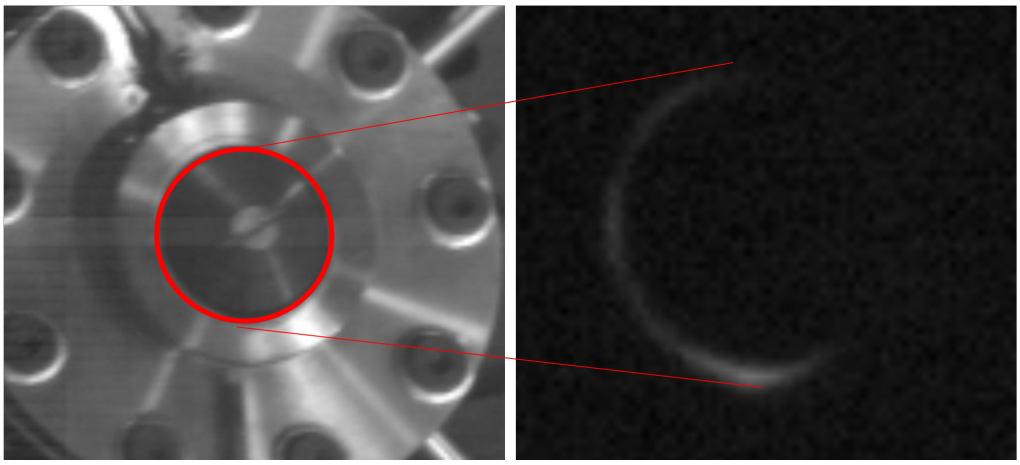

[2]

Figure 60. Schematic of First Configuration of Camera with respect to RDE (top), Picture from Resulting Frame (left), Video from Corresponding Frame (right), adapted from Fiorino

The second configuration was used when gaining optical access into the detonation chamber, and utilized the same "top-down" setup as the first with an additional Phantom camera directly aimed at the side of the RDE. This gave not only the top-down view of the detonation channel but also a side view of the detonation through the transparent Quartz tube as seen in Figure 61. To ensure the videos

were directly synced, the 5V signal that triggered the spark and the camera in the first configuration was also simultaneously sent to the side view camera so the videos started recording at the same time. To capture the entire quartz in the frame, the side view Phantom camera was set to a resolution of 800 x 600 pixels. An exposure time of 10 microseconds was used to filter out other light during the test run and frames were were captured at 13000 frames per second.

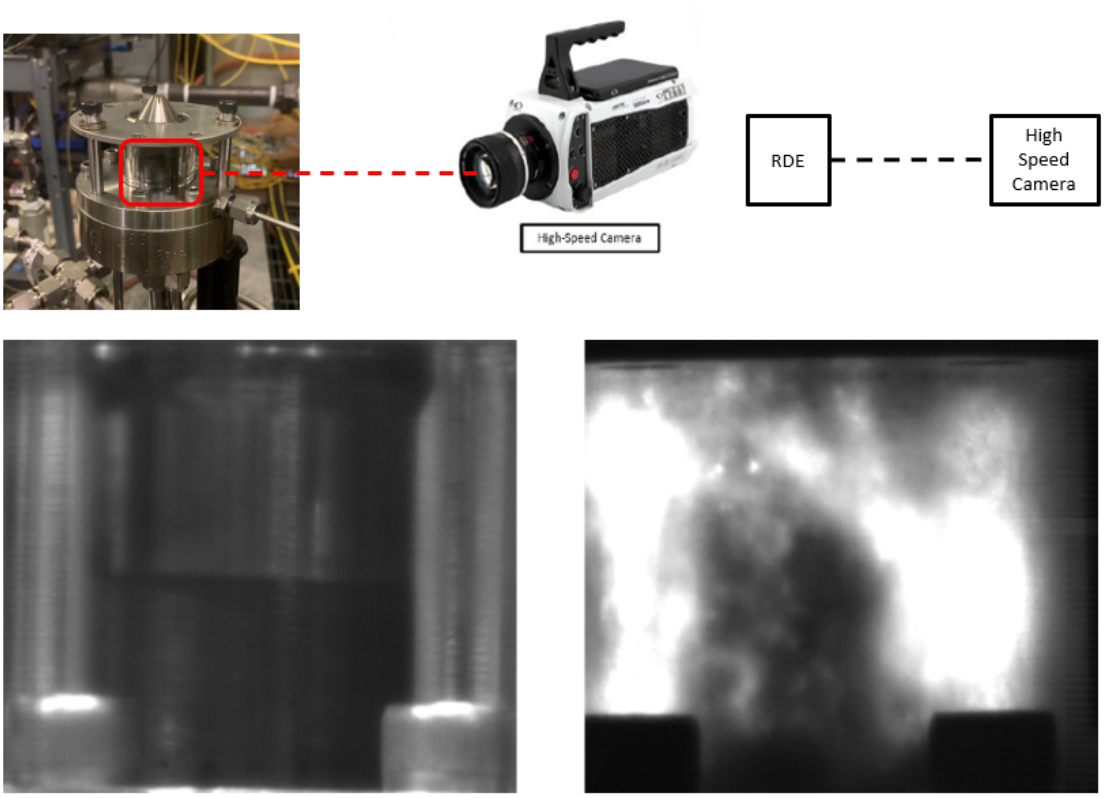

Figure 61. Schematic of Second Configuration of Camera with respect to RDE (top), Picture from Resulting Frame (left), Video from Corresponding Frame (right)

IV. Testing, Results, and Analysis

Using the methods discussed in Chapter III, the Micro-RDE's performance was characterized and compared with previous work to ascertain how the different injection schemes affect its operating map and detonation wave stability. In Section 4.1, the effects of temperature on producing detonations in the Micro-RDE, or the lack thereof, is discussed to establish uniformity of testing. Section 4.3 compares the operability of the Micro-RDE as it changes with the various injection scheme, while Section 4.4 does these same comparisons on injection scheme performance in the Micro-RDE in terms of wave stability. Section 4.2 highlights the settling times of the plenum pressures of the fuel and oxidizer as a function of run time, another sign of detonation stability in the Micro-RDE. Lastly, Section 4.5 highlights the further changes made to optimize the optical configuration along with the analysis of the optical data taken from this portion of the research.

4.1 Micro-RDE Temperature Effect on Detonations

In combustion, the temperature of the engine prior to ignition highly influences the performance or lack thereof of the running engine. Regardless of their composition, all reactants have a specific amount of energy needed to ignite and result in combustion. This amount of energy required is decreased as the initial temperature of the reactants is increased and more ideal combustion conditions are made [3]. In experimental combustion reactions, an external source of heat is typically used to add the necessary heat to the reactants to trigger an ignition. The external source of heat in the case of the Micro-RDE is the pre-detonator. Heating the reactants prior to combustion can be done directly by heating them at their source or achieved indirectly by heating the engine prior to flowing the reactants through it. To further understand the

Micro-RDE and ensure the testing performed was controlled, the temperature of the outerbody and injected reactants were monitored.

Prior to the start of every testing day, the RDE base experienced ambient temperatures of 292 K +/- 2 K. These small deviations were assumed to be influenced by the varying outdoor temperature but were minute enough to assume a constant starting temperature at the beginning of every testing day. While never manually heated, the temperature of the RDE base increased after experiencing detonation events, thus creating more detonable conditions for the next test run. Temperatures of the outerbody after detonation were seen to range between 302 K and 336 K, with the higher temperatures stemming from the heat provided by one or more consecutive detonations. Figure 62 plots the temperature of the RDE base for every run prior to testing.

In Figure 62, it is seen that there are no obvious trends in the influence of temperature on detonability in the Micro-RDE. The base temperature and equivalence ratio are shown for every test along with a legend to show which injection scheme was ran for each specific case. A solid circle denoted a detonation while an open circle denoted no detonation. No apparent trends on the temperature of the base of the RDE were seen to influence the testing of the various injection schemes. While some injection schemes ran at higher temperatures than others, all injection schemes were initially ran at the same temperature and increased detonability for a specific configuration was likely due more to the configuration tested and not the temperature of the RDE base.

The RDE could only be heated by a previous detonation. Since mass flow sweeps were performed from fuel lean to fuel rich equivalence ratios, it was likely that a detonation would already be produced regardless of the temperature since higher fuel ratios have previously performed better in the Micro-RDE. Because some injection

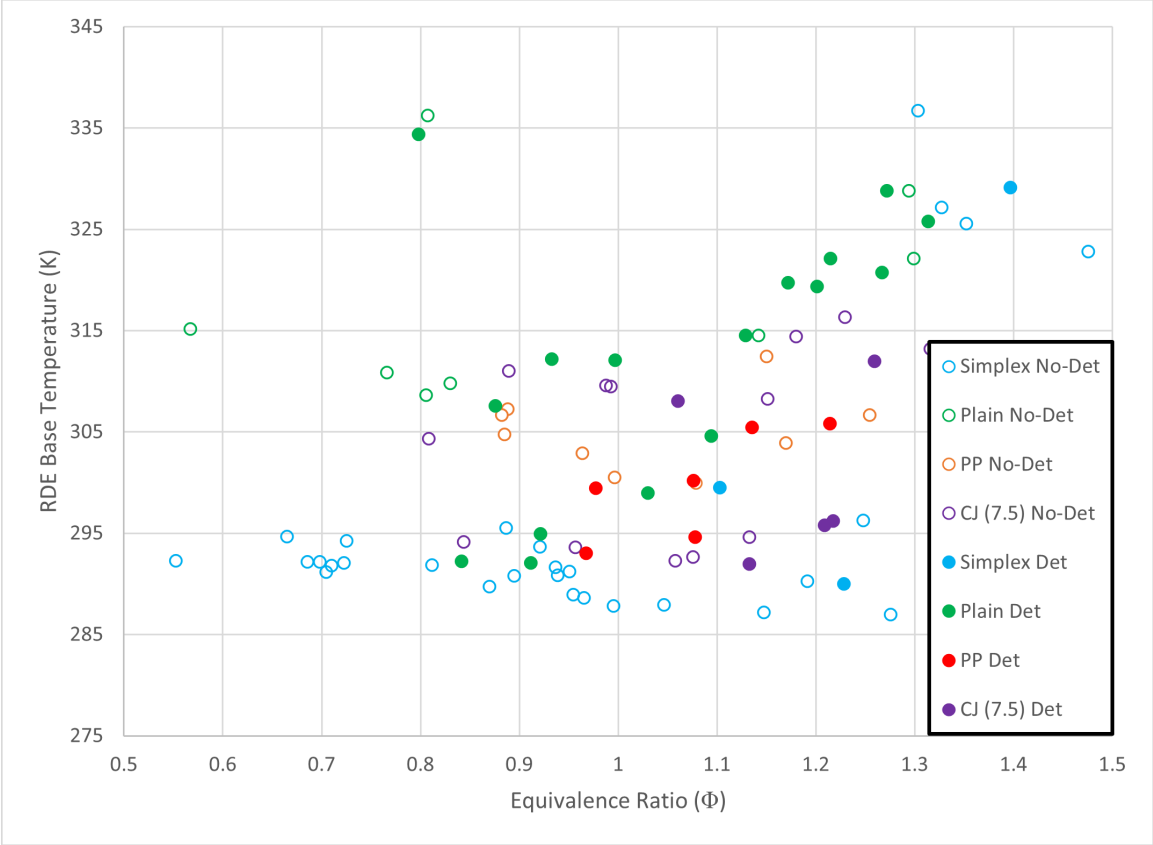

Figure 62. Detonability of Micro-RDE with Changing Base Temperature

schemes had a much larger operating map and consequently ignited more, it is not apparent on whether these injection schemes ignited because of their higher temperature or because they simply detonate at that specific test point.

While it was assumed that increased temperature of the base would help improve detonability, the $\sim$ 40 degrees Kelvin range of temperatures experienced by the RDE during testing did not have a profound impact on the detonability of the injection schemes. The plain injection scheme was the most detonable injection geometry, and produced detonations at both ambient and high temperatures. The simplex typically remained at ambient temperatures and saw few detonations, but when heated there was no consistent sharp rise in detonations. It is also important to note that in this study, plenum temperatures of the reactants were monitored, but not deliberately

changed to avoid an increase or decrease in temperature that would result in a different pressure/mass flow condition other than the one desired by the user. Thus the temperature of the RDE did not play a factor in the comparison of the injection schemes tested in this research.

4.2 Settling Time on Pressure in Plenums

Achieving steady plenum pressure of the reactants during detonation is a key parameter that influences detonation stability. The stability of pressure across the injectors directly affects the mixing of the reactants which in turn affects the stability of the detonation wave. Previous testing by Fiorino saw an inability to settle this pressure during detonation conditions using the Alicat controllers [2]. It was believed that the use of sonic nozzles as the mass flow control system would not only stabilize the flow across the nozzles but also across the injectors. Early testing with the sonic nozzles showed that this was not the case.

Figure 63 shows the pressure time histories of a test ran at 50 g/s $\phi = 1.2$ using Fiorino's Partially-Premixed JIC injection scheme. It is important to reemphasize that this, and all other test sequences, were ran for 4.1 seconds total giving 3.5 seconds for the reactant flow across the sonic nozzles to stabilize and a 0.6 second window for the user to fire the predet to ignite the reactants. However, total "run" times as logged by the LabVIEW code were significantly longer as the test was considered running as soon as pressure and temperature data began being logged. Additionally, the 0.6 second window for detonation did not always translate to a 0.6 second detonation as there was a slight delay for the user to fire the pre-det and ignite the reactants. The window simply translated to a 0.6 second period where the pre-det could be fired. This traditionally resulted in detonations lasting between t = 0.3 – 0.5 seconds.

As seen in Figure 63, the detonation starts at time t = 3.7 seconds marked by the

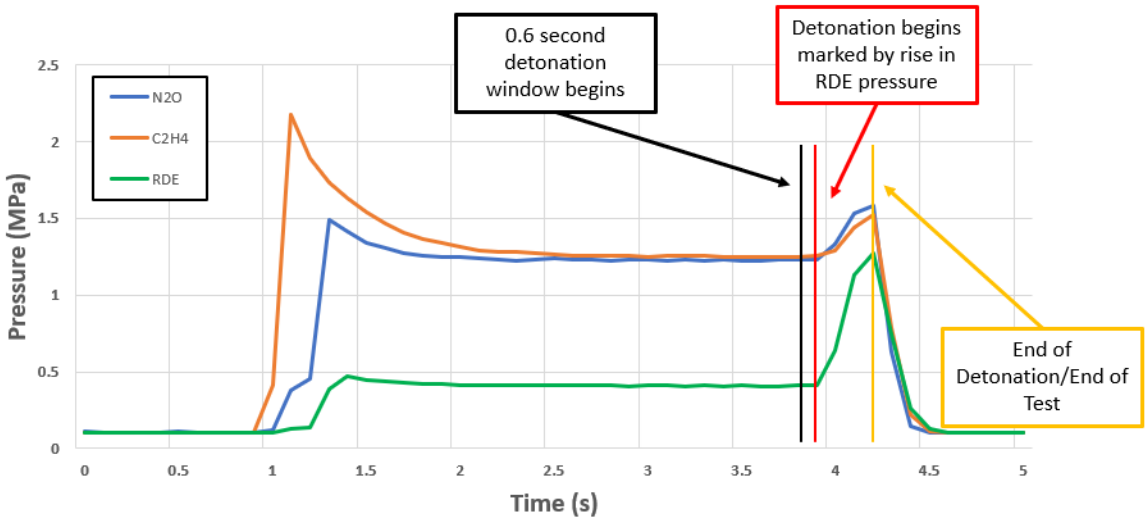

Figure 63. Pressure Time History for Run at 50 g/s and $\phi = 1.2$

beginning of the high-pressure spike in the RDE chamber. This pressure continues to rise until the end of the run at time t = 4.2 seconds where reactants are no longer supplied to the detonation wave. It is seen that with the rise in pressure of the RDE the pressure in the plenum of the nitrous oxide and ethylene also rises and never settles to a steady pressure throughout the detonation. It was hypothesized that the 0.6 second window for a detonation, which usually produced ~ 0.4 second detonations due to the delay of having to manually fire the pre-det from inside the control room, was not enough time for the reactants to settle into a steady plenum pressure after the detonation began. However, this 0.6 second detonation window was specifically chosen to prevent erosion to the Micro-RDE, as longer run times are associated with more energy, higher temperatures and higher pressures.

As shown in Section 4.3, tests using the new Plain JIC injection scheme experienced detonations as low as 12 g/s. Due to the low mass flow rates flowing through the RDE which consequently produce less energy in the detonations, this provided the opportunity to run longer tests to explore the settling time of plenum pressures without the concern of erosion. To explore the settling time three tests were run at

12 g/s $\phi = 1.4$: 1) a normal test with a 0.6 second window for detonation (used as a control) 2) a test with a three second window for detonation and 3) a test with a six second window for detonation. These tests were ran after the vibration of the RDE during testing was identified and mitigated by securing the RDE base to the testing table. Although movement was still present, more and longer periods of a stationary channel in the frame were experienced.

The pressure time histories of these tests are seen in Figure 64 with a), b), and c) representing the tests with 0.6, 3, and 6 second windows for detonation, respectively. All pressure data for these three tests are shown at one second before the beginning of the test (where the fuel valves are opened) to ten seconds after the test began to give sufficient data to capture the behavior of the pressures recorded. Figure 64 a) shows the previously seen phenomenon where the plenum pressures spike with the chamber pressure and do not settle before the end of the test run. The test run with the three second detonation window, pictured in b), shows a trend that appears to begin to settle however never fully reaches steady state conditions before the run ends. However, c) shows that the run with a six second window settles to within 5 % of the final value of the plenum pressure at 1.2 seconds for the fuel and 0.5 seconds for the oxidizer.

Additional data analysis shown in Figure 65 shows that the detonation frequency of the six second detonation window run increases with time and then settles in the middle of the run. This shows possible signs that since the conditions of the plenum pressures are not stable in the shorter runs, the detonation wave does not have adequate time to settle into its final state and thus the observations of the detonation wave (i.e. frequency) could be taken at various conditions. However, when test duration is increased and consequently the conditions are allowed to stabilize, then the detonation wave is able to settle into its true state. This evidence of stable

plenum pressure at longer run times could lead to longer tests in the Micro-RDE to continue improving the stability of the conditions of the detonation wave which will result in more accurate observations of the detonation wave.

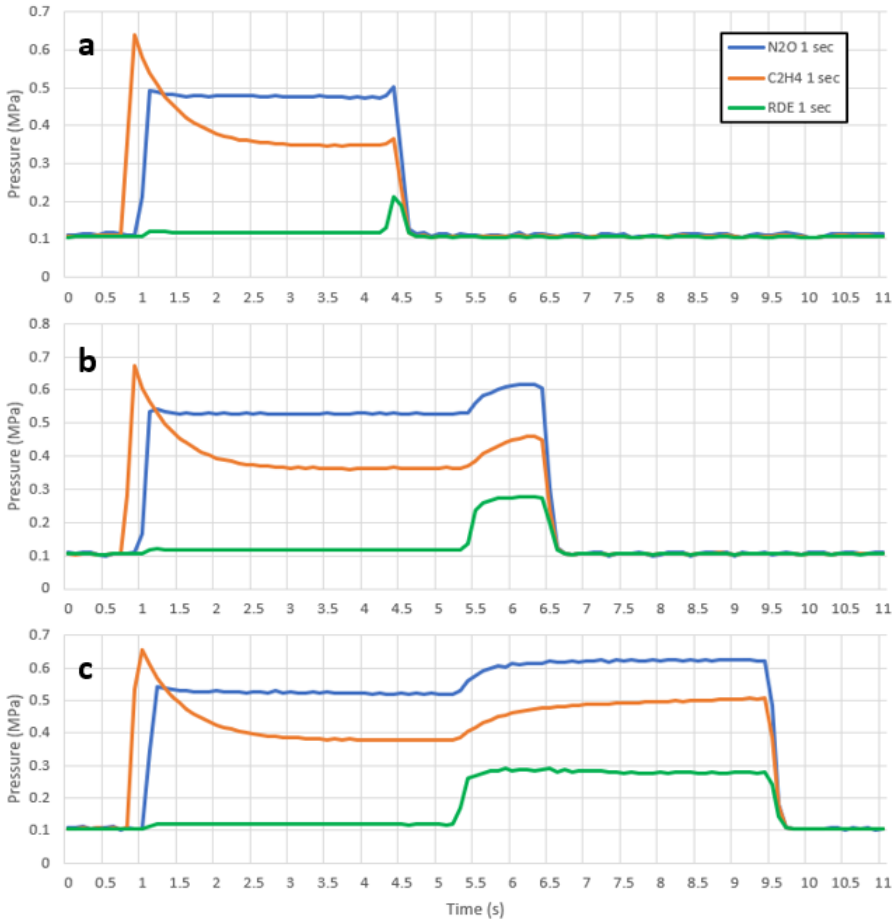

Figure 64. Pressure Time Histories for a) 0.6, b) 3, and c) 6s Run at 50 g/s and $\phi = 1.2$

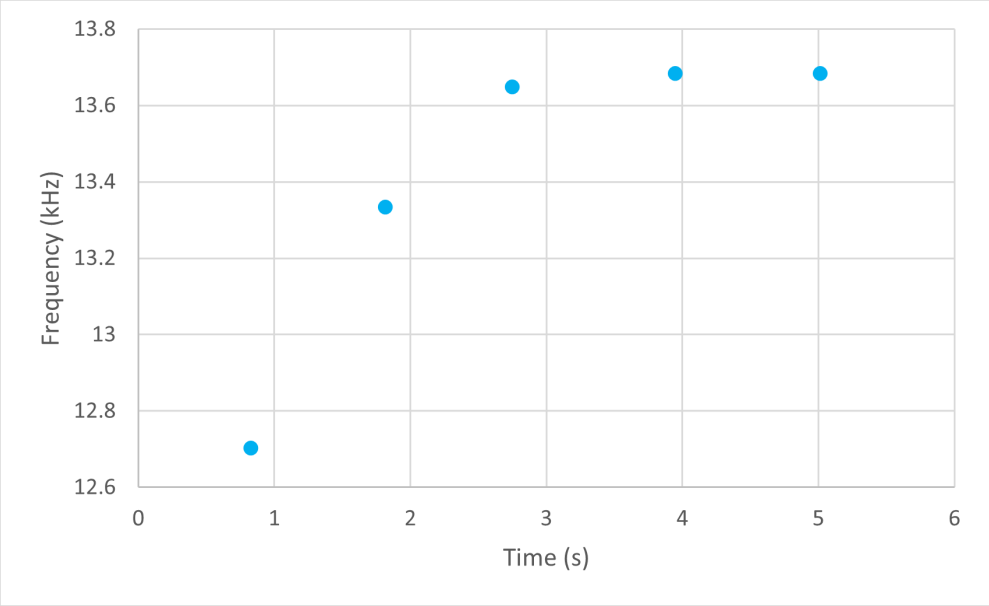

Figure 65. Detonation Frequency versus Time for Run with 6s Detonation Window

4.3 Micro-RDE Operability in Different Injection Schemes

Mass flow rate and equivalence ratio are important parameters in the production of a propagating stable detonation wave. Mass flow rates must be high enough for the detonation wave to be self-sustaining, but low enough for the reactants to be consumed and not blowout the wave. Equivalence ratios must keep the mixture within the flammability limits of the reactants. Too rich or too lean equivalence ratios can keep combustion from occurring. The goal of this part of the research was to find the limits of mass flow rate and equivalence ratio on the various injection schemes outlined in Section 3.4.2.

To compare the operability of various injection schemes in the Micro-RDE (Plain JIC, Partially-Premixed JIC, Simplex, and Counter-jet), tests were ran to see the regimes where detonations were found. Mass flows were tested between 25 g/s and 55 g/s across equivalence ratios between 0.5 and 1.5. The upper end of mass flows at 75 g/s was not tested because it was assumed that injection schemes that produced a detonation at a lower mass flow rate, would also produce a detonation at a higher

mass flow rate. Tests were ran at $\sim$ 50 g/s, and were methodically lowered to lower mass flow rates until detonations were no longer produced, while also sweeping across the full range of equivalence ratios. All configurations used a pre-detonator to ignite along with aerospikes nozzle that produced 0.75 mm channel gaps at the exit of the detonation chamber ($\epsilon = 0.39$). Different outerbodies were used to implement various injection schemes, and pre-ignition chamber pressures and mass flow data were used to track any variations stemming from the different configurations. In general, testing between the various injection schemes was kept as consistent as possible to properly compare their performance. When necessary, specific changes were made to accommodate for the implementation of specific geometries. The results of the tests with the Plain JIC, Partially Pre-mixed JIC, Simplex and Counter-jet are presented individually and then summarized together.

4.3.1 Partially-Premixed Injection Scheme

Tests on Fiorino's Partially-Premixed Jets-in-Crossflow injection geometry were ran to validate its operating map and potentially push its lower limits[2]. As seen in Figure 66, detonations were seen at mass flows between 45 g/s and 55 g/s spanning equivalence ratios from 0.7 to 1.3. An additional single detonation was seen below 40 g/s but was not repeatable and was therefore disregarded as an outlier in the data. It was hypothesized that because of previous detonations the base temperature held more temperature than usual and created more ideal conditions for ignition at this lower mass flow rate (see Section 4.1 for the effects of temperature on detonability).

In previous research Fiorino tested the same configuration except with a variation of aerospike nozzle sizes, using tighter nozzles ($\epsilon = 0.26, 0.33$) in addition to the sole nozzle size used in the current configuration ($\epsilon = 0.39$) [2]. During testing Fiorino saw detonations from experimental tests ranging from mass flow rates between 45 g/s to

60 g/s at equivalence ratios between 0.6 to 1.2 (see Figure 17). Overall, comparing the two operating maps validated the lower limit of 45 g/s with this specific configuration of the Partially-Premixed Jets-in-Crossflow in the Micro-RDE.

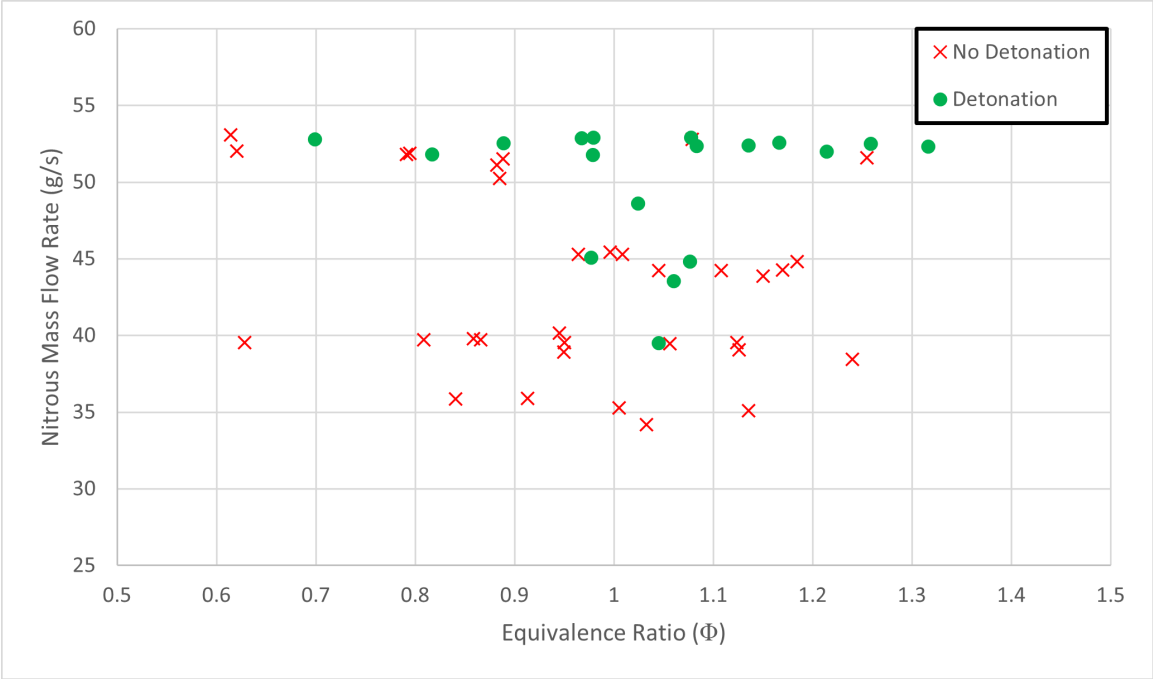

Figure 66. Operating Map of Partially-Premixed JIC Injection Scheme

4.3.2 Plain Injection Scheme

Tests on the Micro-RDE using the Plain JIC configuration were ran to develop its operating map. As discussed in Section 3.4.2, this injection scheme was directly identical to the configuration utilized by Dechert [1]. The difference was that the oxidizer holes were changed from 1.09 mm x 24 NOS holes to 0.89 mm x 16 NOS holes. Through this change a huge expansion to the operating map is seen in Figure 67 as opposed to Dechert's original operating map seen in Figure 15. (It is important to reiterate that Dechert's operating map was a function of his requested mass flow rates and not the observed, as there were issues with his mass flow control system that he was unaware of.)

This new Plain configuration, along with an improved mass flow system, resulted in detonations at 50 g/s with ϕ ranging from 0.7 to 1.4, thus further expanding Dechert's operating map to more lean equivalence ratios. Pushing the bounds of the operating map even further, the plain produced consistent detonations at 30 g/s between equivalence ratios of 0.8 and 1.3. Because of its performance at such low mass flow rates, additional tests were conducted below the initial testing limit of 25 g/s to explore the full limits of this configuration. As shown in Figure 67, detonations were seen as low as 12 g/s, the lowest seen in this Micro-RDE configuration. Tests ran at these mass flow rates only detonated when very rich (between equivalence ratios of 1.4 and 1.5), giving evidence of decreased mixing quality at these lower mass flows although detonations were still experienced.

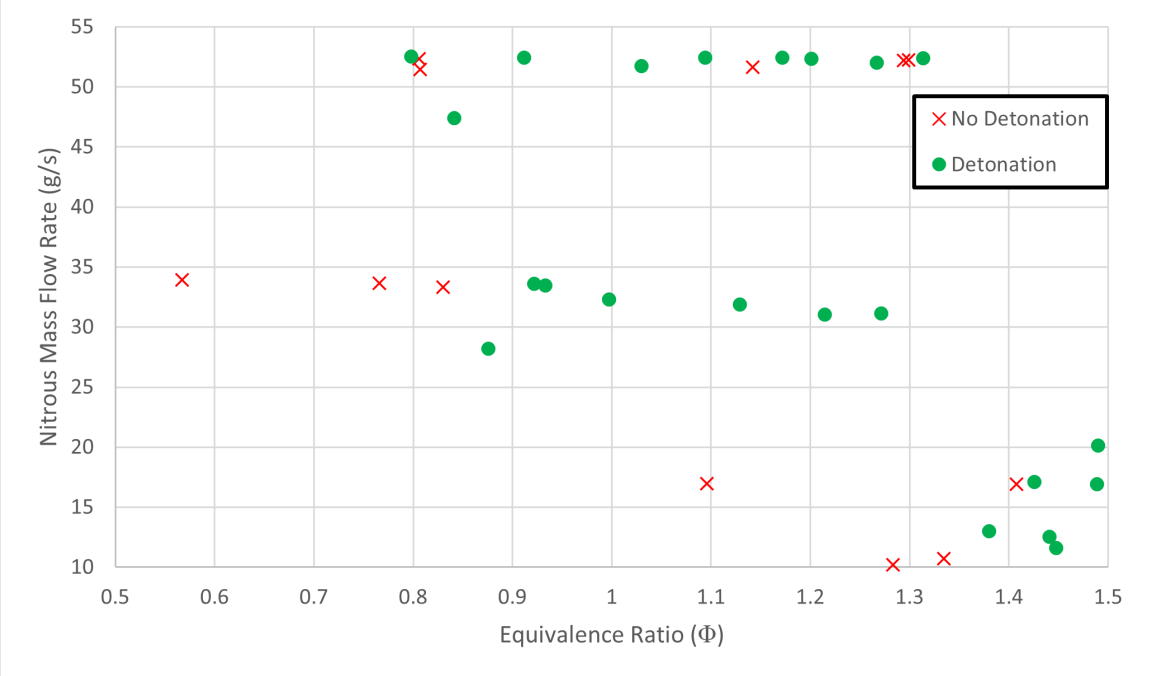

Figure 67. Operating Map of Plain JIC Injection Scheme

4.3.3 Simplex Injection Scheme

The Simplex injection geometry used the same injection hole sizes as the new Plain geometry (see Section 3.4.2) and was designed to produce a swirling phenomenon of the oxidizer while the fuel was injected radially into the detonation chamber. The geometry used was different than a traditional simplex, as liquid fuel reactants are normally used to produce the swirling phenomenon. This configuration used gaseous reactants and swirled the oxidizer instead of the fuel, but was still desired to be tested to explore a different approach of testing of the pressure swirl nozzle. As seen in Figure 68, a much smaller range of detonable equivalence ratios were produced than that of the Plain and Premixed injectors. Detonations were scarcely seen in this configuration, but were predominately seen at $\sim$ 50 g/s between 1.1 and 1.5 equivalence ratios. Tests investigating the lower limit of the operating map proved to further decrease the range of detonable equivalence ratios as detonations below 40 g/s and inside the initial testing range of ϕ were only seen between ϕ = 1.3 – 1.4. At these lower mass flow rates, and in general, detonations were not seen at any fuel lean equivalence ratios.

Additional tests were conducted at equivalence ratios above the initial testing range of ϕ = 0.5 – 1.5 since detonations were found only at the high end of the testing range of the Simplex configuration. At these more fuel rich equivalence ratios, detonations were seen around 28 g/s at ϕ between 1.5 and 1.7. No detonations were seen at equivalence ratios above 1.5 for tests between 40 and 50 g/s. In general, the absence of detonations seen at equivalence ratios around stoichiometric (ϕ = 1) or lower revealed a lack of mixing in this Simplex configuration. It was hypothesized that this configuration did not produce a sufficient spray cone since the reactants used were gaseous and not liquid which is what the original swirl nozzle design was used for. Additional reasons for lack of mixing could stem from the swirling of the oxidizer

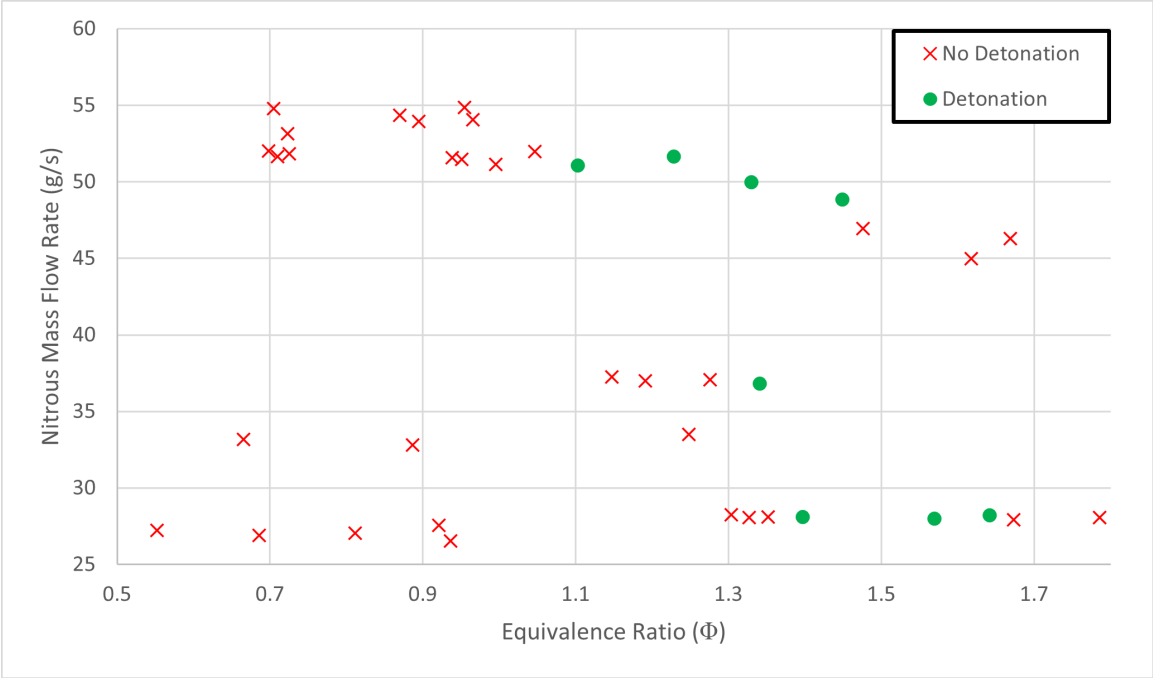

Figure 68. Operating Map of Simplex Injection Scheme

instead of the traditional swirling of the fuel. Producing a swirl of the oxidizer could have further dispersed the nitrous oxide which would require more fuel, ethylene in this case, to be injected to mix with the already dispersed oxidizer.

Further complications with the simplex configuration were revealed when observing the pressure across the sonic nozzles was not consistently choking. As outlined in Section 3.3.2, the choking phenomenon is seen by a 1.2:1 inlet to outlet pressure of the sonic nozzle equating to the downstream pressure being less than 80 % of the upstream pressure. While the simplex had the same injector hole sizes as the plain and was also tested with the same sonic nozzles (fuel = 1.12 mm, oxidizer = 2.67 mm), the simplex teetered the line of being choked and unchoked throughout all its testing. Figure 69 shows the upstream to downstream pressure ratios for every test with each injection scheme. All other injection schemes had consistent ranges of pressure ratios across the sonic nozzles between 0.5 and 0.7, showing a well choked phenomenon throughout testing. However, it is seen that with the simplex configura-

tion, the pressure ratios range from 0.76 to 0.89, revealing that the simplex was often not choked across the nozzles and when it was, the choking state was not as strong.

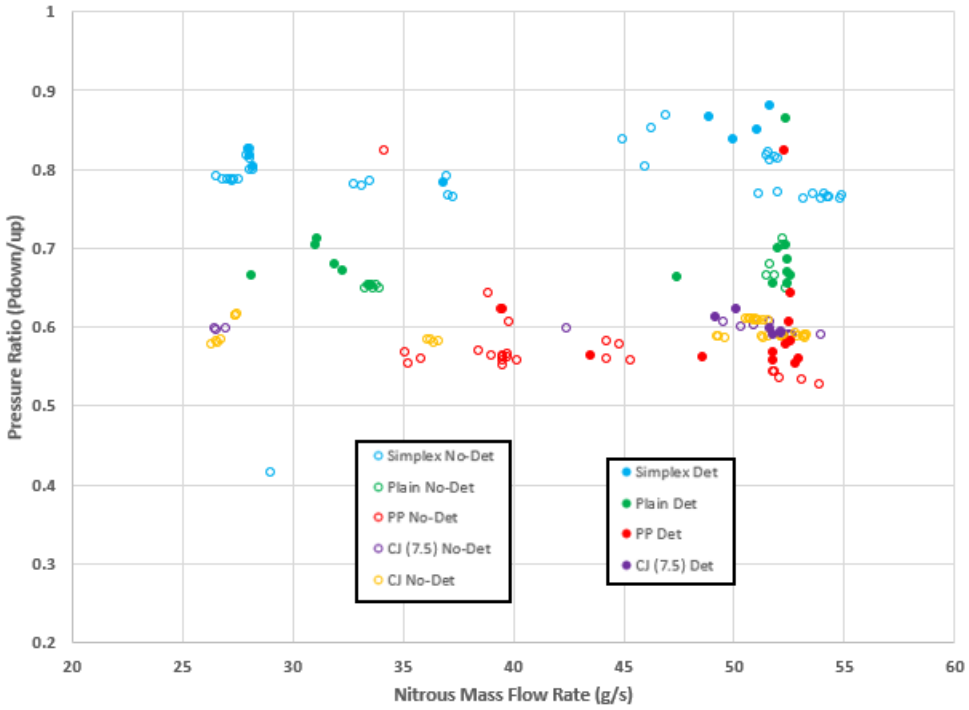

Figure 69. Pressure Ratios Across Sonic Nozzles for All Injection Schemes

The unchoked flow across the sonic nozzle signaled that the flow was instead choked at the injectors. This event did not allow for the user to deduce the true mass flow rate in the RDE system and verify that the mass flow rates observed were equivalent to the mass flow rates desired. It was hypothesized that obtaining choked stable flow across the sonic nozzles would increase detonability, however no trends were seen to verify this claim as detonations were still observed when the Simplex was unchoked. Though the pressure ratio across the sonic nozzle did not seem to have an influence on detonability, it was still desired to produce choked flow in this configuration to at least allow the user to confirm whether specific test points reliably produce detonations in the Simplex. This was not able to be accomplished in this research.

4.3.4 Counter-Jet Injection Scheme

The last injection scheme tested to determine its' operating map was the Counter-jet. Key differences to this geometry included 24 oxidizer injector holes 0.79 mm in diameter and a pre-det entrance hole moved up to 20 mm above the connection plate (see Section 3.4.2). Initial tests with the counter-jet aligned the injectors directly across from each other to produce mixing by the collision of the two reactants. As seen in Figure 70, this initial configuration produced no detonations. Loud "pops" that usually signaled the start of the detonation were commonly seen throughout tests, however the reactants never ignited. It was predicted that since the injectors were directly aligned there was potential for one stream of higher pressure to backpressure the other stream resulting in a disproportionate mixture. However, pressure data, as shown in Figure 71, revealed plenum pressures were steady for the entire duration of the run.

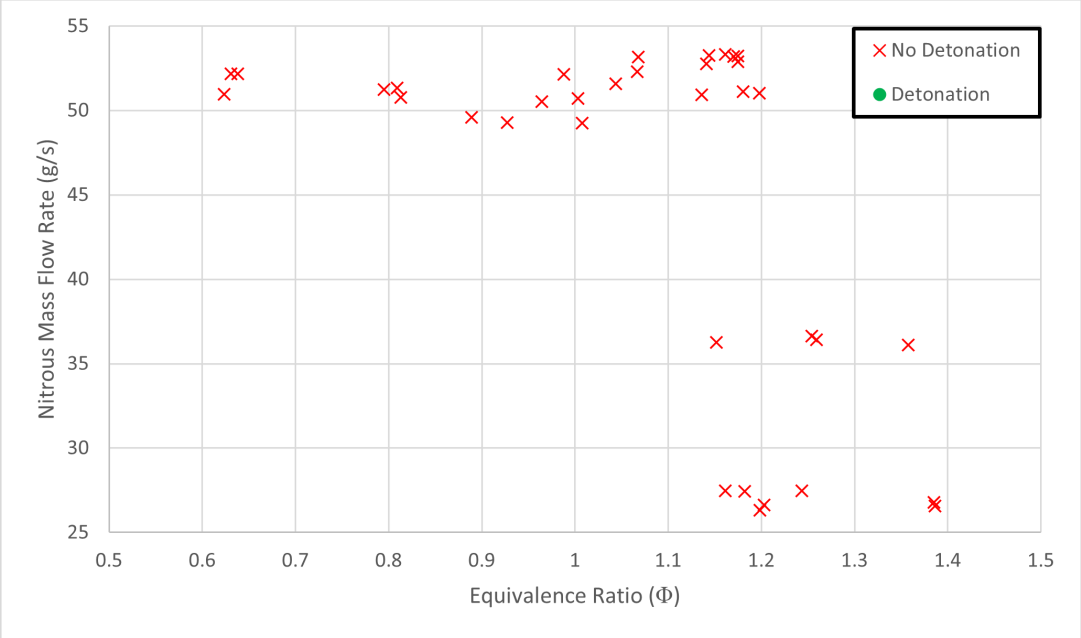

Figure 70. Operating Map of Direct Impinging Counter-Jet Injection Scheme

Because of the consistent "pops" observed, it was hypothesized that the configu-

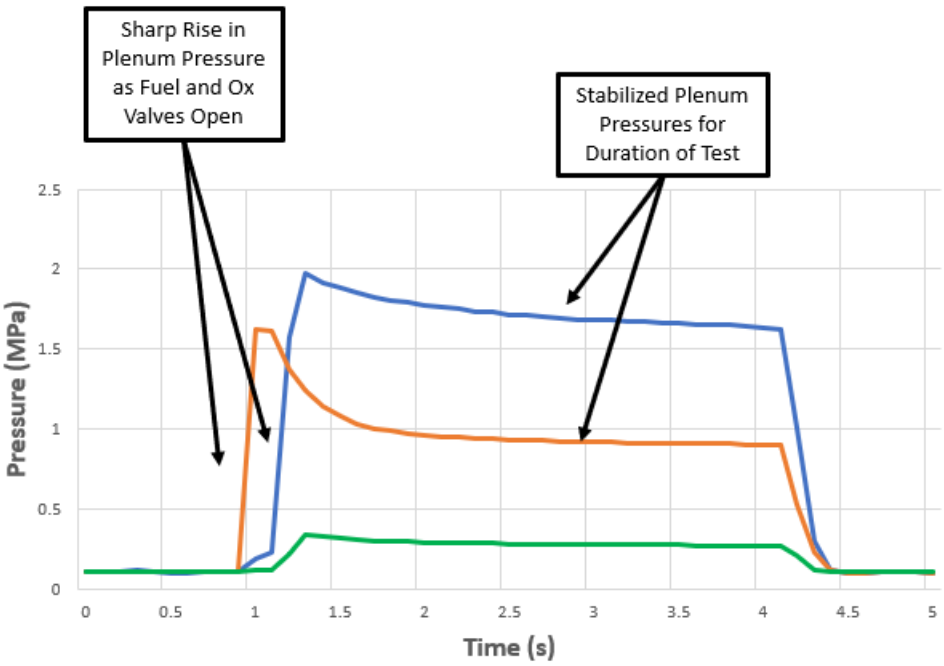

Figure 71. Pressure Time History for Direct Impinging Counter-Jet Scheme at 50 g/s $\phi = 1.0$

ration was close to producing a detonation but needed to retain more pressure in the chamber to allow time for the reactants to ignite rather than it having an issue of a lack of mixing. Thus, for purely exploratory purposes, new tests were ran with a tighter aerospike nozzle with a 0.625 mm gap ($\epsilon = 0.33$) to see if a detonation would be produced and if the issue truly was concerning retaining pressure in the chamber for a sufficient time to ignite. This was the only time the nozzle size was changed throughout the testing of all injection schemes. The tests with the tighter nozzle also failed to produce a detonation. This failure to produce a detonation between 25 g/s to 55 g/s at equivalence ratios between 0.6 and 1.4 revealed that the mixing in this configuration needed to be improved.

It was hypothesized that if the injectors were offset instead of pointed directly at each other, then their collision with the outerwall of the detonation chamber would help disperse the reactants and encourage mixing. Thus, additional tests were con-

ducted where the injectors were offset by 7.5 degrees again for exploratory. This allowed for the 24 injector holes (which were evenly spaced by 15 degrees around the circumference of the fuel/oxidizer plates) to be staggered evenly throughout the configuration and aimed directly between two of the opposite injector holes. This configuration proved to increase the mixing quality as detonations were seen between equivalence ratios of 1 and 1.3 at $\sim$ 50 g/s. Figure 72 shows these detonations and the rest of the operating map of the counter-jet configuration with the 7.5 degree offset. Similar to the direct impinging injectors, pressures in this configuration were also observed to stabilize during the test as seen in Figure 73, so it was assumed that the injection streams of the reactants were not backpressured by the other reactant. While no in depth testing was performed on this configuration of the counter-jet, the result of improved mixing seen manifested in more detonations leaves room for further testing and optimization of the counter-jet.

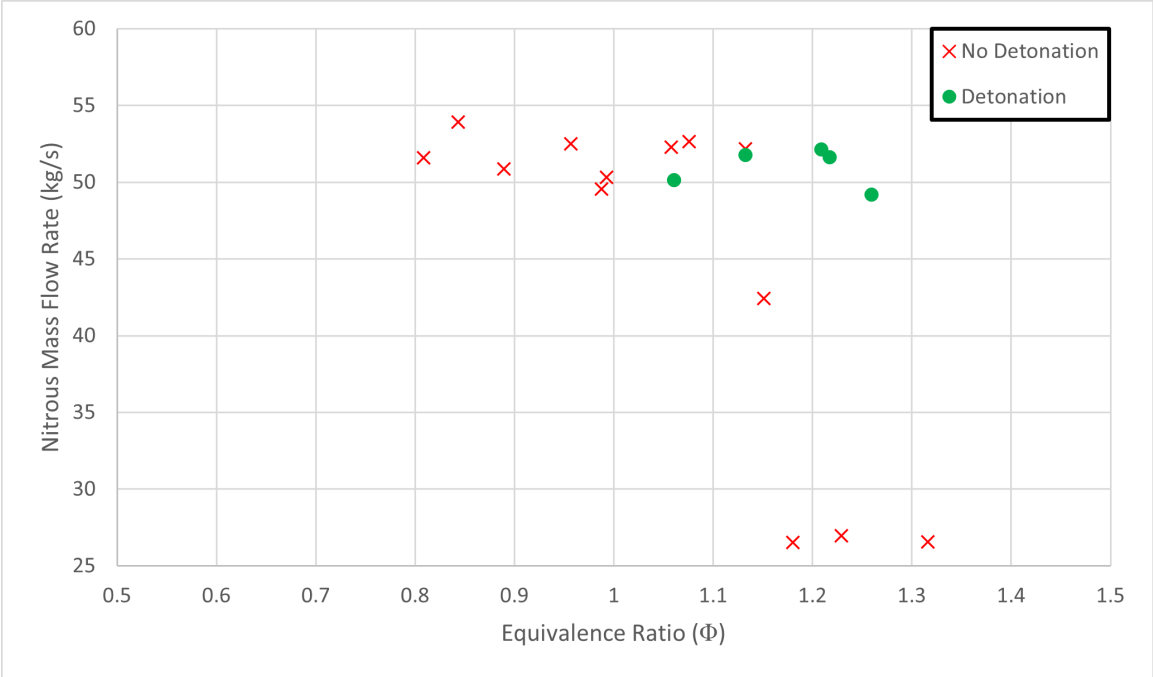

Figure 72. Operating Map of Counter-Jet Injection Scheme with 7.5 Degree Offset

When comparing Figures 71 and 73, it appears that the pressure conditions at

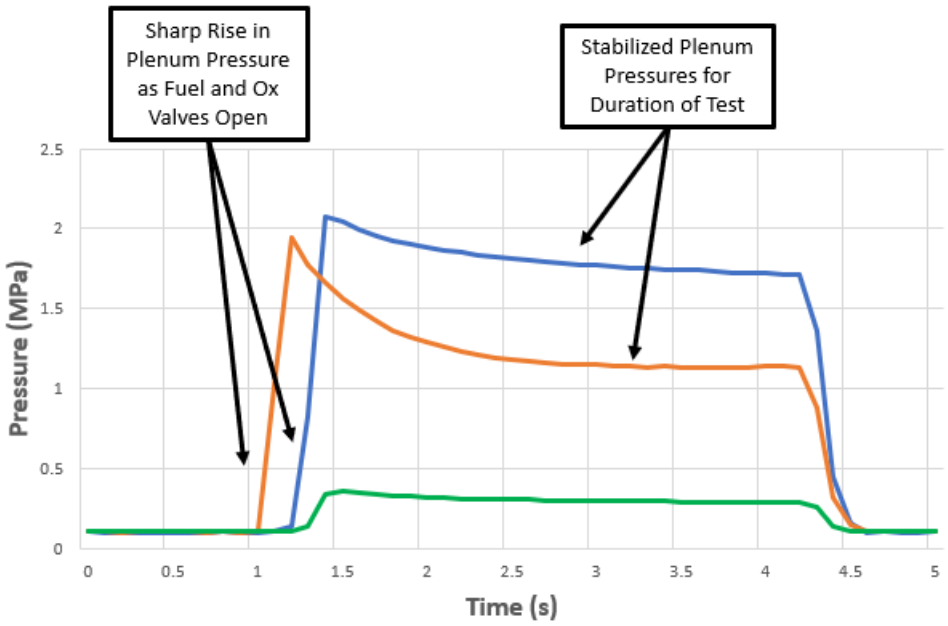

Figure 73. Pressure Time History for Counter-Jet Injection Scheme with 7.5 Degree Offset at 50 g/s $\phi = 1.0$

the inlet varied for the Counter-jet configurations even though they were ran at the same mass flow conditions. The pressures across the oxidizer inlet closely resembled each other as they both stabilized at pressures just below 2 MPa. However, the fuel inlet pressure for the direct impinging Counter-jet and the Counter-jet with the 7.5 degree offset stabilized around 0.9 and 1.2 MPa, respectively. Thus, the increased detonability of the offsetted Counter-jet could be attributed to the increase in fuel pressure across the injector.

4.3.5 Variations in Operating Maps Produced

From examining the various operating maps produced by the injection schemes, it is apparent that the Plain JIC possessed the widest operating map out of all the configurations tested by a big margin. It was desired to further understand the cause of the wide ranges of detonability between the different injection scheme configurations. While all conditions between the testing of the various schemes were

kept as standard as possible, the major difference between the injection schemes apart from their mixing setup was their injector hole size. The fuel and oxidizer injector hole sizes for each configuration can be seen in Table 10.

Table 10. Injector Hole Sizes for the Various Injection Geometries

	Fuel Hole Size	**Oxidizer Hole Size**
Partially-Premixed	24 x 0.40 mm	24 x 0.96 mm
Plain	24 x 0.40 mm	16 x 0.89 mm
Simplex	24 x 0.40 mm	16 x 0.89 mm
Counter-Jet	24 x 0.40 mm	24 x 0.79 mm

The smaller injector hole areas were designed to help retain pressure in the chamber during detonation, and while this did not induce detonability in the Simplex, it vastly increased the operating map of the Plain. Further analysis on the injector hole size analyzed the plenum pressure of the fuel and oxidizer with relation to the average pressure in the chamber. The results, pictured in Figure 74, show that detonability in all configurations highly increases at a P_o/P_c less than 3 and a P_f/P_c less than 2. Thus, it is hypothesized that decreasing the injector hole size of a configuration like the Partially-Premixed, which possesses the largest oxidizer injector hole area, would increase its detonability and widen its operating map.

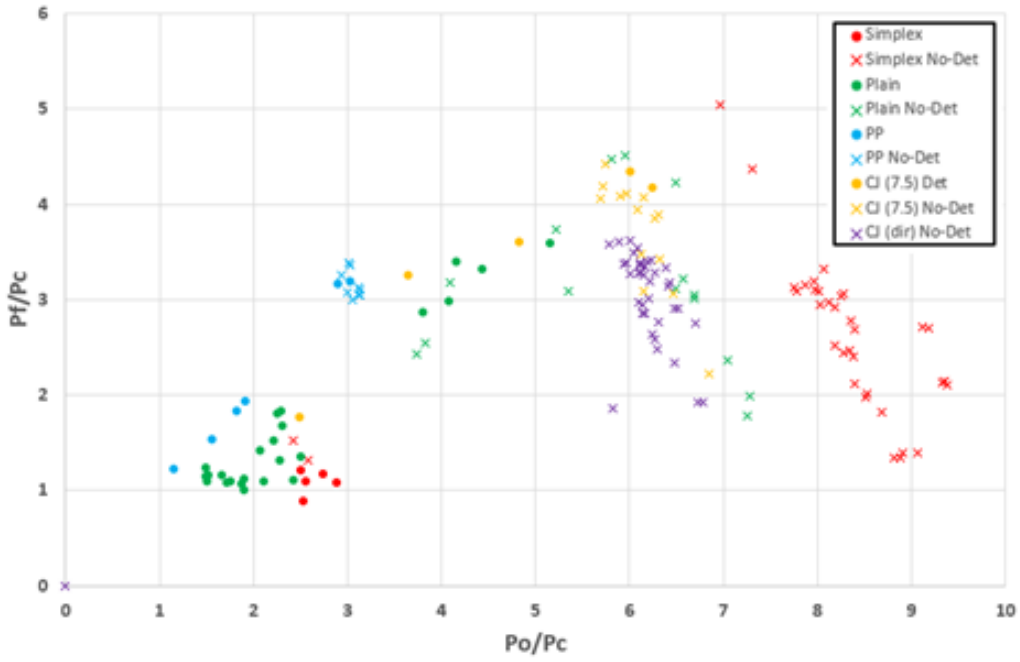

Figure 74. Combined Plot of Oxidizer and Fuel Plenum to Chamber Pressure Ratio

4.4 Micro-RDE Detonation Stability in Different Injection Schemes

The frequency and wave speed of a detonation with relation to the Chapman-Jouget (CJ) wave speed are key indicators of the stability of the detonation wave. Recall from Dechert[1] that the design frequency of the Micro RDE was 20 kHz and the wave speed of a nitrous oxide and ethylene mixture at equivalence ratios of $\phi = 0.6$ – 1.4 was experimentally found to be between 2080 – 2291 m/s through experiments conducted by Fernelius et al. [33]. It is also important to note that the Micro-RDE was designed to reach 80% of the CJ wave speed at ranges between 1664 – 1833 m/s to achieve the desired 20 kHz frequency [1]. For this part of the study, the stability of the detonation waves will be assessed by their relativity to the CJ wave speed and their proximity to the design frequency.

To obtain the detonation wave frequencies, a visual configuration with a high-speed Phantom camera and a mirror allowed for direct view of the detonation cham-

ber during testing (see Section 3.4.3). Frames were taken at 79000 frames per second with a low exposure time of 1 microsecond to ensure outside light would not interfere with capturing the light of the propagating wave. To analyze the data, a Fast Fourier Transform (FFT) was performed using a Python code from Nathan Snow. This code allowed the user to input the outputted frames of a given run from the Phantom camera and select pixels within each of the four quadrants that outlined the detonation channel in the frames (see Figure 75 for details). This ensured that the FFT was executed on the propagating wave and not a blank space in the frame. The FFT was performed on each quadrant of the channel and outputted along with a spectrogram for each corresponding quadrant.

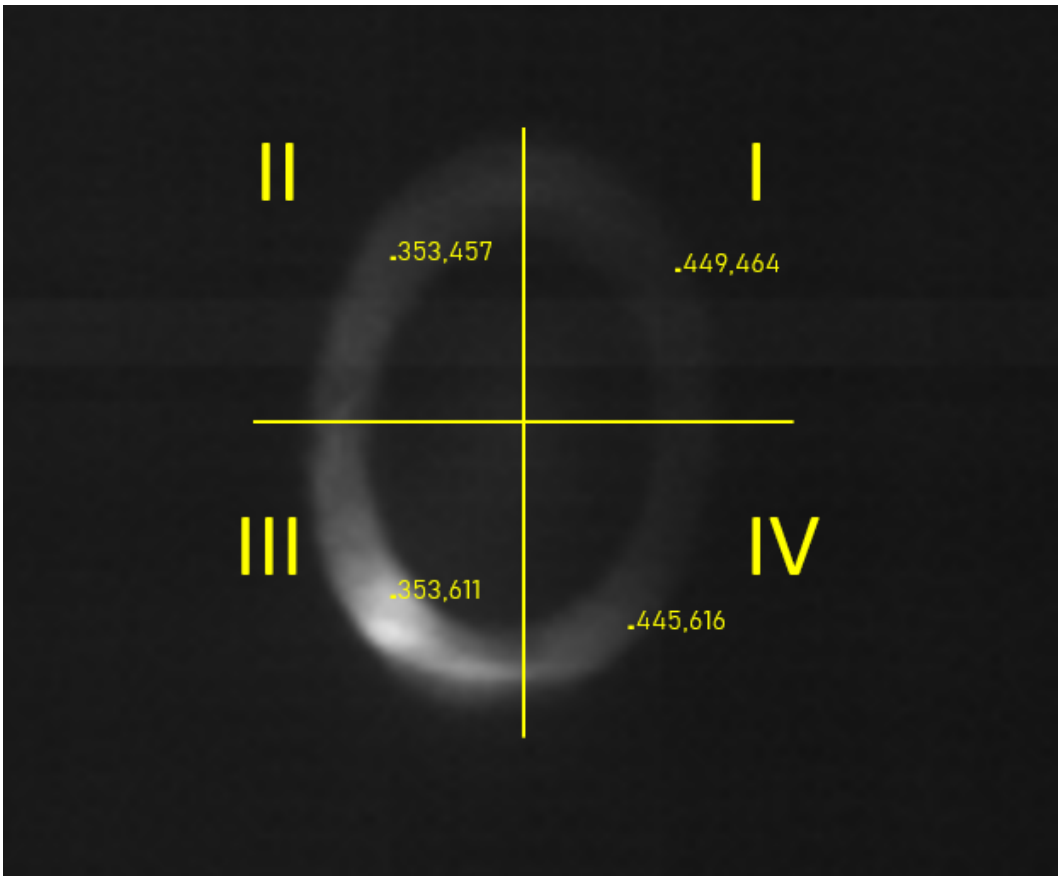

Figure 75. Screenshot of Frame Utilized in Code for Selection of Quadrants for FFT (Quadrants highlighted)

This output from the FFT code, seen in Figure 76, was used to determine the frequency of the detonation (the average of the four quadrants) while the spectrogram gave insight to any possible presence of deflagration acoustics or potential harmonics from the detonation wave. For the case used as an example in Figure 76, a detonation frequency of 17.1 kHZ was found between the averages of the quadrants. This specific spectrogram shows potential evidence for burning and acoustics in the top and bottom left quadrants as seen by presence additional noise frequencies in those outputs.

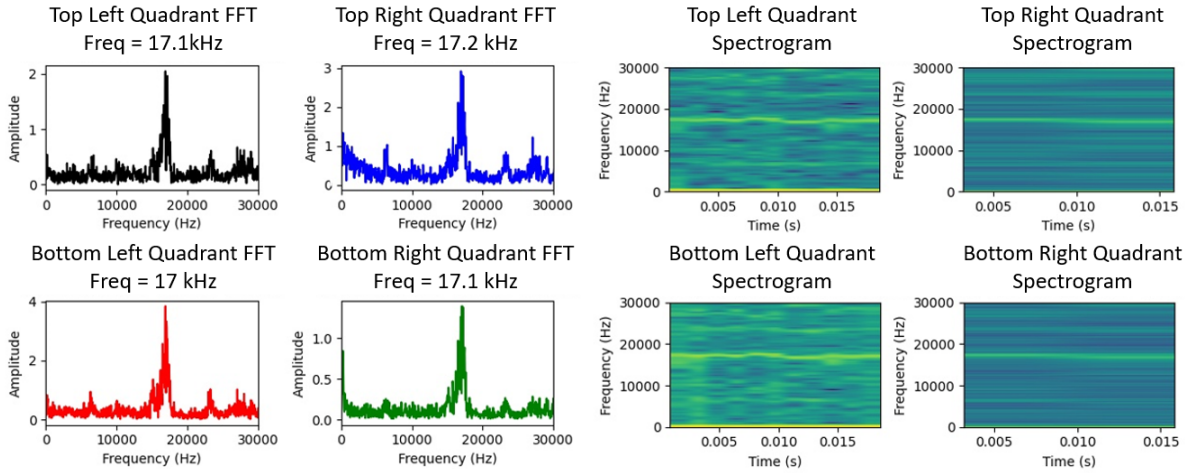

Figure 76. Example Output of Fast Fourier Transform Code: FFT (left) and Spectrogram (right)

While the FFT code utilized helped determine the detonation frequency, issues with securing the Micro-RDE during testing prevented the FFT from being run for the full duration of each test. Small vibrations on the rig due to the detonation events caused the detonation channel to change positions in the frames taken by the camera. This phenomenon can be seen in Figure 77, where at time t = 0.061 s the channel is originally in the center of the frame and gradually changes positions as time goes to t = 0.104 s and t = 0.125 s. This proved problematic because the FFT code was not designed to move with the vibrating detonation channel as it was assumed the channel would be stationary in the frame. Therefore, on average, FFT data was

captured for only 3000 out of the 79000 frames as the channel generally only remained in a single position for that long. Out of 0.6 second run times, this equated to FFTs that spanned an average 0.023 seconds.

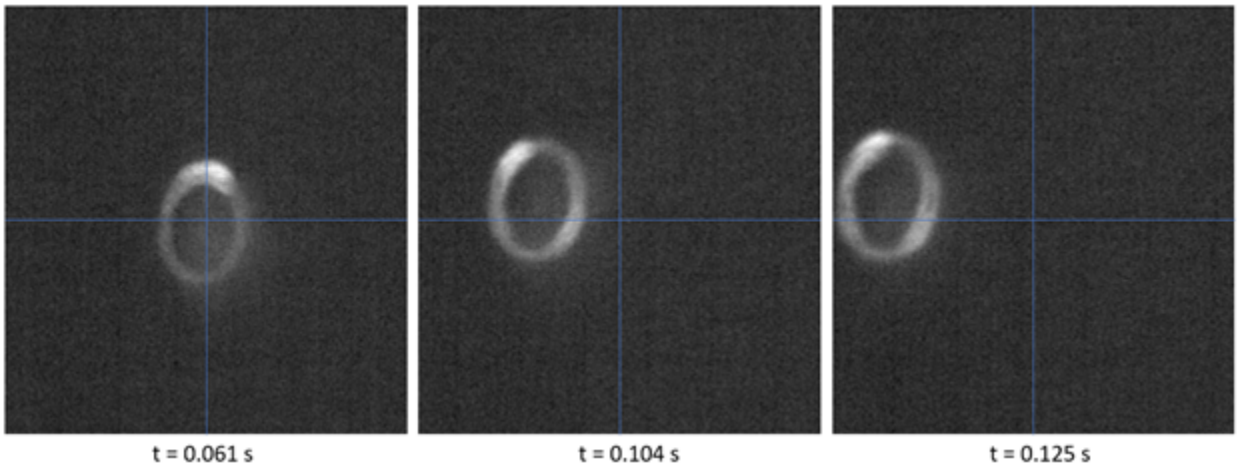

Figure 77. Movement of Detonation Channel from Vibrations During Testing

As previously discussed in Figure 65, the 0.6 second window for detonation was not sufficient time for the detonation frequency to settle to a final value. Thus for this analysis, it could not be assumed that the FFT taken at one point in the run could represent the frequency for the entire duration of the run. To assess the detonation frequency of the entire run multiple FFTs were performed for the periods of time where the channel was stationary in the frame. While some cases had more stationary periods than others, it was standard practice to take at least two FFTs for every test point, one towards the beginning of the run and one towards the end if possible. The frequencies produced at these separate parts of the run were then averaged to produce a general frequency seen by a specific test point.

Using the data gathered from the FFT, the detonation frequencies at the mass flow rate and equivalence ratio limits for each injection scheme were able to be found. This data for the frequency as a function of mass flow and equivalence ratio is presented in Figures 78 and 79, respectively. The average detonation frequency experienced by

each injection scheme is as follows: Partially-Premixed JIC = 16.9 kHz, Plain JIC = 12.6 kHz, Simplex = 13.3 kHz, Counter-jet with 7.5 degree offset = 17.3 kHz.

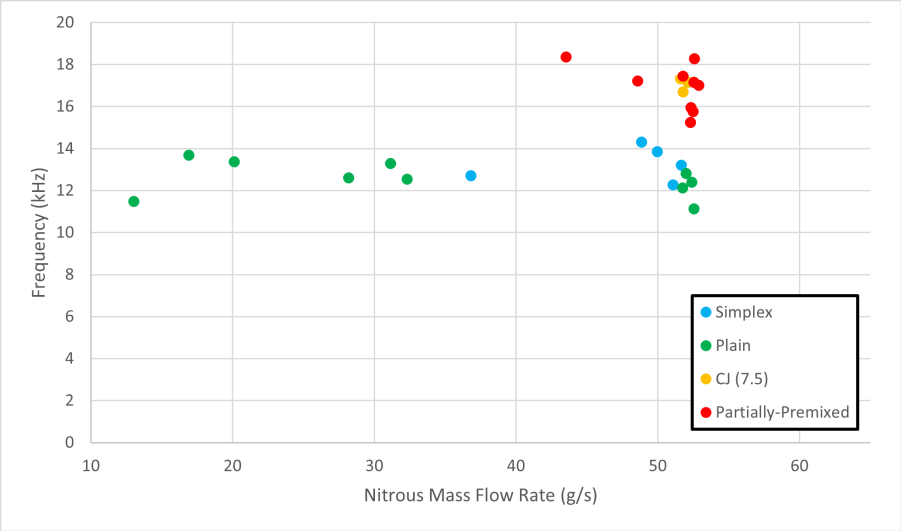

Figure 78. Detonation Frequencies for Various Injection Schemes versus Mass Flow Rate

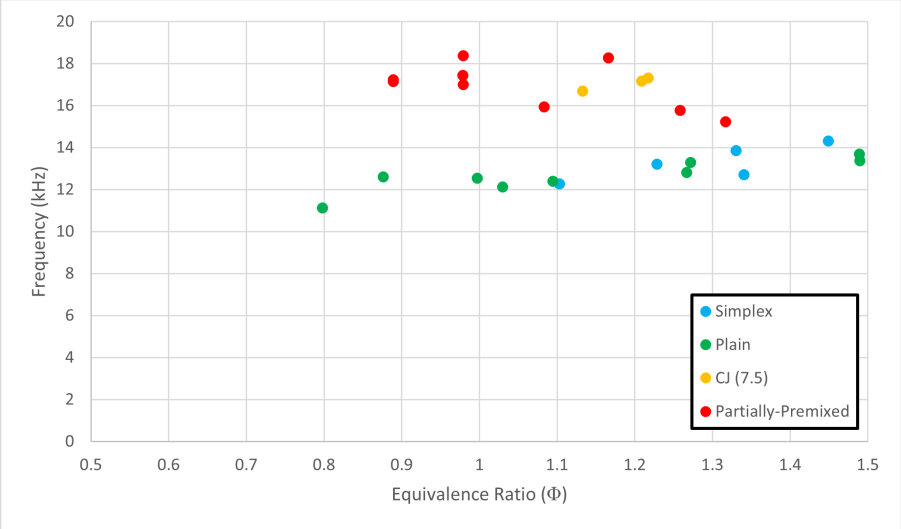

Figure 79. Detonation Frequencies for Various Injection Schemes versus Equivalence Ratio

For this research, the stability of the detonation wave was assessed by its proximity to the design and Chapman-Jouget wave speeds. Wave speeds were calculated using the diamater of the channel, 28 mm, and the detonation frequency using Equation 17.

Additional analysis on the stability of the waves produced by the various injection scheme was performed by examining the spectrograms of their detonations produced at similar conditions.

$$V_{wave} = Freq * \pi D_{channel} \tag{17}$$

Though the Plain JIC had the widest operating map and was the most detonable injection scheme tested (see Section 4.3), it had the lowest average detonation frequency produced out of the injection schemes. Although the widely expanded operating map was surprising, the low frequencies were expected as experiments by Dechert experienced similar unstable detonation frequencies in the Micro-RDE. Wave speeds seen using this geometry ranged from 978 to 1203 m/s. This represents an average of 38.5 % below the design wave speed of 1774 m/s and 51.2 % from the CJ wave speed of 2186 m/s. When examining the spectrogram of the Plain at 50 g/s ϕ = 1.0 pictured in Figure 80, and disregarding the noise seen in the left quadrants, the wave looked somewhat stable at its 12.1 kHz frequency with some harmonics at frequencies around 25 kHz. This showed one wave mode propagation, however because the wave (characterized by the green line) was not very defined it shows that it wasn't completely stable.

The Partially-Premixed injection geometry performed better despite its limited operating map that had a lower limit of 45 g/s. Wave speeds in this configuration ranged from 1339 to 1615 m/s, representing an average 16.8 % below the design wave speed and 32.4 % below the CJ wave speed. At the highest wave speed recorded, the Partially-Premixed scheme produced a detonation less than 10 % from the design frequency of 20 kHz, which corresponded to the highest wave speed recorded throughout this research. These frequencies and wave speeds fell into the range observed by Fiorino, although there were less cases of relatively low detonation frequencies in this

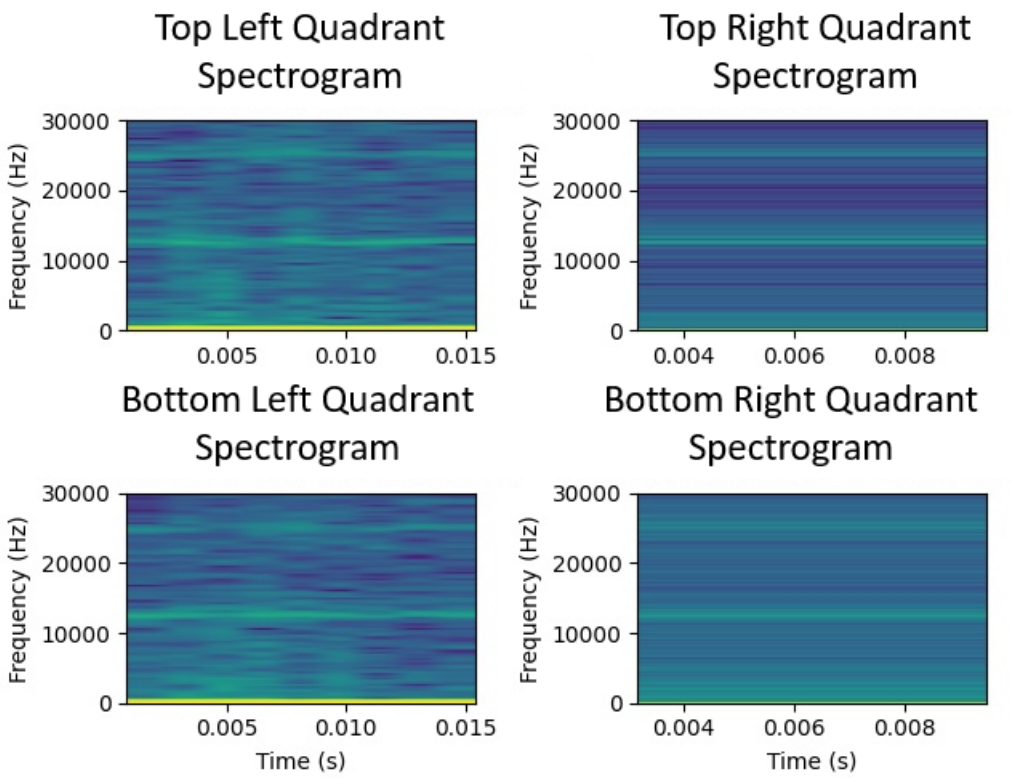

Figure 80. Spectrogram Results for Plain JIC at 50 g/s $\phi = 1.0$

research [2]. Ran at the same conditions as in Figure 80 for the Plain, the spectrogram for the Partially-Premixed JIC is pictured in Figure 81. This spectrogram, once again ignoring the noise in the left quadrants, showed a significantly more defined one wave mode propagation without harmonics or acoustics. This showed not only an increased frequency but also increased stability when running the Partially-Premixed at the same conditions as the Plain.

When compared to the Plain JIC, the significantly higher detonation frequency but significantly smaller operating map of the Partially-Premixed caused high interest in what actually was transpiring in the detonation chamber. Typically, higher detonation frequencies, and thus greater detonation stabilities, are associated with wider operating maps as stable detonations are usually not seen on the limits of an operating map. Further exploration of the dynamics of these injection schemes and the

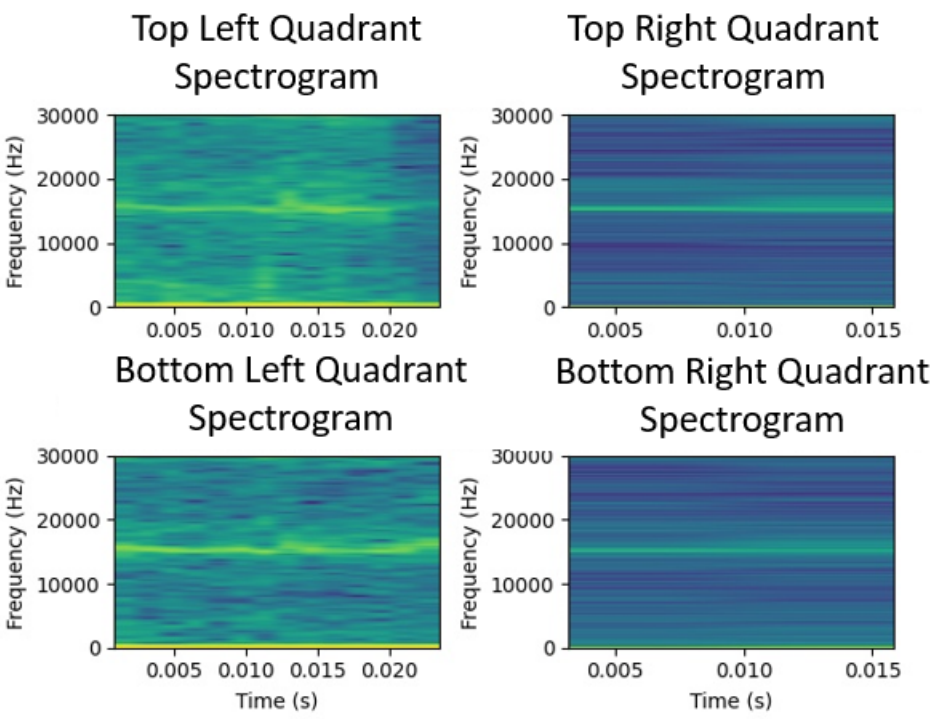

Figure 81. Spectrogram Results for Partially-Premixed JIC at 50 g/s $\phi = 1.0$

detonations they produced were desired to be assessed using the optical configuration (see Section 4.5).

The Simplex configuration produced wave speeds ranging from 1079 to 1258 m/s. This fell to an average 34.2 % below the design wave speed and 46.5 % below the CJ wave speed. This was likely due to the lack of mixing quality in the injection scheme, as discussed in 4.2, and resulted in not only a small operating map but also low frequencies and wave speeds observed in the detonations produced by this specific Simplex configuration. The spectrogram for the Simplex ran at 50 g/s $\phi = 1.1$, no detonations were seen at stoichiometric equivalence ratios in this configuration, is pictured in Figure 82. This spectrogram revealed multiple detonation waves in the chamber in addition to harmonic frequencies. This showed a lack of stability in the waves seen in this configuration. Overall, tests with this variation of the Simplex, which swirled the gaseous oxidizer instead of swirling the liquid fuel, proved to be

unsuccessful in obtaining low mass flow operation and high detonation frequencies.

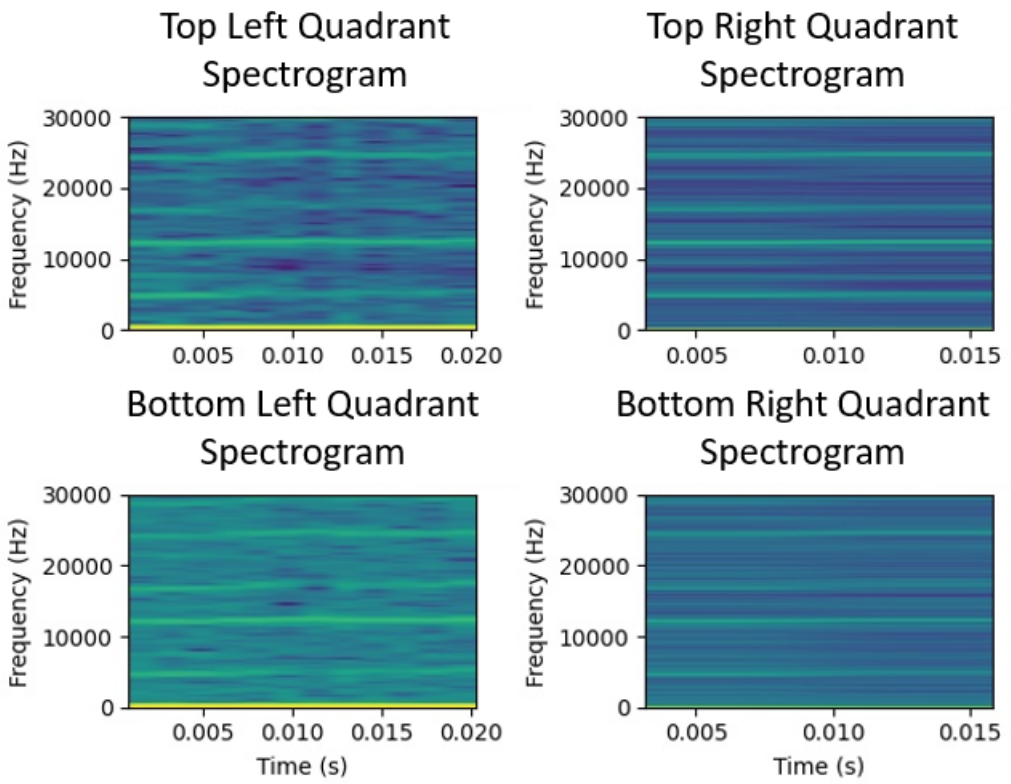

Figure 82. Spectrogram Results for Simplex at 50 g/s $\phi = 1.1$

Lastly, the Counter-jet with a 7.5 degree offset had the highest detonation frequency average out of all the injection schemes tested, having a range of detonation wave speeds from 1468 to 1570 m/s. This equated to a 14.4 % average difference below the design wave speed and a 31.5 % difference below the CJ wave speed. While the Partially-Premixed geometry produced a few detonations with higher wave speeds, the Counter-jet at 7.5 degree offset proved to be more consistent in the detonation wave speeds observed having a standard deviation of only 42 m/s. Granted, not many detonations were observed using this injection scheme, however full sweeps at equivalence ratios and mass flow rates were not done on this configuration since it was tested more out of curiosity because the direct impinging Counter-jet scheme produced no

detonations. Further testing and optimization of the Counter-jet injection scheme with a 7.5 degree offset could continue to see increased detonation frequencies when compared to other geometries used on the Micro-RDE.

The spectrogram of the detonation produced in the offsetted Counter-jet configuration at 50 g/s $\phi = 1.0$ is pictured in Figure 83. As seen in the spectrogram the single detonation wave propagated at a frequency of 17.9 kHz, however the dim green light reveals the lack of strength frequency. The presence of harmonics in the spectrogram is also seen by the green lines above 20 kHz.

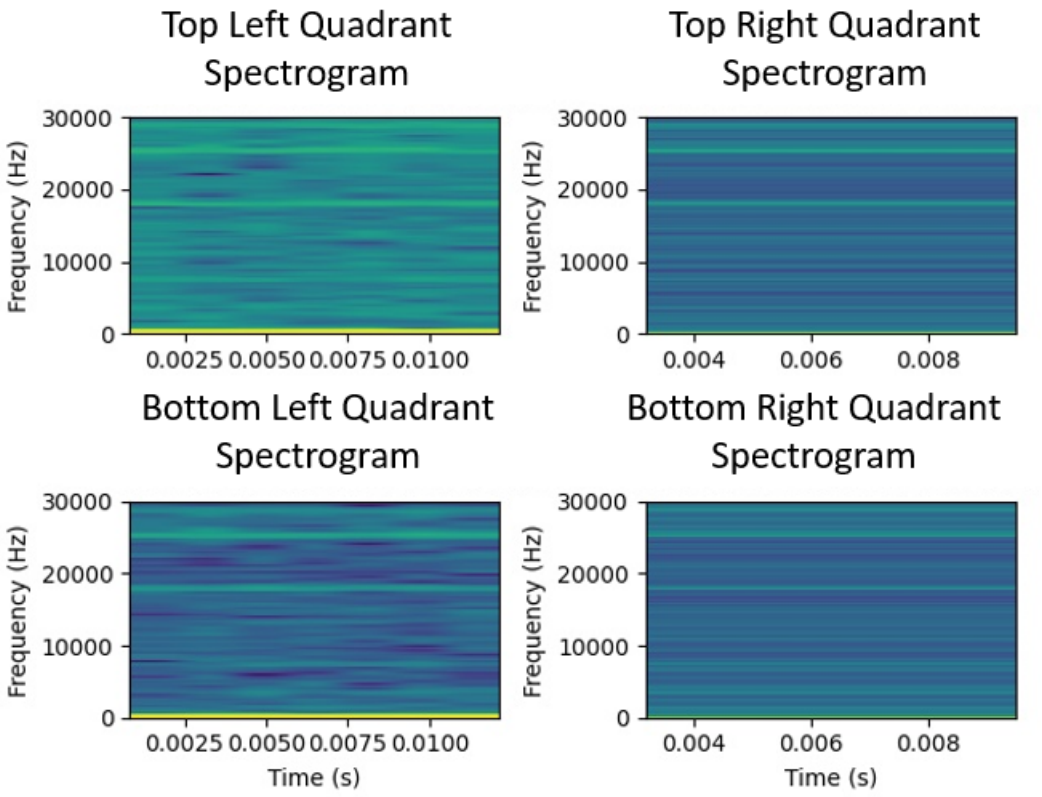

Figure 83. Spectrogram Results for Counter-jet (7.5) at 50 g/s $\phi = 1.0$

4.5 Optical Access Results

To further compare the performance of the various injection schemes, it was desired to use the optical configuration outlined in Section 3.4.3 to observe their influences on the behavior of the detonation wave. Certain key parameters that were to be analyzed included the detonation fill height, wave speed, cell size, and the number of detonation waves propagating in the chamber. Certain changes to the optical configuration were needed to produce the best optical data possible with the high speed cameras utilized. These changes are outlined in Section 4.5.1. The optical data produced by the new configuration is presented and analyzed in Section 4.5.2.

4.5.1 Iterations on the Optical Configuration

The initial optical configuration outlined in Section 3.4.3 was designed to provide optical access into the detonation chamber while still having a setup that could survive detonation conditions. This design was intended to provide images of the propagating detonation wave for three of the four injection geometries tested (Plain JIC, Partially-Premixed JIC, and Simplex) to allow for further comparison of their impact on the performance on the Micro-RDE. Due to multiple issues with the survivability of the optically accessible chamber and the quality of images taken during detonation operation, numerous changes were made to the initial optical configuration. Because the sole purpose of this optical setup was to gather visual data and not additional pressure data (this was already monitored for every injection scheme in the non-optically accessible Micro-RDE), no CTAP was installed on any optical configurations.

Early testing revealed issues of durability with the quartz tubes used as optical outerbodies. A total of six quartz tubes were used throughout the duration of the optical testing. The quartz outerbodies were placed between grooves of the RDE

outerbody and the top plate, with graphite ring sealants placed on the top and bottom of the quartz to prevent it from having contact with the metal pieces. To pin the quartz down between the top plate and RDE outerbody 1/4 20 screws were used. This configuration was designed to prevent vibration during testing while still allowing for the slight expansion of the quartz with the rest of the RDE optical configuration via the placement of springs on the screws (see Figure 56). Due to the desire to pin the quartz down tight enough to prevent vibration while also not over tightening it to allow for expansion, a fine balance of equally distributed tightening was needed on the quartz. This balance proved difficult to find early on, with the first quartz breaking (as can be seen in Figure 84) from violent vibration between the RDE outerbody and top plate because it was not sufficiently pinned in the configuration.

Figure 84. Resultant Quartz Optical Outerbody from Violent Vibration due to Insufficient Support from Top and Base Plate

Following the cracking of the first quartz outerbody, a tighter configuration was needed to prevent the vibration of the quartz during operation. Thus, screws were tightened well past hand tight with a standard wrench (as was done in the first configuration) but due to a lack of lab experience were still unintentionally tightened

unevenly which caused the quartz to crack due to compression during operation. At the time it was believed that this crack was caused by a lack of cushion provided by the graphite sealants on the top and bottom of the quartz. To provide more cushion for the quartz when tightened, as believed was needed, silicone rings were added on the top and bottom of the quartz in addition to the graphite sealants. This proved to be insufficient in allowing for the expansion of the quartz and the quartz once again cracked from compression as seen in Figure 85. Using the expertise from Brian Crabtree and Christopher Harkless from the AFIT model shop, the cracks were assumed to be resulting from excessive and disproportionate compression because of their clean breaks in concentrated areas of the quartz tiles. No detonations or ignitions were experienced from these configurations.

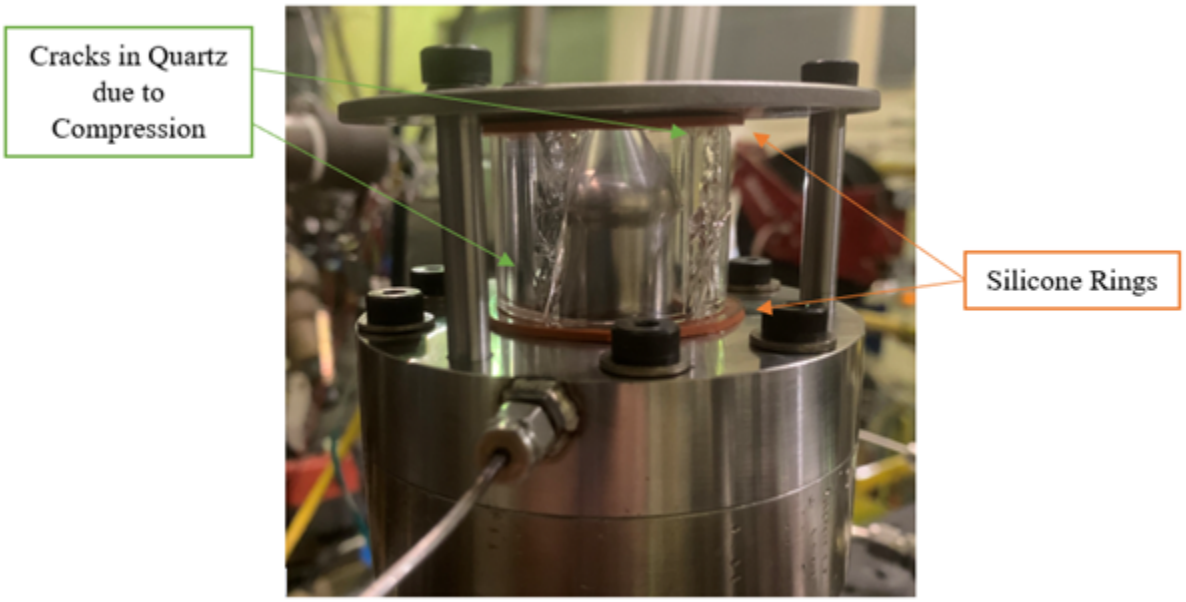

Figure 85. Resultant Cracks in Quartz Optical Outerbody Caused by Unequally Distributed Compression

Additional help from Mr. Crabtree and Mr. Harkless helped resolve the issues of excessive compression on the quartz tube. It was found that the screws were unevenly

tightened on the top plate which caused the pressure on the quartz to be distributed unequally around its circumference thus causing the sharp cracks in the tube. Careful installation and positioning of the quartz directly in the center of the top and bottom grooves, in addition to using two washers on each screw to further evenly distribute the pressure, proved to fix the problem of the quartz breaking due to compression. The silicone rings were not used in any more configurations. No torque wrench was utilized when tightening the screws, however the careful installation with the help of Mr. Crabtree and Mr. Harkless prevented the breaking of any more quartz due to compression. Their method of installation was achieved by approximately two full turns past hand tight on each screw. This also included alternating tightening each screw down so that they were all progessively tightened together.

While inconsistencies in the pressure distribution no longer proved to be an issue for the quartz outerbodies, the quartz was not able to consistently survive detonation conditions. On average, the quartz tubes were only able to survive three detonations before cracking or shattering completely. Because no pressure data in the chamber was recorded during these runs, it is unknown what specific level of pressure caused the quartz to break. However, it was assumed that the chamber pressures experienced in the general configurations were similar to those experienced in the optical, such that at mass flow rates around 50 g/s (where the optical was predominately tested) the Micro-RDE chamber would reach pressures between 0.6 MPa and 1.4 MPa during detonation. It was hypothesized that these pressures, in addition to the thermal shock of running cold flow for stabilization purposes which almost immediately became hot flow after ignition, caused the shattering of the quartz outerbodies.

Figure 86 shows the optical view of a quartz outerbody shattering during a detonation. The illumination of the chamber that is only seen during detonation events (Figure 86 left), was quickly followed by the cracking of the quartz tube as it began

to shatter (Figure 86 right). For reference, a frame taken before the test was taken and added to the figure (top).This led to an almost immediate loss of illumination due to the loss of the detonation wave as the energy was no longer contained by the quartz. Thus, the detonation was gone as quick as it came and no visual data was able to be gathered. This event was also experienced by the last two quartz utilized but not always after only experiencing a single detonation. For the cases where the quartz did not shatter under detonation conditions, the visual data was taken at a frame rate of 13000 frames per second and will be discussed later in the next section.

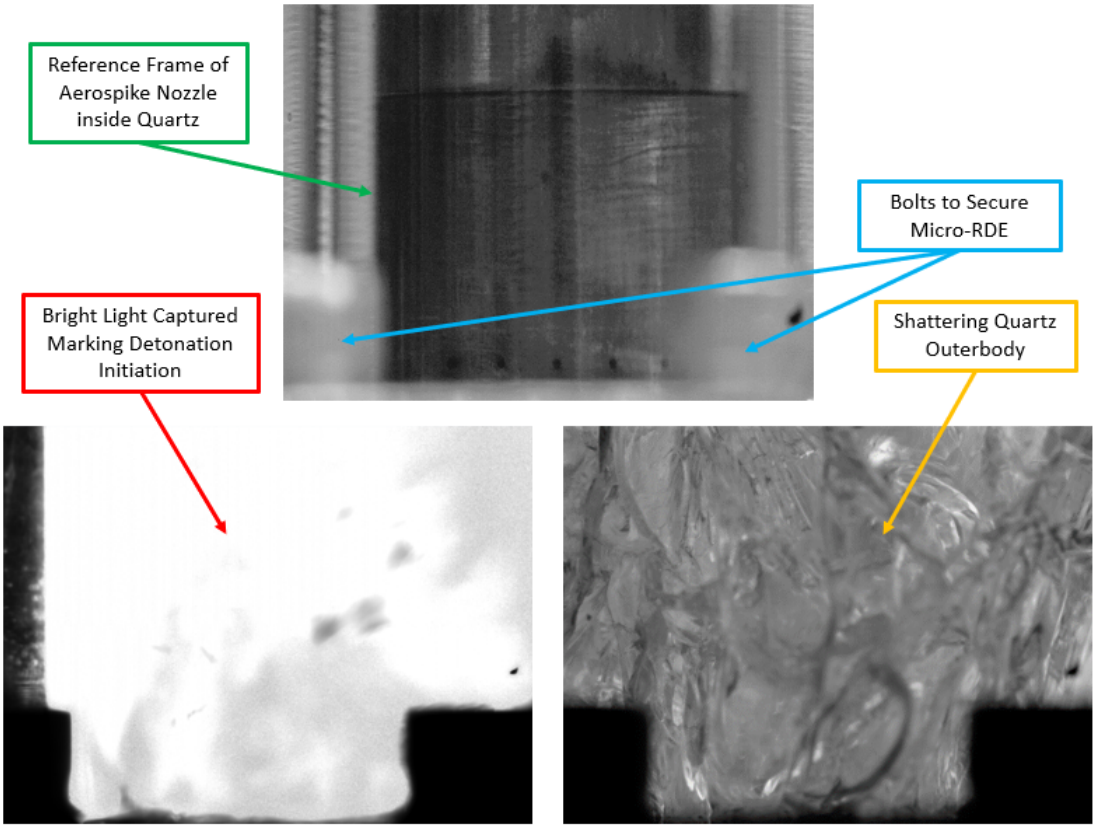

Figure 86. Reference Frame of Chamber Before Detonation (top), Chamber Illuminated by Detonation Initiation (left) Followed by Shattering Quartz (right)

After losing all six quartz tiles to issues of nonuniform compression or detonation events, a new material for of an optical outerbody was needed for visualization into

the detonation chamber. Polycarbonate was used to replace the quartz and was shaped into a cylindrical tube with the same dimensions as the original quartz optical outerbody (ID = 27.9 mm, OD = 41.9 mm, L = 31.75 mm). As seen in Figure 87, the same optical setup was used except the quartz tube was replaced with the polycarbonate. While still somewhat transparent, the polycarbonate did not provide as clear of a view inside the chamber as the quartz tile. Despite its lack of clarity, the polycarbonate was selected for its ability to withstand multiple detonation events, as it had a tensile strength of 64.81 MPa and could withstand temperatures up to 355 K. Additionally, the low exposure time settings on the Phantom camera ensured that only the light produced from the detonation wave was captured so although more clarity was definitely desired, the polycarbonate would prove sufficient because it still allowed for the visualization of the light in the detonation chamber.

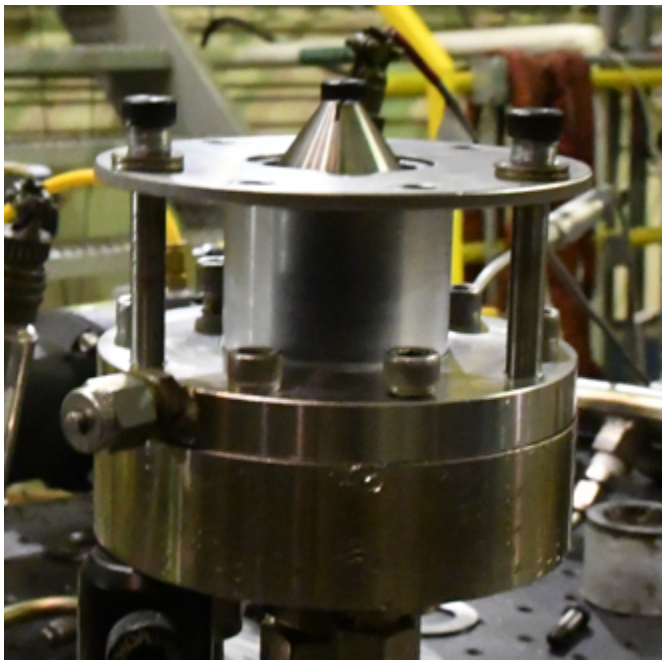

Figure 87. Optical Configuration with Polycarbonate Optical Outerbody

Although more resistant to detonative conditions, the polycarbonate gathered large amounts of soot after every detonation. Figure 88 shows a picture of the poly-

carbonate after a single detonation. Initially having the optical outerbody covered in soot did not prove problematic, as the light produced from the detonation wave was sufficiently bright to shine through the outerbody and be captured by the camera. However, after continuous runs, the polycarbonate outerbody began to experience patterns of burning on its interior circumference. Figure 89 shows a polycarbonate outerbody after eight detonations. After this eighth detonation, visualization of the detonation wave was tainted by pockets of burning throughout the outerbody that caused bright spots throughout the captured frames. These pockets of burning got progressively worse from the first detonation to the eighth, however the eighth detonation proved to be the run that the additional burning blocked out all other visualization into the chamber. The soot on the polycarbonate outerbody was able to be cleaned, but the consistent burning caused for the smooth finish on the interior of the polycarbonate to be compromised thus leading to more burning and even less visualization into the chamber. Thus, multiple polycarbonate outerbodies were needed to continue the optical testing process.

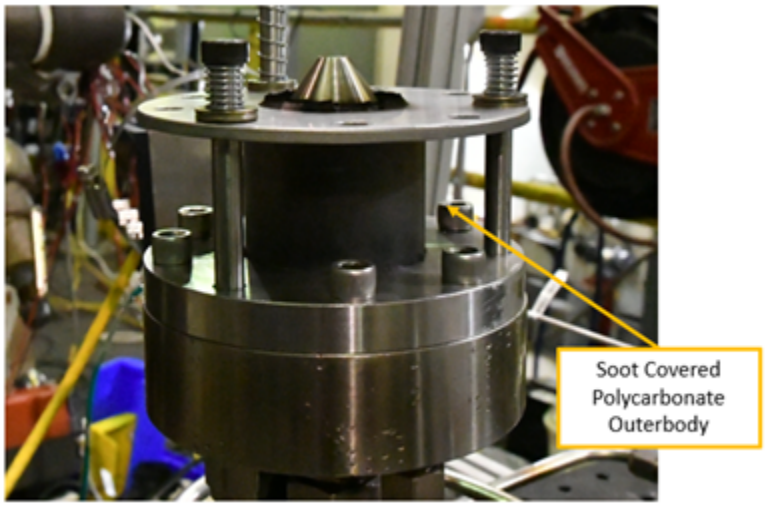

Figure 88. Polycarbonate Optical Outerbody Covered in Soot After a Single Detonation

Additional changes pertaining to the optical setup (outlined in Section 3.4.3) were

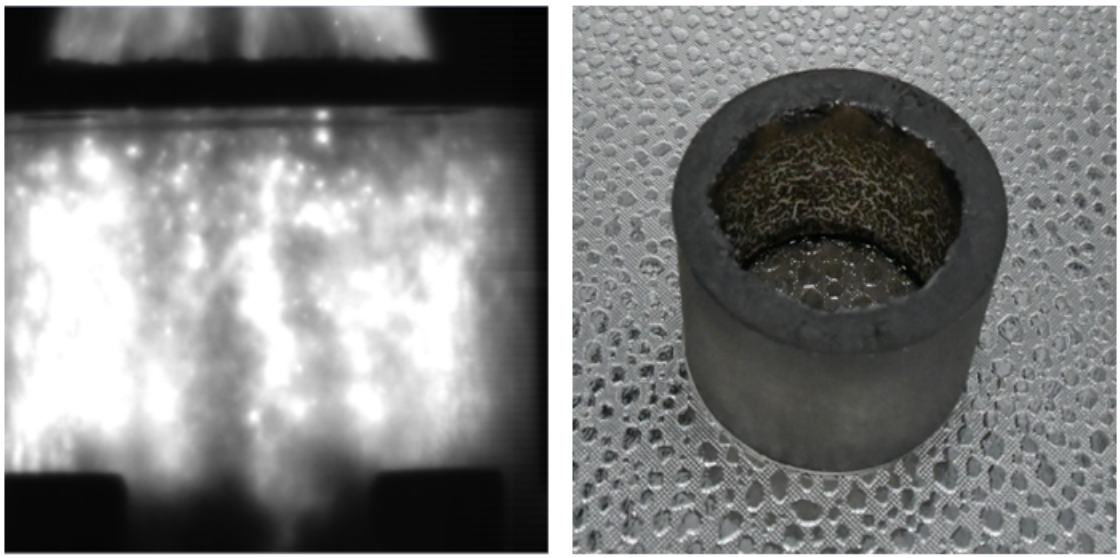

Figure 89. Polycarbonate Optical Outerbody During (left) and After Eight Detonations (right)

made to the side view Phantom camera to optimize visualization into the detonation chamber. Initially, the side view camera was positioned approximately 1.22 m from the Micro-RDE and used a 250 mm Nikon lens to focus in on the optically accessible chamber. This allowed for an 800 x 600 pixel resolution, which on the Phantom camera gave a maximum frame rate of 13,000 frames per second. An exposure time of 10 microseconds was used to capture only light produced by the detonation wave.

A resulting frame taken during a test using the Plain JIC injection scheme and the quartz outerbody can be seen in Figure 90. Pictured is the detonation chamber during a detonation event where the reactant particles that have ignited can be seen propagating from right to left. Although this allowed for visualization into the detonation chamber, this revealed very little information about the structure or behavior of the detonation wave. It was believed that because the detonation frequencies seen from Section 4.4 ranged from 11 to 18 kHz, the 13,000 fps setting on the Phantom initially recommended by a camera expert was too low to capture any behavior of

the wave. A wave frequency that is higher than the data sampling rate translates to information being lost as the detonation could make more than one full revolution before another frame is captured. Thus, a new side view setup with a much higher frame rate was needed to capture more characteristics of the propagating detonation wave.

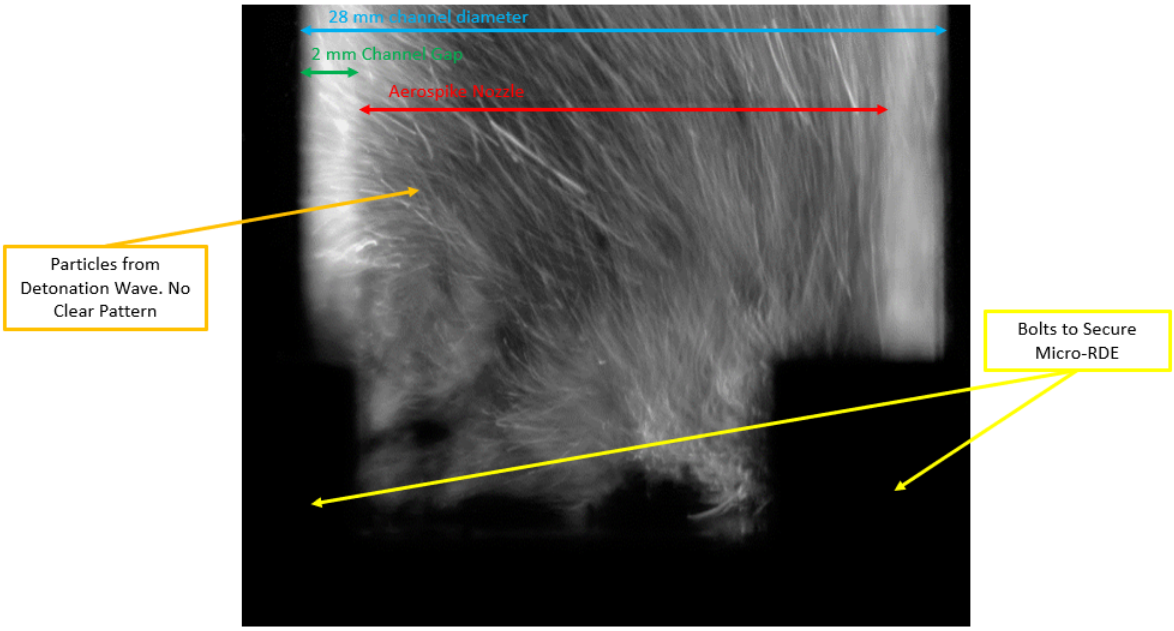

Figure 90. Visual of Frame Taken During Detonation at Frame Rate = 13000 fps

To increase the maximum frame rate possible on the Phantom camera, the camera was moved back to approximately 2.14 m from the Micro-RDE and the 250 mm lens was replaced with a 135 mm lens. This allowed for a smaller resolution (256 x 256 pixels) which consequently allowed for a frame rate of 79,000 frames per second, as smaller resolutions allow for potential of higher frame rates taken. These settings, in addition to the 1 microsecond exposure time, were the same settings used for the top-down view Phantom camera, thus allowing for perfect syncing. The results of

the improved optical configuration with the increased frame rate and new optical outerbody can be seen in Section 4.5.2.

4.5.2 Optical Results

Tests ran using the optical configuration with both the quartz and polycarbonate outerbodies were used to gather optical data on how the different injection schemes (Plain JIC, Partially-Premixed JIC, and Simplex) affected the performance on the Micro-RDE. Using the data from their operating maps discussed in Section 4.3, each injection scheme was retested with the optical configuration at points that previously detonated in their original configurations. It was desired to observe the detonation wave characteristics at the limits of each injection scheme's operating map to determine how to potentially optimize each injection scheme and further expand these. Figure 91 shows the optically accessible Micro-RDE in operation using the quartz optical outerbody while the side view Phantom camera captured frames at a rate of 13000 fps.

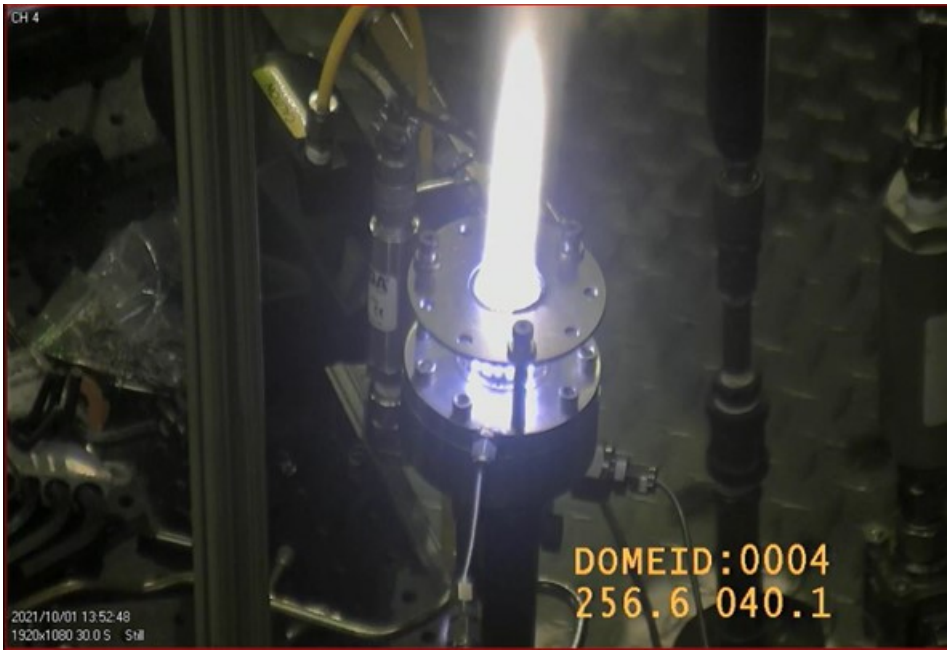

Figure 91. Optically Accessible Micro-RDE in Operation

While testing the Simplex and Partially-Premixed injection geometries, issues arose with the repeatability of detonations in the Micro-RDE optical configuration utilized. Figure 92 shows the operating map of the Simplex in the optically accessible small-scale RDE, where no detonations were produced. While it was desired to retest the points where detonation occurred in the original Micro configuration (shown in Figure 68), test points of the simplex on the optical configuration varied greatly from the previously established detonation points. It was discovered that the problem of choking across the sonic nozzle that was seen in the original configuration had worsened in the optical configuration.

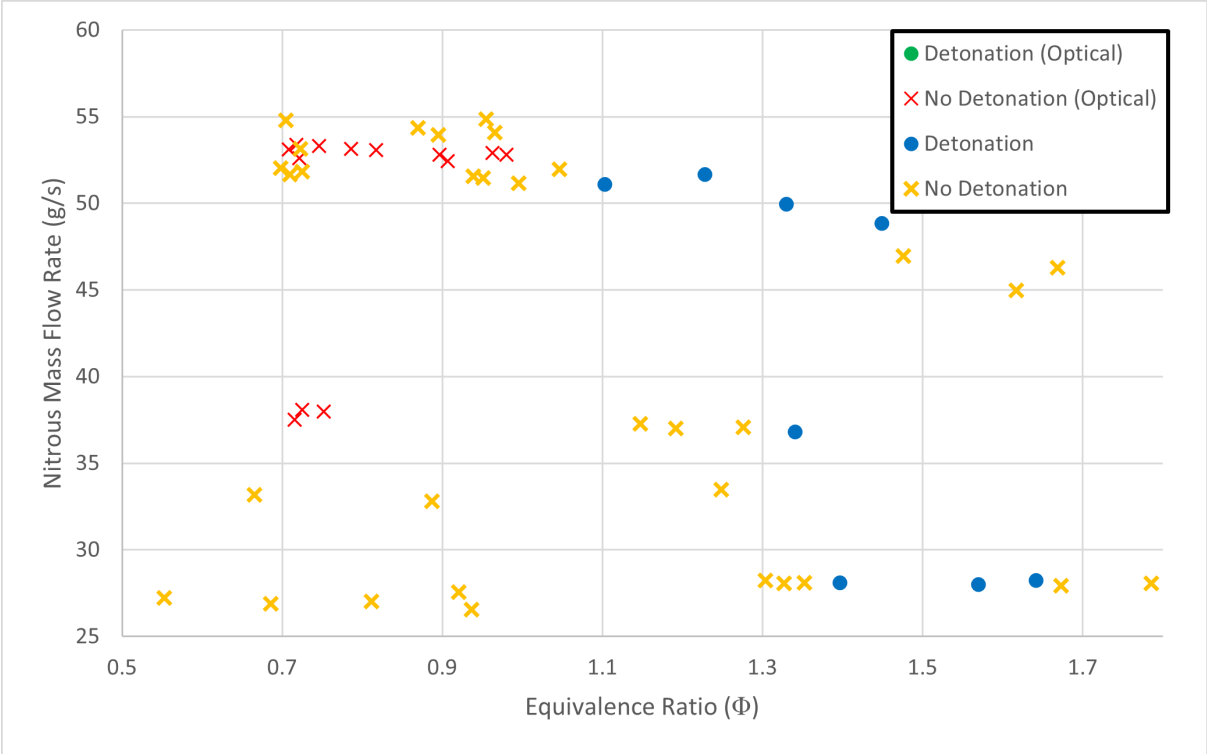

Figure 92. Operating Map of Simplex Injection Scheme in Optically Accessible Micro-RDE

To reach the choking condition, the downstream to upstream pressure ratio across the sonic nozzle must be less than 0.8 (and ideally much less than that). The Simplex pressure ratios across the oxidizer sonic nozzle in the original configuration varied from

0.76 to 0.87 already showing signs of unchoked flow. In the optical condition these pressure ratios in the NOS line ranged from 0.9 to 0.95 for every test point, showing that no choking condition was reached. The cause of this unchoked condition was unknown as the design parameters between the non-optical and optical configurations remained the same. The lack of choking resulted in the extremely fuel lean equivalence ratios tested as seen in Figure 92, as there was no pressure drop in the oxidizer's flow causing for much more NOS than intended to be injected into the RDE. Thus, the fuel rich equivalence ratios that usually caused the Simplex to detonate were not able to be tested.

Tighter nozzles were available which would ensure choking, but these nozzles possessed diameters that would require too high of an inlet pressure (5.18 MPa) which would fall outside the range of 2.07 MPa to 3.45 MPa set by the bottle pressure and the desire to keep the reactants in a gaseous state. As with the lack of choking in the non-optically accessible Simplex configuration, this was unexpected because the Simplex possessed the same injector hole sizes and utilized the same diameter sonic nozzles as the Plain configuration which had no issue choking during testing. Because of this inability to accurately test the Simplex in the optical configuration due to issues with unchoked mass flow, the optical testing of the Simplex was abandoned.

Additional issues arose with detonability in the quartz optical configuration when testing the Partially-Premixed injection scheme. As seen in Figure 93, no detonations were produced using this injection scheme on the optically accessible Micro-RDE. Choking conditions were more than reached in this configuration proven by the 0.44 pressure ratio across the sonic nozzle, thus, mass flow rates and equivalence ratios were able to be reliably tested with each run. Tests were done at the upper limit of $\sim$ 50 g/s to observe the detonation behavior at this portion of its operating map. Ignitions were observed at these mass flow rates, however, no propagating detonation

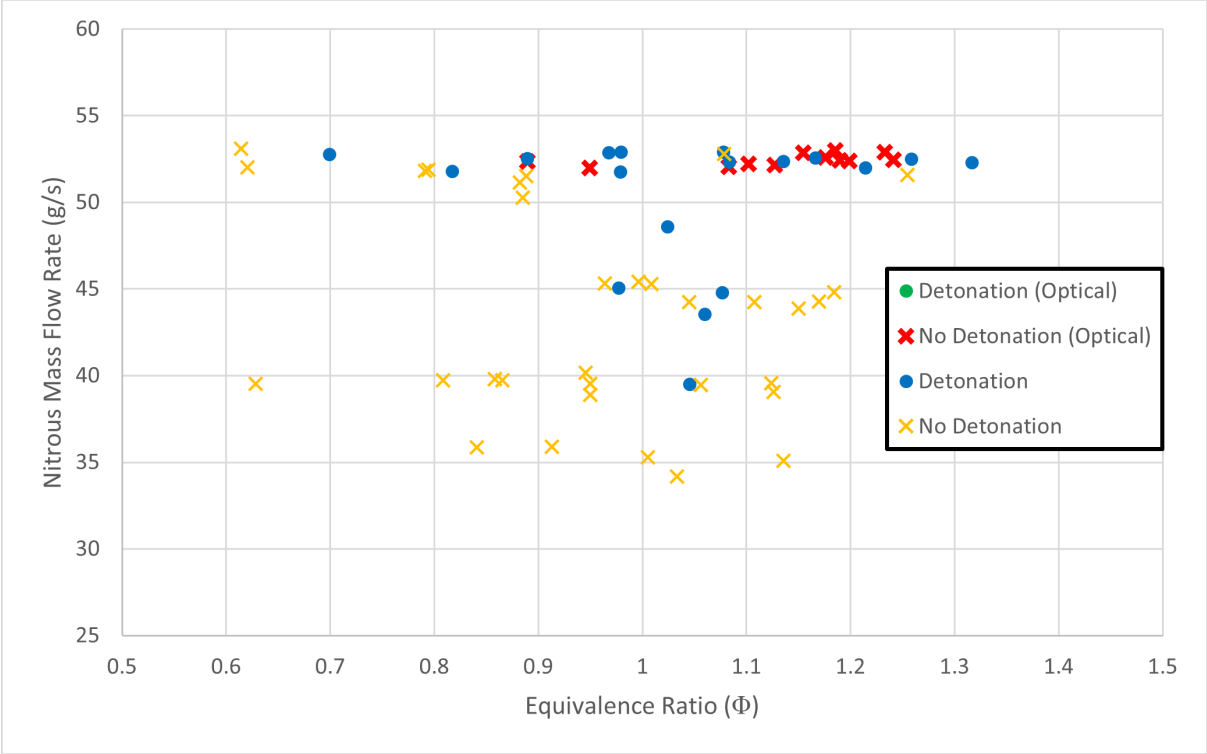

Figure 93. Operating Map of Partially-Premixed Injection Scheme in Optically Accessible Micro-RDE

wave was seen.

Figure 94 pictures the top-down view of the deflagrating flame that was commonly seen when running this configuration, where the reactants ignited but did not produce a detonation. Upon exiting the RDE detonation channel the flame would propagate in irregular patterns as seen in Figure 94 where the flame appeared to be moving towards the bottom of the frame instead of in a streamlined direction from the detonation channel. Because no detonations were observed at its upper limit, it was assumed that detonations would not be produced at lower mass flow rates especially when considering that the injection scheme scarcely produced detonations at oxidizer flow rates less than 50 g/s. Thus, testing of the Partially-Premixed injection scheme was abandoned to pursue the configurations using the Plain injectors.

Because of the lack of detonability in the other injection schemes, it was desired to

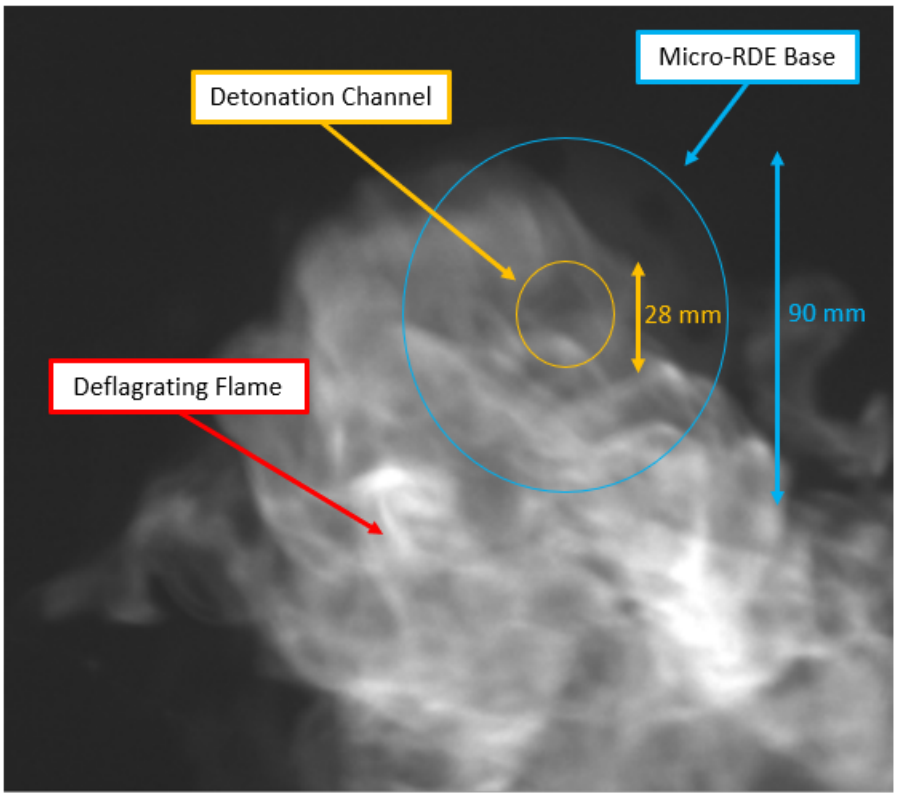

Figure 94. Top-Down View of Deflagration Produced from Partially-Premixed Injection Scheme in Optically Accessible Micro-RDE

focus on the plain injection scheme with the optical configuration. It is important to note that at this point in the testing campaign, no detonations had yet been produced and thus the optical configuration still utilized the quartz as its outerbody. As seen in Figure 95, the operability of the plain injection scheme with the optically accessible Micro-RDE was much more consistent with its original operating map unlike the Partially-Premixed and the Simplex. Initial testing with this configuration began at $\sim$ 50 g/s of oxidizer mass flow rate. While testing at these points, the initial Phantom camera setup that used a frame rate of 13000 fps was being utilized. It was not until detonations were produced in this configuration, which rendered the remaining quartz outerbodies unfit for testing, that it was observed that this frame rate was not sufficient to capture the detonation wave (see Section 4.5.1).

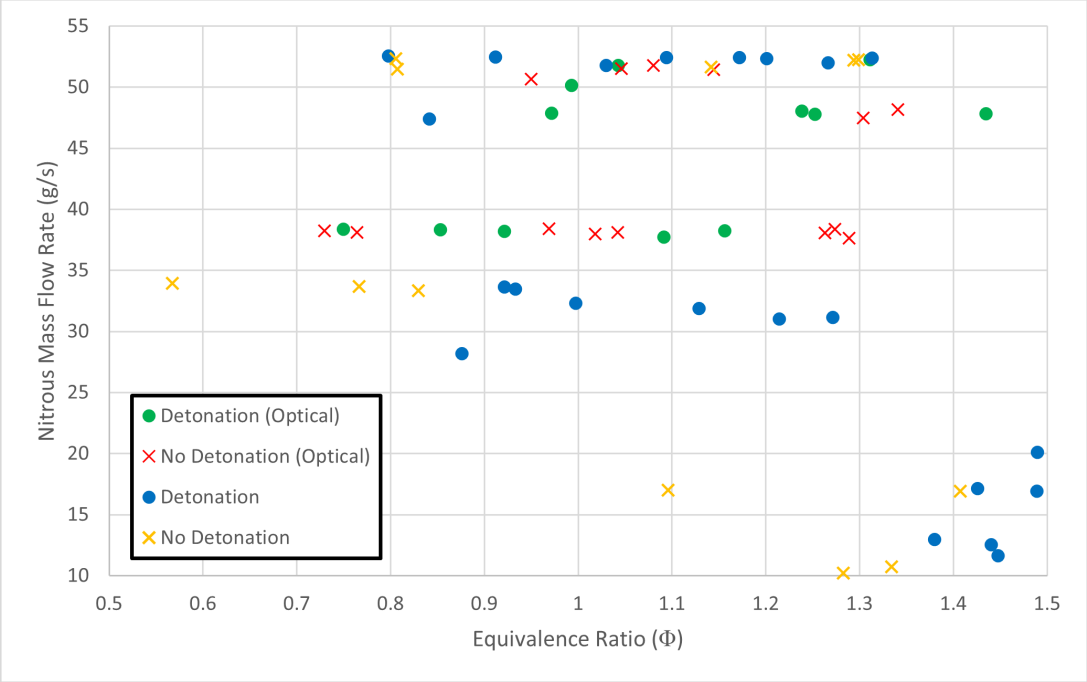

Figure 95. Operating Map of Plain JIC Injection Scheme in Optically Accessible Micro-RDE

Upon changing the optical outerbody to polycarbonate and increasing the frame rate to 79000 fps, the detonation wave was able to be observed, however, the optical data was still limited in its ability to help decipher fill height, cell size, and other properties of the detonation wave. Figure 96 shows the propagation of the detonation wave around the channel for a test at 37.7 g/s and an equivalence ratio of 1.09. Image a) represents the frame captured at time t = 0.26 seconds and images b), c), and d) correspond to the frames captured exactly 1, 2, and 3 frames after image a), respectively. Thus, the time between each of these frames is on the order of 10^{-5} seconds. Figure 96 a) shows the detonation wave on the left side of the Micro-RDE while Figure 96 b) and Figure 96 c) show its propagation around the channel from left to right.

As pictured in Figure 96, the detonation wave propagated almost halfway across the frame (and thus a quarter way across the Micro-RDE), in just a single frame.

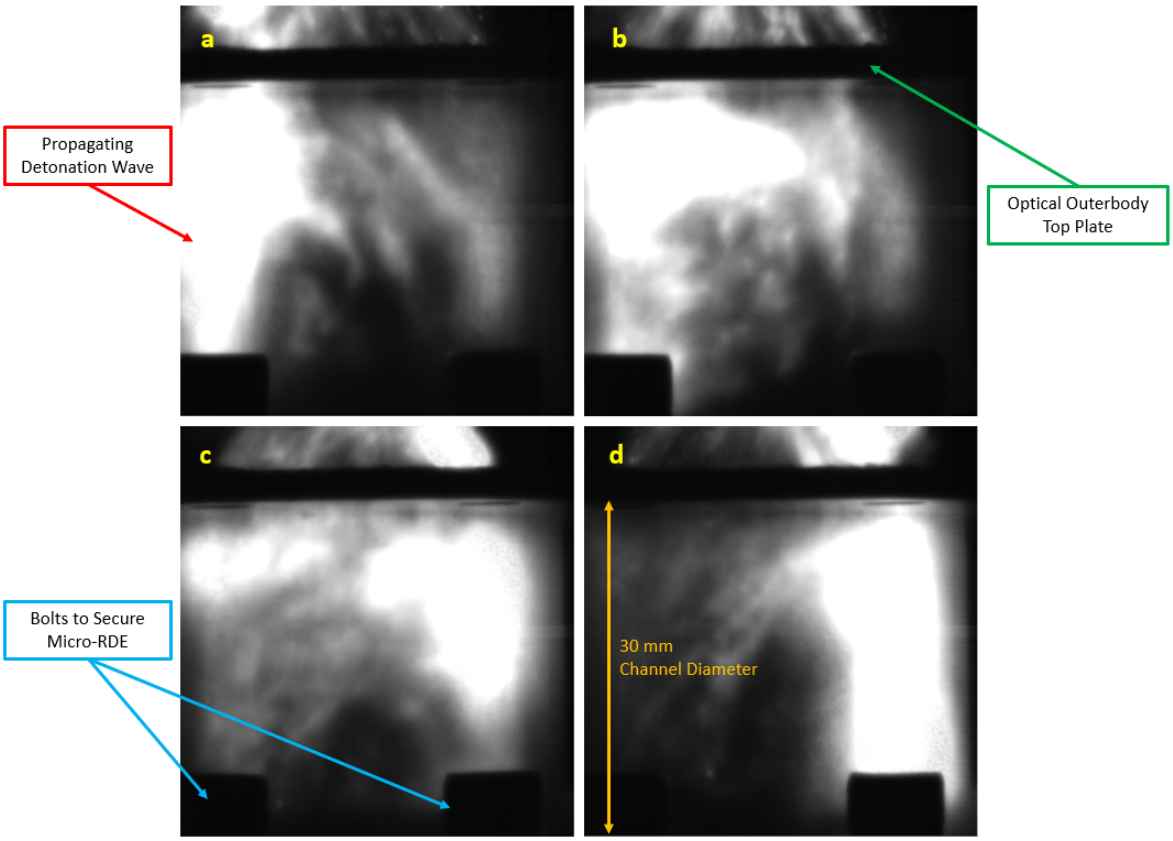

Figure 96. Side View of Detonation Produced from Plain Injection Scheme in Optically Accessible Micro-RDE with Polycarbonate Outerbody

This was likely due to the exposure time setting on the Phantom camera, set at 10 μs, where a detonation wave at 1500 m/s would travel 15 mm in a single frame. Thus, the open shutter time was too long and did not 'stop the flow' while the detonation was propagating which also resulted in the smeared images seen in Figure 96. The exposure time setting used was too large and consequently allowed too much light in causing for an oversaturated and dull image, so vital information concerning the cell size and behavior of the detonation wave was left uncaptured. Furthermore, no visual trends of the detonation wave were seen to allow for the determination of the number of waves propagating in the chamber. The fill height also proved too difficult to decipher from the optical data as the detonation wave seemed to illuminate the entire height of the optical chamber and no clear region of traveling reactants were seen.

Overall, apart from the general direction of its propagation in the Micro-RDE, not enough of the detonation wave is shown in the data to draw conclusions concerning its behavior. Because the use of a camera with a much higher frame rate and lower exposure time was needed to characterize the detonation waves, further testing on the optical configuration of the Micro-RDE was terminated.

V. Conclusion

A small scale rotating detonation engine was developed by Dechert to test the limits of detonability on smaller engines. Also called the "Micro-RDE", it was designed with a channel diameter of 28 mm, a channel gap of 2 mm, and a channel length of 30 mm, making it the smallest RDE at the time of its construction. Detonations in this configuration were designed to reach 20 kHz frequencies and operate between mass flow rates of 25 g/s to 75 g/s [1]. Dechert showed that although detonations were achievable at some of the intended mass flow rates, the detonation waves produced in the configuration were universally unstable as detonation frequencies fell below 30 % of the design frequency. It was hypothesized that this unstable behavior was due to a lack of mixing quality and issues with the ignition mechanism (a spark plug) causing protrusions in the detonation chamber that the wave would attach to. [1].

Building upon Dechert's research, Fiorino made certain modifications to the original Micro-RDE configuration to improve its design. This was done by altering/replacing the mechanisms that were believed to contribute to the wave instability and low detonation frequencies in the RDE: the injection scheme and the ignition mechanism [2]. A new injection scheme was developed, the Partially-Premixed JIC, where the reactants were given more time to mix before reaching the detonation chamber while also allowing for a mixing region uninfluenced by the passing waves in the channel. Additionally, the previous spark plug configuration was replaced with a pre-detonator which used a deflagration-to-detonation transition (DDT) to ignite the reactants without causing a protrusion in the chamber that the detonation wave could attach itself to. These major design changes accompanied by a few minor changes (see [2] for more) resulted in the increased stability of detonations in the Micro-RDE, realized by achieving detonation frequencies of 11 - 18 kHz, representing 84 % of the design frequency. The detonations accompanied by these higher detonation frequencies also

exhibited stable single wave mode behavior showing further improved signs of stability. However, the objective of reaching a stable detonation at the design frequency was still not achieved.

Current research focused on further characterizing the performance of different configurations of the Micro-RDE to allow for potential optimization of the small scale engine in the future. In addition to the injection schemes used by Dechert and Fiorino, two more geometries were tested and their performance characterized on the Micro-RDE: the Simplex and the Counter-jet. The objectives of this research were to explore the operability of these various injection schemes while also comparing their influence on wave stability produced. Further comparisons on their performance were intended to be achieved through an optically accessible configuration that allowed for further visualization and characterization of a propagating detonation wave. It was believed that these assessments would allow for the further understanding of the Micro-RDE and prompt optimization in the rig to achieve the design frequency and wave stability. The following sections recap the steps taken to implement these changes, the results they produced, and potential avenues for future work.

5.1 Methodology

A new mass flow system was designed to replace the previous Alicat Control system used by Dechert and Fiorino to produce more stable and reliable mass flows. The goal of this change was to implement a new system that could continuously pump steady mass flow rates that were not affected by the downstream pressure disturbances during detonations and to meter this flow with reasonable accuracy to the requested mass flow. Sonic nozzles were used as the new mass flow control system to ensure a "choked" state was reached across the nozzles signifying that the flow reached a speed of Mach 1. This assured that the the mass flow was stable as upstream pressure

disturbances could not move past the throat of the nozzle where the velocity of the pressure was at the speed of sound and always greater than that of the pressure disturbances.

Additionally, changes to the centerbody of the Partially-Premixed injection scheme were made to reduce erosion on the aerospike nozzle in the Micro-RDE. The previous interface between the nozzle and the fuel/oxidizer manifold was moved from 15 mm above the injectors to directly above them creating an elongated aerospike nozzle. This was designed to prevent recirculation zones at the interface between the manifold and nozzle as their design prevented them from being completely flush during assembly. To further decrease erosion, these new centerbodies were engineered out of Inconel 625 instead of Stainless Steel 304 for its higher heat resistance.

Multiple injection schemes were tested on the Micro-RDE during this research. These included the Plain JIC (tested by Dechert), the Partially-Premixed JIC (tested by Fiorino), a modified Simplex swirl nozzle, and a Counter-jet injection geometry. The Plain JIC tested on the Micro-RDE during this research utilized fuel and oxidizer streams that were injected radially and axially, respectively, at a 90 degree point of crossflow in the detonation chamber. This was identical to that of Dechert's apart from the tighter oxidizer injection hole areas used in this configuration that were designed to better retain pressure in the detonation chamber. The Partially-Premixed injection scheme moved the point of crossflow from 2 mm into the detonation chamber to 2 mm before the entrance to the detonation chamber to allow for more time and more uninterrupted mixing. This configuration directly mirrored that of Fiorino's and had a larger injector hole area for both the fuel and oxidizer.

The modified Simplex configuration, designed by Nathan Snow, swirled the oxidizer into a spray cone while injecting the fuel radially using both gaseous reactants. The injector hole areas directly matched that of the Plain JIC for direct comparison.

The last injection scheme tested, the Counter-jet, injected the fuel and oxidizer radially into the chamber, where the fuel was injected towards the outer rim of the RDE and the oxidizer was injected towards its center. One configuration of the Counter-jet had the fuel and oxidizer injectors aligned where their streams were directly impinging upon one another, while another had the injectors offset by 7.5 degrees where they would impact the opposite wall of the detonation chamber before mixing. For consistency, all injection schemes tested in this research were performed with a 0.75 mm exit channel gap ($\epsilon = 0.39$). Mass flow rates ranging from 10 g/s to 55 g/s were tested across a range of equivalence ratios ($\phi = 0.5$ to 1.5) on each injection scheme to characterize their operating limits and to help evaluate their performance.

The detonation chamber was replaced with a quartz optical outerbody to allow for optical access into the Micro-RDE during testing. Optical outerbodies made of polycarbonate were also used in this testing. After removing the upper portion of the original outerbodies that made up the detonation chamber, 1 mm grooves were machined into the new optical base plates that allowed for the quartz or polycarbonate to be positioned inside them during testing. On top of the optical outerbody was a top plate used to support the configuration while ensuring the optical outerbodies were secured in place. Graphite sealants were used in between the optical outerbodies and the top/base plates to ensure flow was properly sealed and to protect the optical outerbodies from the hot temperatures experienced by the metals during detonations. Two Phantom cameras were utilized to record the propagating detonation wave from a top-down view of the detonation channel and from a side view of the channel. The top-down view, utilized in previous research by Dechert and Fiorino, was used to gather optical data that would later be used to determine the frequency of the detonation wave. The side view was intended on gathering optical data that would lead to the determination of the cell size, fill height and other key parameters of the

detonation wave's behavior. Iterations to the side view configuration were made to optimize this data given the cameras utilized.

Pressure and temperature data were also monitored during this research. Pressure transducers and thermocouples were placed inside the plenums for both the fuel and oxidizer to monitor the pressure injected into the chamber. Another pressure transducer was situated in the detonation chamber to capture a capillary tube average pressure measurement of detonation chamber conditions. Additional pressure and temperature sensors was used to upstream and downstream the sonic nozzle mass flow control system to monitor mass flow rates and ensure steady flow throughout testing.

5.2 Results

Tests were conducted on each injection scheme to characterize their performance and influence on the operating map and wave stability produced in the Micro-RDE. To first ensure that every injection scheme was tested under similar conditions, the temperature on the base plate of the RDE, which heated up after experiencing a detonation, was monitored. In this research the temperature was never deliberately changed to influence the performance of the injection geometries. While it was hypothesized that the $\sim$ 40 K range of temperatures experienced by the RDE would help improve detonability in some configurations, the temperature made no profound impact on the operating maps. The plain injection scheme detonated at both ambient and higher temperatures, and the simplex did not see a major increase in detonability after it was heated from the few detonation events it produced. Thus, it was concluded that the temperature was not hot enough to play a factor in the comparison of the injection schemes tested in this research.

Since temperature was found to not influence detonability and the uniformity

of testing was established, research was conducted on the injection schemes in the Micro-RDE. The results of settling time of the plenum pressures, another sign of stability of conditions in detonations is presented in Section 5.2.1. Section 5.2.2 and Section 5.2.3 compare the results of the injection schemes in the Micro-RDE by their operating maps and detonation frequencies, respectively. Lastly, the results of the visual data produced by the optical configuration is discussed in Section 5.2.4.

5.2.1 Settling Time

Additional analysis was done on the settling time of the plenum pressures of the reactants during detonation, another key sign of stability during detonation. Tests by Fiorino observed plenum pressures sharply rising during detonation events and never settling to a steady state condition before the test run was terminated. Initial concerns for elongating the run time included extreme erosion to the Micro-RDE and a decrease in reusability of parts, but changes to the metal contents of the RDE in addition to the ability of running at significantly lower mass flows instilled confidence in comparing the effects of longer runs on settling time. Pressure readings for a standard 0.6 second detonation window test along with elongated 3 and 6 second detonation window tests were monitored to explore the time needed for plenum pressures to settle in detonation events. Analysis revealed that the elongated run times allowed for the pressures to settle within 5 % of the final steady state value within 1.2 seconds for the fuel and 0.5 seconds for the oxidizer. The standard tests with a 0.6 second detonation window average $\sim$ 0.4 second detonation times which is not long enough for these pressures to settle, hence the reason why plenum pressures never stabilized beforehand. This evidence of stable plenum pressure at longer run times could lead to the increased stability of detonations in the future.

5.2.2 Operating Maps

To analyze the performance of the various injection schemes through the comparison of the operating maps they produced, mass flow rates between 10 g/s and 55 g/s were tested across a range of equivalence ratios between $\phi = 0.5$ - 1.5. This was changed from the operating regimes of Dechert and Fiorino (25 g/s to 75 g/s) because discovering the lower limits of the operating map were deemed more important for this research as it was assumed that if a configuration could detonate at a low mass flow rate then it would also detonate at a higher one. Tests were ran on every injection scheme at $\sim$ 50 g/s and were gradually lowered until no more detonations were produced and the lower limit was reached. This was done while simultaneously sweeping the desired range of equivalence ratios. All configurations used a pre-detonator as an ignition mechanism and a 0.75 mm gap aerospike nozzle ($\epsilon = 0.39$).

The largest operating map was observed in the Plain JIC injection scheme which produced detonations at oxidizer mass flow rates as low as 12 g/s. This drastically expanded the operating map of this injection scheme tested by Dechert which had a lower limit of 40 g/s to produce detonations. While the detonations at these lower mass flow rates were only experienced at more fuel rich equivalence ratios, detonations between $\sim$ 30 g/s and $\sim$50 g/s were observed at equivalence ratios between 0.8 and 1.4. The operating map of the Partially-Premixed JIC injection scheme produced a lower limit of 45 g/s, but detonated consistently at mass flows $\sim$ 50 g/s from equivalence ratios between $\phi = 0.7$ - 1.3. These results closely resembled those produced in tests by Fiorino, which also had a lower limit of 45 g/s.

Detonations in the Simplex were not as prevalent, as detonations were only produced on the fuel rich side of equivalence ratios between $\phi = 1.1$ - 1.5 at mass flow rates $\sim$ 50 g/s. However, in spite of its limited ability to detonate at lower equivalence ratios, detonations were observed in the Simplex configuration at mass flow rates as

low as 28 g/s. These detonations were produced at fuel rich equivalence ratios outside the general operating space (ϕ = 1.56, 1.64), yet they contributed to a detonations at low mass flow rates. The last operating map was characterized for the Counter-jet configuration. The first initial configuration of the Counter-jet directly aligned oxidizer and fuel injectors across from each other such that there streams were directly impinging on one another. Although many loud "pops" were experienced in this first configuration, which usually signal the start of a detonation, no detonations were experienced. It was decided to test a second configuration where the injectors were aligned to be offset by 7.5 degrees each such that their streams would collide with the opposing detonation channel wall as opposed to the other stream. This resulted in detonations seen at $\sim$ 50 g/s between equivalence ratios of ϕ = 1.1 - 1.3. No further testing was done on the second configuration, as it was tested purely out of curiosity and not an original configuration desired to be tested.

Thus, it was concluded that for the tested configurations the Plain possessed the widest operating map by a significant margin. To assess potential reasons for the wide variations in the operating maps observed by the different injection schemes, analysis was done on the plenum to chamber pressure ratios produced by the configurations. By assessing this injector stiffness and where it detonates, it was hoped to find a trend that revealed a correlation between injector stiffness and detonability which would translate to better injection desing in the future. It was found that detonability in all configurations highly increases at a P_o/P_c less than 3 and a P_f/P_c less than 2. These conditions were most often reached in the Plain, thus giving reason for its highly expanded operating map. Reaching these conditions with the other injection schemes will allow for the expansion of their operating maps and increase their detonability.

5.2.3 Detonation Stability

Performance comparisons of the various injection schemes also included the assessment of the proximity of the detonation wave frequencies and speeds produced to the design frequencies and speeds. Dechert designed the Micro-RDE to operate at 20 kHZ and produce wave speeds between 1664 – 1833 m/s which equate to 80 % of the Chapman-Jouget wave speed for a nitrous and ethylene mixture (2080 - 2291 m/s). The detonation frequencies for each run were found using FFT methods executed in a Python code written by Nathan Snow. An FFT and spectrogram were outputted for each run which allowed the user to determine the frequency of the detonation along with verify the presence of any acoustic burning or harmonics inside the detonation channel.

Although it produced the largest operating map, the Plain JIC produced detonation frequencies ranging from only 11.1 kHz to 13.7 kHz, an average 38.5 % below the design frequency of the Micro-RDE configuration. This equated to wave speeds between 978 to 1203 m/s. Spectrogram results for this injection scheme revealed single wave mode propagation however with unstable behavior. Despite its more limited operating map, the Partially Premixed produced detonation frequencies between 15.2 and 18.4 kHZ, equating to wave speeds between 1339 and 1615 m/s. TIn addition to the increased frequencies, the spectrogram output from this injection scheme showed a more stable single wave propagating detonation with no harmonic frequencies.

The Simplex configuration produced wave frequencies between 12.3 and 14.3 kHz, an average 34.2 % below the design frequency and only slightly higher than those produced by the Plain. These corresponded to wave speeds between 1079 and 1258 m/s. Spectogram outputs from the Plain revealed multiple detonation waves in the detonation chamber all exhibiting unstable behavior. As previously stated, no detonations were produced in the direct impinging configuration of the Counter-jet injection

scheme. However, analysis on the Counter-jet with the 7.5 degree offsetted injectors revealed detonation frequencies between 16.7 and 17.8 kHz, producing the highest average of detonation frequencies in the Micro-RDE testing (it is important to note that not as many tests were conducted on this configuration as the others, which could be a potential cause of its consistency). These frequencies, averaging 14.4 % below the design frequency, equated to wave speeds from 1468 to 1570 m/s. Spectrograms produced by the Counter-jet showed single wave mode propagation however the strength of the detonation was weak and harmonic frequencies were present.

Thus, the Partially-Premixed and 7.5 degree offsetted Counter-jet produced the highest frequencies in this research. Despite their limited operating maps when compared to the Plain, they possess the highest stability of detonations when comparing their frequencies to that of the design frequency. When observing wave behavior, the Partially-Premixed produced the most stable wave modes producing single wave propagating detonations. Future research that is focused on stability and the production of high frequencies should utilize these configurations.

5.2.4 Optical Configuration

Concerning optical access, multiple iterations on the original optically accessible Micro-RDE configuration were made to attempt to obtain the best optical data possible that clearly defined the detonation wave and its properties. Tests were performed on the Plain JIC, Partially-Premixed JIC, and Simplex in the optical configuration (note: no accommodations for the Counter-jet were made for optical access). These tests were conducted at the mass flow rates and equivalence ratios that experienced detonations in their original configurations to further observe the behavior of the detonation wave at the previously tested points. Initial issues of detonability in the optical configuration were realized in the Partially-Premixed JIC and Sim-

plex injection schemes as no detonations were produced for these geometries in the optically-accessible Micro-RDE. Ignitions were observed in the Partially-Premixed configuration, however later analysis shows that these events were deflagration and no propagating detonation wave was found. Only the Plain JIC injection scheme produced detonations in the optical configuration, so testing was streamlined to focus on the optical data produced by this geometry.

Other initial issues were experienced with the durability of the quartz optical outerbody. Some quartz outerbodies utilized were rendered unusable due to issues with the installation that caused unequally distributed pressure around the quartz during testing that resulted in cracks on the surface of the outerbody. The rest of the quartz were shattered from detonation conditions experienced during testing. Optical data from tests with the quartz was also limited due to the initial 13,000 frames per second setting used on the side view Phantom camera which only captured the motion of particles and the presence of flames in the detonation channel.

A more durable but less transparent material, the polycarbonate, replaced the quartz as the optical outerbody and the frame rate on the Phantom camera was set to its maximum (79,000 fps) for the specific resolution needed to capture the entire detonation channel. Improvements on the optical data gathered from this configuration were seen as the detonation wave was seen propagating around the channel. However, the frame rate was still insufficient in capturing the fill height, cell size, and other important parameters that describe the behavior of the detonation wave. Even visualization of the detonation wave, although visible, was not as defined as was expected. Thus, no optical data was able to be used to compare the performance of the various injection schemes and their impact on detonation wave stability in the Micro-RDE.

5.3 Future Work

There still exists a multitude of ways to further characterize and optimize the performance of the Micro-RDE configuration, both the optical and non-optical. Concerning injection schemes, it was hypothesized that further iterations to the Partially-Premixed JIC, Simplex, and Counter-jet geometries should increase their ability to outperform the Plain JIC which is a standard and basic injection mechanism. Future testing should consider decreasing the oxidizer injection hole areas for the Partially-Premixed JIC. This decrease in the oxidizer injection hole area for the Plain JIC allowed for the lower limit of its operating map to decrease by 30 g/s from lower limit in its original configuration. It is believed that decreasing the oxidizer injection hole diameters and their quantity will allow for more pressure to be retained in the chamber as it did for the Plain, and thus create more detonable conditions and expand its operating map.

Additionally, the Simplex configuration must be modified to ensure flow is choking across the sonic nozzles during testing. This can be accomplished by increasing the area of the injector holes or by decreasing the area of the sonic nozzles. Decreasing the sonic nozzle size used also will require more pressure to choke across the nozzle to obtain the same desired mass flow rate, which would further complicate the configuration because the inlet pressure would require more than can be supplied by the bottle or it would reach a certain pressure where the reactants begin to phase into liquids. Thus, it is recommended that the injector holes simply be opened or that an additional sonic nozzle with a smaller diameter that doesn't require more than 3.45 MPa to be choked be obtained. It is also highly encouraged to flip how the reactants are injected in this scheme back to a more traditional Simplex where the fuel is swirled and the oxidizer is axially injected and not the other way around. Testing on how reversing the direction of the injected reactants affect mixing quality

should not be limited to the Simplex, as there are potential changes in detonability if the two reactants are reversed in all the injection schemes tested.

While testing in the Counter-jet configuration with direct impinging produced no detonations, the operating limits of the Counter-jet with the 7.5 degree offsetted injectors should be further explored. Testing on this configuration was limited since it was not a part of the original objective of characterizing the Counter-jet's performance, but the consistently high frequencies produced show potential for creating a stable detonation wave at the design frequency using this injection scheme.

For the testing in this research, all injection schemes were tested with aerospike nozzles that created 0.75 mm channel gaps at the exit for continuity purposes. While this allowed for the controlled testing of the injection schemes, it did not allow for the observation of how the various injection schemes run with tighter or looser nozzle gaps. Because the use of tighter aerospike nozzles are another way of retaining more pressure in the detonation chamber, a testing sweep of nozzles sizes that create 0.625 mm ($\epsilon = 0.33$) and 0.50 mm ($\epsilon = 0.26$) channel gaps could allow for more detonations and expanded operating maps for all injection mechanisms. Testing using the various nozzles sizes will lead to further understanding and optimization of the Micro-RDE.

The goal of testing in the Micro-RDE is to push the boundaries of small-scale rotating detonation engines and detonate at the lowest mass flow rates possible. While detonations in this configuration were seen as low as 12 g/s, testing by Law et al. produced detonations in their small-scale RDE at mass flow rates as low as 3.5 g/s [34]. It is important to note that the RDE designed by Law et al. uses an ethylene-oxygen mixture instead of the ethylene-nitrous oxide mixture used in this research. The ethylene-oxygen mixture used had an estimated cell size of 0.465 mm while the estimated cell size for the ethylene-nitrous oxide reactants in this research had an estimated cell size between 0.5 and 1.75 mm [34, 1]. The smaller cell size of

reactant mixture with oxygen created more detonable conditions and allowed for the propagation of a detonation wave at a lower mass flow rate. It is recommended that to further push the limits of detonating at low mass flow rates that the Micro-RDE replace nitrous oxide with oxygen as the oxidizer of the reactants. Law et al. produced detonations at these low mass flow rates using a 75 mm RDE while the one used in this research has only a 28 mm channel diameter, so theoretically a switch to oxygen should allow for detonations at mass flows even lower than 3.5 g/s.

While switching the oxidizer to oxygen is the ideal course of action in further expanding the operating map of the Micro-RDE, additional changes would be have to be made to account for the oxygen in the RDE. A metal more resistant to oxidation, such as Monel, should be used to create the new parts of the Micro-RDE. This nickel alloy that is primarily composed of nickel and copper will be less susceptible to metal oxidation as opposed to the Inconel and Stainless Steel parts used on the Micro-RDE. Additionally, lines previously holding the traveling nitrous-oxide would need to be purged prior to running oxygen through the lines to prevent an unwanted mixture of reactants.

Lastly, certain changes to the optical configuration must be made to capture a propagating detonation wave in the Micro-RDE should it be desired in the future. It is suggested to develop a more survivable optical configuration with the quartz cylinder that can consistently endure detonation conditions without having to sacrifice clarity of visualization into the chamber by using a more durable yet less clear optical outerbody such as the polycarbonate. Other materials for an optical outerbody such as sapphire or zirconium could also be explored in their ability to allow visualization into the chamber without being destroyed in the process. It is also imperative that a different high-speed camera be used for the side-view visual to properly capture the desired properties of the detonation wave. Experiments by Santiago in the Air Force

Research Labs (AFRL) at Wright-Patterson Air Force Base, Ohio used a Shimadzu high speed camera to monitor a propagating detonation created by electric wires. This high-speed camera, which takes a maximum 14,000,000 fps allowed for him to compare the differences of the detonation waves produced by various equivalence ratios in his configuration. It is highly suggested that this camera along with a lower exposure time setting be used to gather optical data in the Micro-RDE so that the desired characteristics of the propagating detonation wave may be observed and characterized for the various injection schemes and mass flow conditions.

Bibliography

[1] Dechert, J. R., *Development of a Small Scale Rotating Detonation Engine*, Master's thesis, Air Force Institute of Technology, WPAFB, OH, 2020.

[2] Fiorino, N. T., *Improving the Stability and Operability of a Small Scale Rotating Detonation Engine*, Master's thesis, Air Force Institute of Technology, WPAFB, OH, 2021.

[3] Turns, S. R., *An Introduction to Combustion: Concepts and Applications*, WCB/McGraw-Hill, 3rd ed., 2020.

[4] Lee, J. H. S., *The Detonation Phenomenon*, Cambridge University Press, Cambridge, 2008.

[5] Schwer, D. A. and Kailasanath, K., "Rotating Detonation-Wave Engines," 49th AIAA Aerospace Sciences Meeting including the New Horizons Forum and Aerospace Exposition, 2011.

[6] Thomas, L., Schauer, F., Hoke, J., and Naples, A., "Buildup and Operation of a Rotating Detonation Engine," American Institute of Aeronautics and Astronautics (AIAA), 2011.

[7] Paxson, D. E. and Kaemming, T. A., "Foundational Performance Analyses of Pressure Gain Combustion Thermodynamic Benefits for Gas Turbines," 50th AIAA Aerospace Sciences Meeting Including the New Horizons Forum and Aerospace Exposition, 2012.

[8] Paxson, D. E. and Kaemming, T., "The Influence of Unsteadiness on the Analysis of Pressure Gain Combustion Devices," 51st AIAA Aerospace Sciences Meeting, 2013.

[9] Wintenberger, E. and Shepherd, J. E., "Thermodynamic Cycle Analysis for Propagating Detonations," *Journal of Propulsion and Power*, Vol. 22, 2006, pp. 694–697.

[10] Vutthivithayarak, R., Braun, E., and Lu, F., "Examination of the Various Cycles for Pulse Detonation Engines," 47th AIAA/ASME/SAE/ASEE Joint Propulsion Conference, 2011.

[11] Nicholls, J. A., Wilkinson, H. R., and Morrison, R. B., "Intermittent Detonation as a Thrust-Producing Mechanism," *Journal of Jet Propulsion*, Vol. 27, No. 5, 1957, pp. 534–541.

[12] Schwer, D. and Kailasanath, K., "Numerical Investigation of Rotating Detonation Engines," 46th AIAA/ASME/SAE/ASEE Joint Propulsion Conference, 2010.

[13] Braun, E. M., Dunn, N. L., and Lu, F. K., "Testing of a Continuous Detonation Wave Engine with Swirled Injection," 48th AIAA Aerospace Sciences Meeting Including the New Horizons Forum and Aerospace Exposition, 2010, p. 146.

[14] Fiorino, N. T., Schauer, F. R., Polanka, M. D., Schumaker, S. A., and Sell, B. C., "Use of a Partially Pre-Mixed Injection Scheme and Pre-Detonator in a Small Scale Rotating Detonation Engine," AIAA Propulsion and Energy 2021 Forum.

[15] Tieszen, S. R., Sherman, M. P., Benedick, W. B., and Berman, M., "Detonability of H2-Air-Diluent Mixtures," *Technical Report*, 1987.

[16] Bykovskii, F. A., Zhdan, S. A., and Vedernikov, E. F., "Continuous Spin Detonations," *Journal of Propulsion and Power*, Vol. 22, 2006, pp. 1204–1216.

[17] Batista, A., Ross, M., Lietz, C., and Hargus, W. A., "Detonation Wave Interaction Classifications in a Rotating Detonation Rocket Engine," American Institute of Aeronautics and Astronautics Inc, AIAA, 2020, pp. 1–21.

[18] Lu, F. K., Braun, E. M., and Powers, J., "Rotating Detonation Wave Propulsion: Experimental Challenges, Modeling, and Engine Concepts," Vol. 30, American Institute of Aeronautics and Astronautics Inc., 2014, pp. 1125–1142.

[19] Shepard, J. E., "Detonation in Gases," *Proceedings of the Combustion Institute*, Vol. 32 I, 2009, pp. 83–98.

[20] Kudo, Y., Nagura, Y., Kasahara, J., Sasamoto, Y., and Matsuo, A., "Oblique Detonation Waves Stabilized in Rectangular-Cross-Section Bent Tubes," Vol. 33, 2011, pp. 2319–2326.

[21] Duvall, J., Chacon, F., Harvey, C., and Gamba, M., "Study of the Effects of Various Injection Geometries on the Operation of a Rotating Detonation Engine," American Institute of Aeronautics and Astronautics Inc, AIAA, 2018.

[22] Amini, G., "Liquid Flow in a Simplex Swirl Nozzle," *International Journal of Multiphase Flow*, Vol. 79, 3 2016, pp. 225–235.

[23] Giffen, E. and Muraszew, A., *The Atomization of Liquid Fuels*, Chapman and Hall, London, 1954.

[24] Kaneshige, M. J. and Shepard, J. E., "Detonation Database," Graduate Aeronautical Laboratories California Institute of Technology, Pasadena, CA, 1997.

[25] Rankin, B. A., Richardson, D. R., Caswell, A. W., Naples, A., Hoke, J. L., and Schauer, F. R., "Imaging of OH* Chemiluminescence in an Optically Accessible Nonpremixed Rotating Detonation Engine," American Institute of Aeronautics and Astronautics Inc, AIAA, 2015.

[26] Naples, A., Hoke, J., Karnesky, J., and Schauer, F., "Flowfield Characterization of a Rotating Detonation Engine," American Institute of Aeronautics and Astronautics Inc., 2013.

[27] Unruh, E., Spaulding, M., Lineberry, D., Xu, K. G., and Frederick, R., "Development of an Optically Accessible Racetrack-type Rotating Detonation Rocket Engine," American Institute of Aeronautics and Astronautics Inc, AIAA, 2020, pp. 1–16.

[28] Gavrikov, A., Efimenko, A., and Dorofeev, S., "A Model for Detonation Cell Size Prediction from Chemical Kinetics," *Combustion and Flame*, Vol. 120, No. 1, 2000, pp. 19–33.

[29] Stainless, N. A., *North American Stainless Long Products Stainless Steel Data Sheet*, North American Stainless, 2020.

[30] a POC Company, S. M., *INCONEL Alloy 625*, Special Metals Corporation Group, 2013.

[31] Engineering, F., *Sonic Nozzles*, Critical Flow Nozzles, accessed Aug 23 2013.

[32] ToolBox, E., *Universal and Individual Gas Constants*, The Engineering Toolbox, accessed 23 Aug 2021.

[33] Fernelius, M., Sell, B., Moosmann, K. J., Andrus, I. Q., Hoke, J. L., and Schauer, F. R., "Characterization of a Premixed Laboratory Scale Pulsed Detonation Burner," 2018 AIAA Aerospace Sciences Meeting.

[34] Law, H., Baxter, T., Ryan, C. N., and Deiterding, R., "Design and Testing of a Small-Scale Laboratory Rotating Detonation Engine Running on Ethylene-Oxygen," AIAA Propulsion and Energy 2021 Forum.

REPORT DOCUMENTATION PAGE

Form Approved
OMB No. 0704–0188

1. REPORT DATE *(DD–MM–YYYY)*	2. REPORT TYPE	3. DATES COVERED *(From — To)*
23–12–2021	Master's Thesis	June 2020 — December 2021

4. TITLE AND SUBTITLE

Injection Studies on a Small-Scale Rotating Detonation Engine with Improved Flow Control

5a. CONTRACT NUMBER

5b. GRANT NUMBER

5c. PROGRAM ELEMENT NUMBER

6. AUTHOR(S)

Wyatt, Jonathan J., 2d Lt, USAF

5d. PROJECT NUMBER

5e. TASK NUMBER

5f. WORK UNIT NUMBER

7. PERFORMING ORGANIZATION NAME(S) AND ADDRESS(ES)

Air Force Institute of Technology
Graduate School of Engineering and Management (AFIT/EN)
2950 Hobson Way
WPAFB OH 45433-7765

8. PERFORMING ORGANIZATION REPORT NUMBER

AFIT-ENY-MS-D-080

9. SPONSORING / MONITORING AGENCY NAME(S) AND ADDRESS(ES)

Air Force Research Lab Aerospace Directorate
Combustion Branch, Turbine Engine Division
1790 Loop Road North
WPAFB OH 45433-7765

10. SPONSOR/MONITOR'S ACRONYM(S)

AFRL/RQTC

11. SPONSOR/MONITOR'S REPORT NUMBER(S)

AFIT-ENY-MS-D-080

12. DISTRIBUTION / AVAILABILITY STATEMENT

Approval for public release; distribution is unlimited.

13. SUPPLEMENTARY NOTES

14. ABSTRACT

The Rotating Detonation Engine (RDE) has gained increasing attention in recent years for its potential advantages over typical deflagration combustion. A Micro-RDE design with an outer diameter of 28mm operating on Nitrous Oxide and Ethylene was recently developed, which stretched the limits of small-scale detonation engines. The testing on this rig has shown a stable one wave mode detonation with frequencies reaching 16.8 kHz. Key parameters that influence the detonation wave mode are cell size, fill height, and wave speed, which are heavily influenced by injection schemes. Previous testing utilized a partially premixed jets in crossflow (JIC) injection scheme, while tests before that used a traditional JIC scheme. A Simplex and Counter-jet injection scheme were added to the configuration to explore other options of injecting the fuel and oxidizer. The goal of this research was to characterize the operating limits of the injection schemes and understand their effects on the detonation wave stability in a small-scale RDE.

15. SUBJECT TERMS

Rotating Detonation Engine, Small Scale, Pressure-Gain Combustion, Detonation Combustion, Detonation Frequency

16. SECURITY CLASSIFICATION OF:			17. LIMITATION OF ABSTRACT	18. NUMBER OF PAGES	19a. NAME OF RESPONSIBLE PERSON
a. REPORT	b. ABSTRACT	c. THIS PAGE			Dr. Fred R. Schauer, AFIT/ENY
U	U	U	UU	177	19b. TELEPHONE NUMBER *(include area code)* (937) 255-3636, x4204; fschauer@afit.edu